ASTROCYTE SIGNALING IN TRAUMATIC BRAIN INJURY

YungChia Chen

A DISSERTATION

in

Bioengineering

Presented to the Faculties of the University of Pennsylvania

in Partial Fulfillment of the Requirements for the

Degree of Doctor of Philosophy

2014

_____

David F. Meaney
Solomon R. Pollack Profressor
Supervisor of Dissertation

_____

Jason A. Burdick
Graduate Group Chairperson

Dissertation Committee
Beth A. Winkelstein, Ph.D., Professor Bioengineering
Andrew Tsourkas, PhD, Associate Professor, Dept. of Bioengineering
Douglas H. Smith, MD, Robert A. Groff Professor of Neurosurgery, Dept of Neurosurgery

ASTROCYTE SIGNALING IN TRAUMATIC BRAIN INJURY

To my parents.

Acknowledgements

Before embarking on my doctoral journey, I would not have been able to tell anyone any bit about the brain much less how it functions. Now I could talk someone's ear off on this finding, that new study, possible connections, and exciting new theories, all related to one particular cell type in the brain, astrocytes. That and mice behavior. I have spent some time with them after all. And it's not just knowing facts or findings, but seeing how different studies (including my own) start to fit into a greater picture. To this, I have my thesis advisor, Dr. David Meaney, to thank. Our conversations – "what if this really means…", "wouldn't it be cool if we found this (*insert something that would change the field here*)…", "did you see this study where (*insert some new finding here*) and maybe it could mean (*insert some new amazing idea here*)" – have honed my ability as a scientist to see the bigger picture and how generally amazing the world of science really is. Dave, here's to mice driving buses.

And to my committee, Drs. Winkelstein, Tsourkas, and Smith, for making sure that I was solidly in the realm of the practical and real. I also need to acknowledge Drs. Abel and Hernandez for giving me greater insight to mice and their many, many behaviors.

Most of my time was spent in the lab with mice. But the few times I spent with people (Meaneylab and Margulieslab) have been when some of the most enlightening and entertaining conversations occured, and not all of it about science.

Lastly, to my taciturn siblings and dad and my talkative mom, thank you guys for your support. It's something that I know I can count on always. I say no more on this subject. Anymore and sap would flow.

ABSTRACT

ASTROCYTE SIGNALING IN TRAUMATIC BRAIN INJURY

YungChia Chen

David F. Meaney

Traumatic brain injury (TBI) is a major and costly epidemic in the United States and around the world. There are little treatment options and currently no cure. Past research aimed at treating neurons as a therapeutic target have not been successful treatments clinically. Recent interest has turned to another cell type, the astrocyte, as a potential therapeutic target. In this dissertation, we expand upon past findings by further exploring the role of astrocytes and astrocytic signaling in TBI *in vivo*. Creating a new mild TBI model based on human mild TBI biomechanics, we produced behavioral deficits and histopathological changes similar to mild human TBI. We modified and applied the new TBI model to see if the *in vitro* astrocytic response to mild mechanical injury could be reproduced *in vivo*. By imaging the intracellular calcium in cortical astrocytes after mechanical impact *in vivo* with a 2-photon microscope, we found that mild mechanical injury produced a strong intercellular calcium wave originating from the site of injury. Drug applications to determine the mechanism of calcium wave showed that ATP signaling, and not gap junction coupling among the astrocytes, was responsible for this immediate effect of mild mechanical injury. Next we tested two transgenic animals, each with a different aspect of inhibited astrocyte signaling to determine the effect on TBI recovery. The first transgenic line, VIPP, had an over expression of IP_3 phosphatase and was able to reduce the injury induced

intercellular calcium wave in astrocytes. Reducing IP_3 signaling specifically in astrocytes led to a worse behavioral outcome in a more severe TBI model and no significant difference in the mild TBI model. The second transgenic line, dnSNARE, was used to study the role of inhibited vesicular release from astrocytes. Reducing gliotransmission in this manner improved outcome in both the severe and the mild TBI models. In both cases, baseline behavior did not differ from wildtype littermates suggesting that targeting either pathway may have limited side effects. Histopathologies revealed significant reduction of astrogliosis in both VIPP and dnSNARE injured mice compared to WT. Together these results suggest that injury level can affect the effectiveness of a particular pathway as a therapeutic target and that overall targeting gliotransmission is an effective strategy.

Table of Contents

List of Tables

List of Figures

Chapter 1 Background and Significance

INTRODUCTION

According to the Center for Disease Control (CDC), there are currently 1.7 million new cases of traumatic brain injury (TBI) annually (Faul et al., 2010) with about 75% of these cases being diagnosed as mild (mTBI) (National Center for Injury Prevention and Control, 2003). Typical symptoms include headache, nausea, slurred speech, imbalance, sleep disturbance, and fatigue (Kushner, 1998). Even mTBI sufferers can experience symptoms for years (Signoretti et al., 2010). This is especially true in pediatric populations where there is a higher risk of developing negative psychosocial behavior such as mood disorder and substance abuse later in life (Hamilton and Keller, 2010). Current diagnosis for TBI relies on clinical assessment and neuroimaging techniques. Computed axial tomography (CT), magnetic resonance imaging (MRI), and diffusion tensor imaging (DTI) can help identify intracranial injuries that may require surgical intervention (Andriessen et al., 2010). Once diagnosed however, there is no cure for TBI; the only recourse is rehabilitation. Many of the therapeutic treatments found in animal models have yet to translate clinically (Andriessen et al., 2010). A major reason for this is the limitation of animal TBI models to accurately mimic clinical conditions as well as a suitable therapeutic target.

BACKGROUND

Traumatic Brain Injury – mechanical causation

The most common causes of TBI are from falls followed by motor vehicular accidents (Faul et al., 2010). Head injuries can be categorized into three groups based on the manner of insult loading (Goldmsith, 1972). The first is an impact or blow involving a collision with another object. The second is an impulsive loading causing a sudden change in head motion without direct impact. Sudden acceleration/deceleration loading of a car accident is one such example. The third is static

or quasi-static loading to the head. Generally, contusions and focal injuries are produced by the first type of loading and diffuse injuries are produced by the second.

The mechanical loading to the head results in cellular dysfunction and degeneration stemming from physical damage and chemical overstimulation (Lusardi et al., 2003; Spaethling et al., 2007). Primary brain injury occurs during the moment of impact or loading and can only be prevented through precautionary safety measures. Secondary brain injury is the degeneration resulting from pathological processes that arise from primary injury (Werner and Engelhard, 2007). Much of the subsequent biochemical and behavioral changes after TBI that have been elucidated were done so with a variety of *in vitro* and *in vivo* models.

Animal models of traumatic brain injury

Animal models of TBI have been vital to our understanding of TBI pathology sequelae and behavioral changes. A "good" animal model will be able to capture the biochemical changes and some of the behavioral alterations seen in the human condition. However, there is widespread recognition that no one animal model captures the whole spectrum of human TBI (Cernak, 2005; Gennarelli, 1994; Xiong et al., 2013). Past animal models have focused on specific injury factors such as location and type of damage, injury severity, and time course. The guiding hypotheses in developing an animal model were

> "…(1) human TBI can be duplicated in nonhumans and (2) nonhuman TBI replicates human injury." And "…the assumptions implicit in animal models are (1) that the mechanism of production of the traumatic brain injury is not important and (2) that species differences can be ignored…it may be argued that so long as the end result type of brain injury can be produced, the mechanism by which that injury is produced can be ignored…" (Gennarelli, 1994).

This guiding theme produced many different animal TBI models, involving different species, each replicating a specific injury type. As a result, in many of these models, the manner of inducing was not based on human TBI biomechanics. Here, we will focus on rodent TBI models. These models can be classified into groups based on the mechanism of injury. They are

(1) direct brain deformation, (2) closed head impact, (3) acceleration only, (4) cryogenic injury, and (5) blast injury. However, blast TBI is not a typical civilian injury and the exact biomechanics of loading on the brain is unknown. Therefore blast TBI will not be discussed here.

Direct Brain Deformation Models: There are several animal TBI models where the main mechanism of injury is from direct deformation to the brain. The two most commonly used models are the fluid percussion injury (FPI) and the controlled cortical impact (CCI) models. Other brain injury models that directly deform the brain are the dynamic cortical deformation (DCD) and a penetrating ballistic-like model.

With FPI, a pulse of fluid is used to dynamically deform the cortex through a craniotomy. The severity of injury is controlled through increasing the volume and velocity of the fluid pulse. Initially developed in the rabbit (Lindgren and Rinder, 1966), it has since been adapted for cat (Sullivan et al., 1976), rat (McIntosh et al., 1987, 1989), mouse (Carbonell et al., 1998), pig, dog and sheep (Gennarelli, 1994). Histopathologically, this model generates a number of changes seen in human TBI such as vascular permeability changes, neuronal degeneration, and petechial hemorrhaging[1] (Thompson et al., 2005). Studies into the biomechanics of FPI have shown that most of the strain is localized in the brain stem region (Thibault et al., 1992) which potentially explains the concussion symptoms of FPI (C. Edward Dixon et al., 1987; Gennarelli, 1994; Thompson et al., 2005). A major drawback to this model is the variability in fluid loading (Dixon et al., 1988) among animals even within a single group where the pressure and duration are tightly controlled. This variability makes it difficult for a finite element analysis (FEA) simulation to capture biomechanics in the model limiting further understanding of tissue tolerances. In addition, it makes the resulting behavioral changes in the model more likely to vary compared to other models where the biomechanical loading can be controlled more directly.

[1] Petechial hemorrhage is a form of hemorrhage which causes distinctive petechiae (pinpoint, round spots) markings.

The CCI model was first developed by Lighthall to induce a controlled injury in the ferret that could be simulated with FEA (Lighthall, 1988). This injury model has since been adapted to the rat (Dixon et al., 1991), mouse (Smith et al., 1995), and pig (Manley et al., 2006). A piston driven by compressed nitrogen impacts the cortex exposed by a craniotomy. The speed and depth of impact can be controlled independently, unlike with FPI, to create graded injury severity. A newer version of the CCI that is electromagnetically (EM) controlled was created to reduce the variability of the pneumatically driven device (Brody et al., 2007). The consistent interaction between a solid indenter and the brain, allows for the CCI to be modeled with FEA for both rat and mouse (Mao and Yang, 2011; Mao et al., 2010a, 2010b; Pleasant et al., 2011). These FE models have helped to further understand the CCI generated stress-strain distribution as well as understand tissue tolerances by comparing FE results with injury patterns in the brain.

Two other models directly deform the brain, yet with less precise control. The weight drop model developed by Feeney (1981) involves dropping a weight onto a footplate resting on the cortex. Like the CCI, this model creates mainly focal contusion injuries. Alternatively, the dynamic cortical deformation model (DCD) developed by Shreiber (1998) uses a vacuum pulse through a craniotomy to deform the cortex with the dura removed. Both the vacuum pulse duration and the vacuum pressure can be independently altered to generate a variety of loading conditions. This model determined the *in vivo* threshold for blood brain barrier (BBB) breakdown using the maximum principal logarithmic strain to be 17.2% (Shreiber et al., 1997). It generates a hemorrhagic lesion, glial reactivity, and cell death in the CA1 of the hippocampus, a contrast to the CCI where the neuronal degeneration in the hippocampus occurs in the CA3 (Smith et al., 1995).

The last type of direct brain deformation model is the penetrating ballistic-like brain injury (PBBI) (Williams et al., 2005). This model was created to mimic the permanent injury tract created by a penetrating bullet and the temporary cavity generated by energy dissipation of the

bullet. In this model a probe is inserted into the brain and a balloon is rapidly inflated to mimic the temporary cavity created. This model creates intracerebral hemorrhaging, inflammation, and neurodegeneration (Williams et al., 2005, 2006, 2007).

Closed Head Impact Models: Closed head Injury (CHI) models do not require much pre-injury manipulation, and some cite these models as more clinically relevant than direct deformation models because CHI involve impact to the scalp/skull, often a causative feature of human TBI. Most CHIs employ the use of weights dropped onto the skull, either directly or over a metal plate glued to the head. The Marmarou model uses a weight dropped onto a steel helmet placed over exposed skull (Marmarou et al., 1994). The animal is placed on foam during the injury and the head is allowed to accelerate downward. The Shohami weight drop model for rats (Shapira et al., 1988; Shohami et al., 1988) and mice (Chen et al., 1996; Flierl et al., 2009) uses a metal rod dropped directly onto the skull on one side. The head is placed on a hard surface and not allowed to move during or after impact. This model creates concussion symptoms, contusions, hemorrhages and skull fractures. It has been noted that the Shohami weight drop is not highly reproducible and has a high mortality rate (Albert-Weissenberger and Sirén, 2010). The Maryland model (Kilbourne et al., 2009) modified the traditional weight drop models to produce a frontal impact. A steel ball rolls down a ramp and impacts a coupling arm which is in contact with the malar processes of the rat. The coupling arm prevents direct contact of the steel ball with the rat and eliminates damage to the rat's facial bones. This model creates subarachnoid hemorrhages, concussion symptoms and motor deficits.

Another type of closed head non-acceleration injury model uses the controlled cortical impact device. However, instead of impacting the cortex through a craniotomy, these models impact the skull directly. Creed et al used the pneumatic controlled cortical impact device directly impacting the skull to induce a concussion injury (Creed et al., 2011). Depending on the speed and depth of impact, contusion and skull fracture can occur. Replacing the metal tip of the CCI

device with a silicone tip eliminated skull fractures and contusions creating a milder injury useful for the study of repetitive brain injury. In these studies a single injury produced no long lasting behavioral dysfunction (Bennett et al., 2012; Longhi et al., 2005; Shitaka et al., 2011). A second impact exacerbated both the histopathological and behavioral deficits from the first injury.

Acceleration Only Injury Model: Head acceleration models in the primate (Gennarelli et al., 1982; Ommaya and Gennarelli, 1974; Ommaya et al., 1966) and later in the swine (Ross et al., 1994) are difficult to replicate in the rodent model due to the small size of their brains. Holburn theorized that

> "the level of rotational acceleration required to produce injury in brains with similar properties and shapes is inversely proportional to the 2/3 power of the masses of the brains."(Ommaya et al., 1967)

Therefore to reproduce a similar level of injury in the rodent as seen in human mTBI, much greater the rotational accelerations are needed. However, a rotational acceleration injury model scaled to the rat (Ellingson et al., 2005; Fijalkowski et al., 2007) based on Holburn's scaling laws was successfully created. This model uses a helmet to transfer a linear acceleration into a rotational acceleration; rats are injured in the coronal rotation. Histopathology of the brain showed subarachnoid hemorrhaging and intraparenchymal lesions in most of the mice with no evidence of varicosities in the white matter tracts. Behaviorally, this model did produce concussion like symptoms.

Cryogenic Injury Model: The cryogenic injury model is unlike other TBI models. It uses either a chilled copper cylinder (Rákos et al., 2007; Raslan et al., 2010, 2012) or dried ice (Pifarré et al., 2010) contacted to the cortex or skull to induce a lesion to the brain. The major drawback to this model is that the injury method has no biomechanical relevance to human TBI. It however does produce consistent and reproducible lesions, BBB breakdown, subsequent upregulation of inflammation and gliosis (Albert-Weissenberger and Sirén, 2010).

Astrocytes and TBI

Using the above models allows us to study the role of astrocytes in TBI, a field that has been relatively understudied in the past. This is because astrocytes have historically been viewed as brain "glue" providing only basic and structural support to neurons, the excitable cells. Since the 1990's, this view has taken a drastic turn. As the most abundant cell type in the brain, astrocytes are responsible for a variety of physiological and pathophysiological functions (Agulhon et al., 2008; Laird et al., 2008; Perea et al., 2009; Sofroniew and Vinters, 2010). Combining animal model behavior, histopathology, and FEA, we can start to understand how astrocytes respond to a variety of mechanical insults. This combination of techniques can also allow us to understand the mechanical thresholds and link the biochemical response from a biomechanical input.

Currently we know that after TBI, astrocytes become reactive, characterized by cellular hypertrophy and increased expression of glial fibrillary acidic protein (GFAP), and contribute to the inflammatory response through release of cytokines (Franke et al., 2012). Prolonged, excessive inflammation in the brain has been shown to be a potential driver for neurodegeneration and depression (Hashmi et al., 2013; Paradise et al., 2012; Patki et al., 2013). However, studies that ablated reactive astrocytes in a CCI model resulted in increased lesion due to greater infiltration of inflammatory agents into the penumbra region (Faulkner et al., 2004; Myer et al., 2006), possibly due to the lack of a glial scar to wall off the injured region. Reactive astrocytes are also important in blood brain barrier (BBB) repair. Ablating reactive astrocytes after TBI prevented repair of the BBB and increased vasogenic edema (Bush et al., 1999; Faulkner et al., 2004). Grafting astrocytes from nontransgenic animals into transgenic animals with ablated reactive astrocytes allowed for BBB repair, demonstrating an integral need for reactive astrocytes in TBI recovery (Faulkner et al., 2004). Increased GFAP expression also reduces the elastic modulus of astrocytes, making them softer (Miller et al., 2009). Neurons preferentially grow on softer substrates and an increase in GFAP expression may aid in regeneration after injury.

Astrocytes can also promote degeneration and dysfunction and have been linked to several degenerative diseases. More and more research indicates that astrocytes undergo calcium excitability, releasing signaling molecules in a calcium dependent process called gliotransmission that can modulate neuronal activity (Agulhon et al., 2012; Fellin et al., 2004; Perea et al., 2009). Increased calcium signaling in both frequency and duration has been noted in status epilepticus (Ding et al., 2007), Alzheimer's disease (AD) (Kuchibhotla et al., 2009), and cortical spreading depression (CSD) models (Peters et al., 2003). *In vitro* studies showed astrocytes produce intercellular calcium waves (ICW) in response to stretch (Choo et al., 2013; Miller, 2009). Stretch induced release of extracellular adenosine triphosphase (ATP) from astrcoytes contributes to neuronal death after injury. Treatment with apyrase reduced ICWs, GFAP expression to naïve levels (Miller et al., 2009), and subsequent degeneration (Choo et al., 2013; Miller, 2009). The initial ICWs induce further release of ATP and glutamate from astrocytes, enhancing excitotoxicity. Inhibition of the purinergic receptors have been shown to be neuroprotective *in vitro* and *in vivo* and improved functional outcome (Choo et al., 2013; Miller, 2009). Blocking the calcium wave specifically in astrocytes with BAPTA-AM also provided a similar level of neuroprotection (Choo et al., 2013; Miller, 2009).

SUMMARY OF CHAPTERS

The goal of this dissertation was to determine the effect of astrocytic calcium signaling on the recovery of TBI *in vivo*. To achieve these research goals, we first looked at the biomechanics of the different animal TBI models. We adapted an existing injury model to better mimic the biomechanics of mild TBI in humans (Chapter 2). We next verified if past *in vitro* findings with astrocytes and stretch injury could be validated *in vivo* (Chapter 3). Using this new and preexisting model of TBI, we tested two transgenic mice lines each with reduced astrocytic signaling and studied their recovery (Chapter 4 and 5). The overall hypothesis is that

gliotransmission (rapid and regulated exocytosis of gliotransmitters by astrocytes in a calcium-dependent manner, (Agulhon et al., 2012)), is a source of excitotoxic factors that contribute to neuronal death post TBI and that blocking this response will improve outcome.

In chapter 2, we adapted the CCI brain injury model and used parameters that would produce the same injury biomechanics found in human mild TBI in the mouse. In the past, animal TBI models especially rodent models strived towards replicating specific injury types. Although all models cite that injury is created by a mechanical event and that species differences were assumed to be negligent, our review and analysis of common CCI conditions indicate the use of impact speeds that produce strain rates in the mouse that are twenty to eighty times higher than strain rates found in human TBI. Slowing down the impact speed and changing the material of the impactor tip allowed us to create a non-hemorrhagic injury and transient behavioral deficits. Biomechanically and symptomatically, the modified CCI created an injury that is consistent with human mild TBI.

In chapter 3, we adapted the mechanism of the newly developed mild TBI model and made it possible to perform *in vivo* imaging during injury. We showed that strain induced injury does cause an astrocytic calcium wave *in vivo*. Purinergic signaling was the dominant pathway in the production of this pathophysiologic calcium signaling. Past *in vitro* research also showed that purinergic signaling was a dominant pathway in the propagation of calcium signaling after stretch.

Once we validated *in vitro* findings *in vivo*, we were able to proceed with further *in vivo* studies. In chapter 4, VIPP transgenic mice were subject to both traditional and modified CCI. With the traditional CCI, VIPP mice performed worse in a hippocampal dependent task on day 7. There were no behavioral differences in the more immediate time points. This worse outcome was unexpected and did not support our hypothesis. There was less GFAP expression with VIPP injured mice than with WT littermates; however, there was no increased lesion volume. With the modified CCI, behavioral deficits were less apparent in VIPP mice than WT suggesting that the

difference in injury mechanism may affect subsequent biochemical pathways, highlighting the importance of accurately modeling injury mechanics.

In chapter 5, dnSNARE transgenic mice were subjected to both traditional and modified CCI. With the traditional CCI, dnSNARE mice overall performed no differently than WT littermates except on day 7 in the watermaze. They did also have a slightly improved rate of spatial learning. There was less GFAP expression in the dnSNARE mice and no difference in lesion volumes. When subject to the modified CCI, dnSNARE mice showed significant behavioral improvement over WT mice. In the rotarod, dnSNARE injured mice had the same latency times as dnSNARE and WT sham mice.

Finally, Chapter 6 provides a summary of the important findings discovered throughout this research. It highlights some of the limitations, overall conclusions, and future work that could improve our current understanding.

Chapter 2 Modifying the Controlled Cortical Impact Based on Mild TBI Biomechanics in Humans

ABSTRACT

For the past 25 years, controlled cortical impact (CCI) has been a useful tool in traumatic brain injury (TBI) research, modeling injury patterns that include primary contusion, neuronal loss, and traumatic axonal damage. However, when CCI was first developed very little was known about the underlying biomechanics of mild TBI. This paper seeks to use the information generated from recent computational models of mild TBI to alter the CCI technique to better reflect the biomechanical conditions of mild TBI. We adjusted three primary features of CCI: the speed of the impact to achieve strain rates within the range associated with mild TBI, the shape and material of the impounder to minimize strain concentrations in the brain, and the impact depth to control the peak deformation that occurred in the cortex and hippocampus. With these modified cortical impact conditions, we observed breakdown of the blood-brain barrier (BBB) but no primary hemorrhage. Moreover neuronal degeneration, axonal injury, and both astrocytic and microglia reactivity were observed up to 8 days after injury. Significant deficits in rotarod performance appeared early after injury. We observed no impairment in spatial object recognition or fear conditioning response 5 days and 8 days after injury. Together, these data show that simulating the biomechanical conditions of mild TBI with a modified cortical impact technique produces regions of cellular reactivity and neuronal loss that coincide with only a transient behavioral impairment.

INTRODUCTION

Traumatic brain injury (TBI) is a significant public health problem. Of the 1.7 million people diagnosed with TBI, about 75% of them are considered to have experienced mild (mTBI) (National Center for Injury Prevention and Control, 2003). Although most mTBI patients do not have long term impairments (Dikmen et al., 2001), approximately 15% may experience symptoms for years, and these persisting deficits are a major contributor to the morbidity associated with the disease (Hamilton and Keller, 2010; Signoretti et al., 2010). Current diagnosis for TBI relies on clinical assessment (Malec et al., 2007; Saatman et al., 2008; Teasdale and Jennett, 1974); neuroimaging techniques such as computed axial tomography (CT), magnetic resonance imaging (MRI), and diffusion tensor imaging (DTI) are all used to better detect structural and functional changes in TBI patients (Bigler and Maxwell, 2012; Le and Gean, 2009; Lee and Newberg, 2005). Diagnosis for mTBI in particular is more difficult than either moderate or severe TBI, due in part to the rapid recovery of symptoms and the lack of a universal definition (McKinlay, 2010; Powell et al., 2008; Ruff et al., 2009; Yeates, 2010). However, once diagnosed, there are very few treatment options outside of rehabilitation as successful pre-clinical treatments have yet to translate to the clinical population (Beauchamp et al., 2008).

Creating an experimental model to reproduce faithfully human mTBI is challenging, yet can offer an important new tool to study mTBI in the laboratory. With differences in the anatomy, functional organization, and phylogenic development, no one experimental model in a single species can fully capture human mTBI. Past animal models of TBI often reproduced specific brain injuries observed, such as contusions, acute subdural hematoma, and diffuse axonal damage (Duhaime et al., 1994; Gennarelli, 1994; Lighthall, 1988; Lindgren and Rinder, 1966; Marmarou et al., 1994; Rinder, 1969; Ross et al., 1994; Shreiber et al., 1999; Sullivan et al., 1976). These injury techniques were used to model mild TBI by adjusting the input parameters (eg, shallower

impact depth, smaller fluid pulse, smaller weight dropped) or by altering the methodology to create closed head impact models (Bennett et al., 2012; Creed et al., 2011; Huh et al., 2007; Longhi et al., 2005; Shitaka et al., 2011; Spain et al., 2010; Ucar et al., 2006). A critique for this manner of adaptation is that for some models, a smaller load or shallower impact depth, biomechanically does not equate to generating an mTBI injury. This is because while a smaller load may reduce the volume of damage, the type of injury produced is less consistent with the bulk of mTBIs seen in humans.

In the past 10 years, biomechanics research successfully coupled finite element (FE) analyses (FEA) to existing TBI models and human accident reconstructions to produce a more detailed picture of the *in vivo* mechanical loading associated with concussions. (Levchakov et al., 2006; Ruan et al., 1994; Viano and Pellman, 2005; Viano et al., 2005, 2007; Ward and Thompson, 1975; Willinger et al., 1999) These computational models analyzed the relationship between mechanical stress/strain and resulting structural/functional damage to tissue(Bain and Meaney, 1999, 2000; Bayly et al., 2006; Elkin and Morrison III, 2007; Margulies and Thibault, 1992; Margulies et al., 1990; Meaney and Thibault, 1990; Morrison III et al., 2000, 2003, 2006; Pfister et al., 2003; Rashid et al., 2012; Shreiber et al., 1997; Singh et al., 2006) to provide estimates on injury volume, and injury thresholds based on strain and strain rate for specific loading conditions(Dokko et al., 2003; Kimpara and Iwamoto, 2012; Kleiven, 2007; McAllister et al., 2012; Ruan et al., 1993; Viano et al., 2005; Zhang et al., 2004). In parallel, physical models of the brain also offered estimates of the tissue biomechanics associated with injury in the white matter (Margulies and Thibault, 1992; Margulies et al., 1990; Meaney et al., 1995). Among rodent mTBI models, strain rates of fluid percussion (FPI) and the dynamic cortical deformation (DCD) injury models have similar ranges estimated in human mTBI (Shreiber et al., 1999; Thibault et al., 1992; Zhang et al., 2004) (Figure 2.1). Closed head injury (CHI) rodent models may also yield strains and strain rates in the range of human TBI (Albert-Weissenberger et al., 2012; Chen et al., 1996;

Creed et al., 2011; Ellingson et al., 2005; Feeney et al., 1981; Fijalkowski et al., 2007; Kilbourne et al., 2009; Longhi et al., 2005; Marmarou et al., 1994; Shohami et al., 1988). The biggest drawback to FPI and CHIs is that FE analyses of these models are difficult. Only recently was the foam used in the Marmarou weight drop test modeled (Zhang et al., 2011). And translating the FPI to a computational model is difficult because of variability in fluid loading at the dural surface (Dixon et al., 1988). While DCD has been simulated and used for other 3D FE model validation (Lamy et al., 2013; Mao et al., 2006; Shreiber et al., 1997), this method of injury induces hemorrhage in the shape of the craniotomy, likely from the bone cutting into the cortex

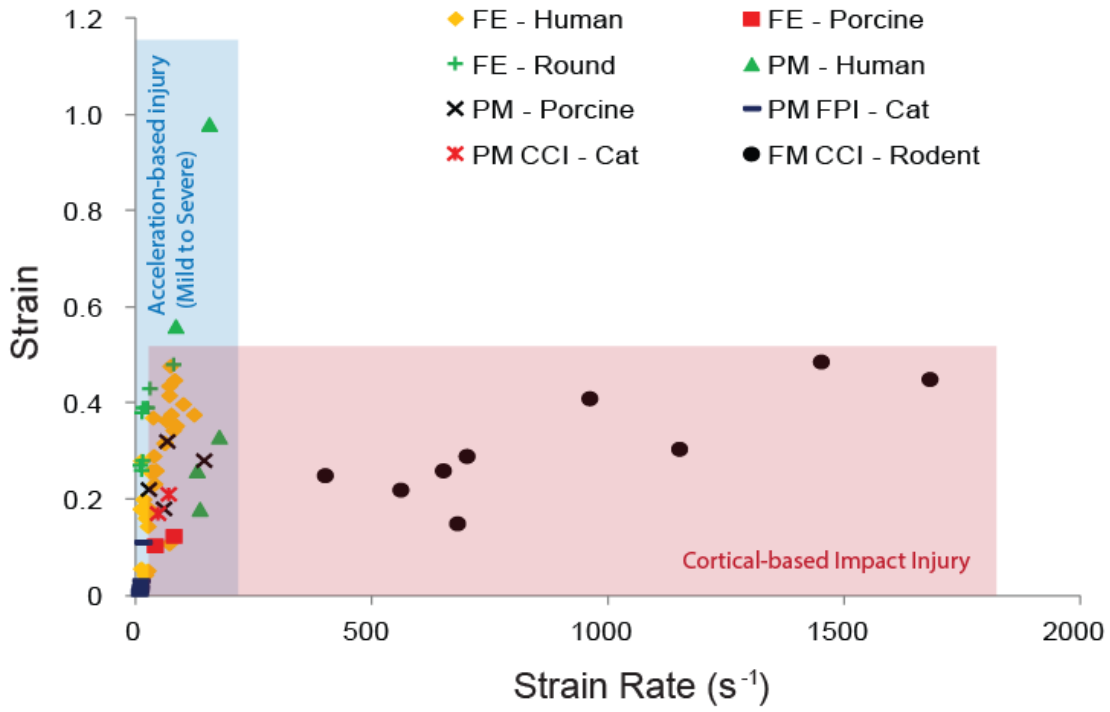

Figure 2.1. Comparison of strains and strain rates in human and animal TBI models. References used: FE-Human (Cloots et al., 2012; Ho and Kleiven, 2007; Kleiven and Hardy, 2002; McAllister et al., 2012; Viano et al., 2005; Zhang et al., 2001, 2002, 2003); FE-Round (Yoganandan et al., 2008); FE-Porcine (Miller et al., 1998); PM-Human (Meaney and Thibault, 1990); PM-Primate (Margulies et al., 1990); PM-Porcine (Meaney et al., 1995); FE CCI-Rodent (Mao et al., 2006, 2010a); PM CCI-Cat (Meaney et al., 1994); PM FPI-Cat (Thibault et al., 1992). FE = Finite Element; PM = Physical Model.

during the vacuum pulse. A coronal rotational head injury in the rodent that uses accelerations scaled from human TBI was created and simulated in a 2D FE model (Fijalkowski et al., 2007, 2009). However, this diffuse brain injury (DBI) model failed to show axonal histopathological changes that are considered the hallmark for human mTBI; over 50% of the animals had hemorrhaging and lesions, pathologies that are not typical of mTBI.

The bulk of rodent TBI FEMs are of CCI (Levchakov et al., 2006; Mao et al., 2010a, 2010b; Peña et al., 2005). However, CCI loading conditions do not generate similar biomechanics to human TBI. Currently, even at slower speeds, CCI produces strain rates of $400s^{-1}$ and over (Mao et al., 2006), well over the higher strain rates of moderate to severe human TBI (Figure 2.1). At more typical CCI speeds, the cortex sees strain rates in the range of $1150\text{-}1450s^{-1}$ (Mao et al., 2010a). Therefore, we revisited the biomechanics of traditional rodent CCI and altered it to produce injury conditions in the rodent that better approximate the loading seen in human mTBI. In addition, it was important that the injury would induce no hemorrhagic contusions in the cortex, a common injury in cortical impact models but rarely observed in human mTBI (Alexander, 1995). Finally, it was important to use impact conditions that generated a measurable behavioral impairment.

To achieve these three design criteria, the impact velocity was reduced to achieve tissue strain rates more consistent with mild TBI, the cortical impact tip was modified to distribute the strains throughout the cortex, and the impact depth adjusted (Figure 2.2A-C). CCI was selected over FPI because the biomechanics of the loading are more directly controllable. With CCI, we can alter strain rate independently from strain by changing the parameters of the injury. In this study, the combination of reducing impact velocity (strain rate) while maintain impact depth (strain) changes the morphology of the injury to include blood brain barrier (BBB) opening, glial reactivity, neuronal degeneration and microglial activation without significant hemorrhage and lesions often associated with cortical impact. Moreover, this modification achieves a slight, but

temporary, behavioral deficit. The improved biomechanical fidelity of this model now provides a new tool to determine the tissue tolerance criteria associated with neuronal and glial changes in the brain after mTBI, as well as a scientific tool to compare the effects between a hemorrhagic and nonhemorrhagic injury.

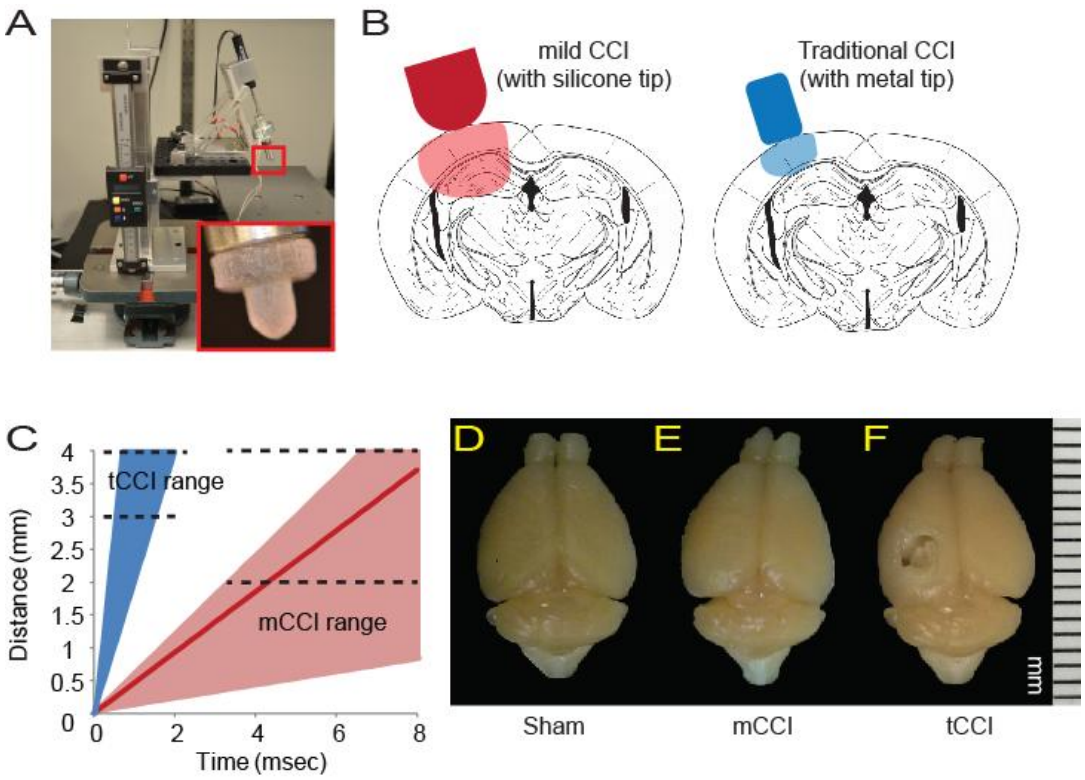

Figure 2.2. Parameters of mild CCI.
The mild CCI (mCCI) uses a hemi- spherical silicone tip, actuated by a solenoid (A). A potentiometer was used to measure the displacement of the impactor. The angle of the impactor and the height of the impactor are adjustable. A comparison of displaced tissue volume between mild CCI (2mm impact depth) and traditional CCI (1mm impact depth) is shown in B. C shows the range of impact speeds between tCCI (2.0 -6.0m/s) and the velocity range that would generate clinical TBI strain rates ($17s^{-1}$ – $104s^{-1}$ for 0.1 -0.6m/s respectively). The red line is the impactor speed used in this study (0.43m/s for a strain rate of $80s^{-1}$). Brains perfused 8 days after a sham injury (D), mCCI with 2mm impact depth (E), and tCCI with an impact depth and speed of 1mm and 6.0m/s respectively (F).

METHODS AND MATERIALS

Modified CCI (mCCI) device

The traditional CCI (tCCI) model scaled down to the mouse as first described by Smith et al (1995) produces a focal contusion and hemorrhage, symptoms more normally associated with moderate to severe TBI cases. This model generates reproducible, graded injury that is amenable to FEA. For these reasons, the pneumatic CCI device was improved upon and a electromagnetic (EM) version was created (Brody et al., 2007). However, the electromagnetic version uses similar speeds and creates similar injury profiles. We sought to increase the injury spectrum of CCI to explore mild TBI injuries. The mCCI model has very many similarities to tCCI (Figure 2.2A). Two main differences are the use of a rounded silicone tip (4mm in diameter; tip was made by injecting Sylgard 184 – mixed and vacuumed – into a 3-D printed mold; Figure 2.2A insert) and a slower impact speed (Fig 2B, C).

To reproduce a mild injury in the rodent, we sought to replicate the lower strain rates seen in clinical mTBI. A pneumatic CCI and the electromagnetic CCI produced first described by Brody et al 2007 have similar velocity ranges of 1.5 to 6.0m/s. At these speeds, a deformation of 1-3mm on tissue will have strain rate ranging over $400s^{-1}$ (Mao et al., 2006). These are much higher than those seen in mild TBI which range from $23s^{-1}$ to $140s^{-1}$ (Zhang et al., 2003). Studies with physical models have shown strain rates between $10s^{-1}$ to $50s^{-1}$ to be injurious (Figure 2.1).

Therefore to scale mTBI strain rates to a mouse required velocities well below tCCI ranges. The mCCI velocity uses an impact velocity that is one-tenth of those used in tCCI (0.2-0.6m/s versus 2.0 – 6.0m/s, Figure 2.2C). The actual impact speed of the solenoid used in this study is the line in red at 0.43m/s (Figure 2.2C; the solenoid has a retraction velocity of 0.20m/s; SoftShift 2EPM, Ledex, USA), producing during the 2mm impact a calculated 14ms tissue displacement duration (not including the dwell time). Bayly et al (2006) showed that a 0.34m/s

impact velocity produced strain rates of around $40s^{-1}$ in rat pups. A linear potentiometer (LP803-1, Omega, USA) measured the actuation of the solenoid and a custom Matlab (Mathworks, MA, USA) program controlled the solenoid and collected the potentiometer readings. The angle of the impactor was set to 20° from vertical (measured with a digital angle meter), similar to other lateral CCI models.

It is important to note that dwell times are a byproduct of the response times of electromechanical devices. As the effect of varying dwell times on injury have not been studied, it was important to maintain a similar dwell time to those seen in literature. In this study the dwell time used was consistently around 72.6ms with an overshoot of 0.19mm. These parameters were within the dwell time ranges (25ms to 250ms) for rodent CCI as cited in the literature (Cernak, 2005). The overshoot from the solenoid increases the actual impact depth slightly, however, this overshoot is not larger than the pneumatic or electromagnetic CCI (Brody et al., 2007). The variability of overshoot from the solenoid did not vary as this was determined by the physical stroke length of the solenoid.

For simplicity, only one impact velocity was used in combination with one impact depth. This study uses a 2mm impact depth; 1mm failed to generate measurable behavioral deficits and 3mm caused hemorrhaging upon impact (data not shown). The approximate resulting strain rate for a 2mm impact depth with this solenoid is $80s^{-1}$. We replaced the rounded cylindrical 3mm metal tip with a custom made silicone, hemispherical tip of 4mm diameter. The larger impact diameter and increased impact depth creates a larger volume of injury (Figure 2.2B). Despite the larger injury volume, the slower strain rates used did not result in a necrotic lesion, a contrast from tCCI (Figure 2.2D-F).

Cortical Injury

All animal procedures were approved by University of Pennsylvania's Institutional Animal Care and Use Committee (IACUC). Sixty C57Bl6 mice (Jackson Laboratory, Maine, USA) were divided into sham and injured for three different time points: a one hour time point to determine extravasation (sham=3, injured n=6); 24hr time point to determine early neurodegeneration (sham n=5, injured n=10 each); 8 day time point to determine longer term behavioral and histopathological changes (sham n=17, injured n=19).

On the day of injury, mice were anaesthetized with isoflurane (5% induction, 2% maintenance) and placed in a stereotaxic frame. A 4-mm diameter craniotomy was produced on the left hemisphere, midway between bregma and lambda. CCI injuries were produced with a modified impactor at a speed of 0.43m/s to a cortical impact depth of 2mm (Figure 2.2B,C). The estimated center of the impact was -2.5mm bregma. The solenoid has a full stroke length of 4mm. The baseline point was set by lowering the impactor tip to the cortex with the solenoid in the fully actuated position and the linear stage position set to zero. Once baseline was set, the impactor was retracted and the impact depth was adjusted using 1.0mm shims. After injury, the cranial exposure was sutured closed and the animals were placed in a warmed cage to recover until ambulatory.

Histology

Mice were anaesthetized with an overdose of sodium pentobarbital. Animals were transcardially perfused with 30ml of ice-cold phosphate buffered saline (PBS) (pH 7.4) and then with 40mls of ice-cold 4% paraformaldehyde. Brains were harvested, post-fixed overnight in 4% paraformaldehyde at 4°C and then cryoprotected in 24% sucrose. Brains were mounted in Tissue-Tek® and frozen in isopentane cooled with dry ice. Brains were cryosectioned at 20 μm. Sections

were taken 500µm apart starting from bregma -1.5 to -3.5 mm, therefore spanning the entire injury area.

Blood brain barrier compromise: For identification of extravasation, animals were injected with Evans blue (EB, 100µL of 4%) 15min prior to the injury or sham surgery. One hour post injury, animals were perfused. Brains were removed, post-fixed, cyroprotected, and frozen. Equally spaced, serial tissue sections of the brain were mounted on slides and rinsed several times in phosphate-buffered saline (PBS). The slides were coverslipped with ProLong Gold (Invitrogen, USA; #P36934). Sections were imaged with a Leica SP5 confocal microscope (Leica, Germany). The same laser settings were used with all sections.

Neuronal degeneration: Fluoro-jade® B (FJB) labeling detected degenerating neurons. Histological sections were rehydrated in graded ethanols (100%, 95%, 80% 70%; 2 min each) followed by distilled water. They were then incubated in a solution of 0.06% potassium permanganate on a rotating stage for 20 min. The sections were then rinsed in distilled water for 2 min and placed in fresh 0.0005% FJB solution made by adding 5mL of a 0.01% stock solution of FJB to 95 mL of 0.1% acetic acid. After 30 min in the FJB staining solution, the sections were rinsed through three changes of distilled water for 1 min per change. Excess water was drained onto a paper towel, and the sections were then air dried in an oven at 37° for 30 min. The dry sections were cleared by immersion in xylene for at least 2 minutes before coverslipping with permount (Fisher Scientific, USA). The sections were viewed with a Leica SP5 confocal microscope (Leica, Germany).

Astrocyte and microglial reactivity: Sections were rehydrated in 1×PBS (3x 5min) and then incubated with 10% normal goat serum for 30 mins with 0.1% triton-X. To measure astrocyte reactivity, sections were incubated overnight at room temperature in polyclonal anti-GFAP (Neuromics, MN, USA; #CH22102; 1:500). Microglial reactivity was assessed using the polyclonal anti-Iba-1 (Wako, VA, USA; #019-19741; 1:1000). After rinsing with 1×PBS,

sections were then incubated with Alexa 546 conjugated secondary antibodies (Invitrogen, USA; #A-11035; 1:250) for 1hr at room temperature. Sections were mounted with ProLong Gold antifade (Invitrogen, USA; #P36934).

Axonal injury: Sections were dried and washed in 0.1M TBS for 5 minutes. Sections were heated in 10mM sodium citrate at 75°C for 30 minutes and allowed to cool to room temperature. Endogenous peroxidase activity was blocked with incubation in 3% hydrogen peroxide in methanol for 30 minutes with shaking. Sections were rinsed with running water for 10min, after which they were placed in blocking buffer (0.1M TBS and 2% FBS) for 5 minutes before blocking with 10% NGS for 30 minutes in 0.1M TBS with 0.2% Triton-X. This was followed by overnight incubation at 4°C with anti-APP (Invitrogen, USA; #36-3900; 1:1000). Sections were washed in 0.1M TBS, placed in blocking buffer and then incubated in biotinylated goat anti rabbit secondary (Jackson Labs,#111-065-003; 1:250). Sections were washed and placed in blocking buffer again prior to incubation in Elite ABC (Vectastain, CA, USA; #PK-6100) for 30 minutes. Sections were washed and incubated in DAB (Vectastain, CA, USA; #SK-4100) for 5min. Sections were washed in running water for 5 minutes and stained with Hematoxylin for 30 seconds. Sections were washed, dehydrated (alcohol 70%, 80%, 95% 2x, 100% 2x, xylene 2x) and coverslipped in Permount.

Behavior Tests

A series of behavior tests were conducted in the order that placed the test that required the least of amount of mouse handing first and the most stressful test last. The behavior schedule is listed in Table 2.1. The rotarod training was conducted the day before the injury. On the day of injury, no behavioral test was given. On days 1 – 3 after injury, mice were tested on the rotarod; on days 4 – 5, mice were tested on the spatial object recognition (SOR), on days 7 – 8; mice were trained and tested in contextual fear conditioning (CFC).

Table 2.1. Behavioral Schedule

Day -1	Day 0	Day 1	Day 2	Day 3	Day 4	Day 5	Day 6	Day 7	Day 8
RR training	Injury	RR	RR	RR	SOR	SOR		CFC	CFC

Cortical motor function: The rotarod protocol was adapted from Oliveira et al 2011 (Oliveira et al., 2011). In short, the rotarod apparatus (Med Associates Inc, VT, USA) has a 3.2 cm diameter rotating rod raised 16.5 cm above a platform and divided into five sections for testing multiple mice simultaneously. The rotarod gradually increased its rotation speed from 4 to 40 rpm over the course of 5 minutes. Latency to first fault (defined as the mouse riding with the platform in a single rotation) and fall time was recorded. Mice were trained on the rotarod at 4 rpm for 60 seconds one day before injury. Three trials a day were given during three consecutive days with an inter-trial interval of 1 hour. Each trial started at the same time every day and ended when mice fell or when mice ran for 300 seconds.

Hippocampal function: The SOR protocol was adapted from Oliveira et al (2010). In short, the experimental apparatus consisted of a gray rectangular open field (60 cm × 50 cm × 26 cm) with a visual cue placed on the arena wall. Prior to training, mice were handled for 1 minute per day for 3 days. During the training day, mice received four 10 minute training sessions. Between sessions, mice were placed back in their home cage for 3 minutes. During the first session, mice were habituated to the gray rectangular open field in the absence of objects, but with an internal cue on one of the four walls. For the next three sessions, mice were placed in the same box but now with two distinct objects. The objects consisted of a glass bottle (100 mL volume) and a metal tower (1.5625 square inches). Mice were allowed to freely explore the environment and the objects for 10 minutes. Mice that climbed the objects were eliminated from behavioral analysis. After 24 h, mice were placed back in the rectangular environment for testing. The two objects were again present, but one of the two objects was now displaced to a novel

spatial location. Mice were again allowed to freely explore the environment and the objects for 10 minutes. Both the object identity and spatial location was balanced between subjects. The response to changing the spatial location was assessed by comparing the mean time the mice spent exploring the objects (when mice were facing and sniffing the objects within very close proximity and/or touching them) belonging to each category (displaced and non-displaced) in the test session minus the mean time spent in contact with the same object category in the last training session. A positive value indicates recognition of the spatial change.

In the CFC test, mice were placed in a testing chamber (Coulbourn, PA, USA) on training day for 3 minutes. Two minutes and 28 seconds after mice were placed into the testing environment, mice were given a single 2 second, 1.5mA shock. Twenty four hours later, mice were place in the same testing chamber and their percent freezing was calculated across the course of 5 minutes.

Statistical Analysis

All statistical tests were carried out using JMP10. The variance among groups was first tested for normality (Shapiro-Wilks test) and then equality (Bartlett test). When the variance among groups was not similar, the two sample t test was used, otherwise a one way analysis of variance (ANOVA) was used. A linear regression model was used to look for significance between injured and uninjured groups. A repeated measures ANOVA was used in the rotarod behavior test.

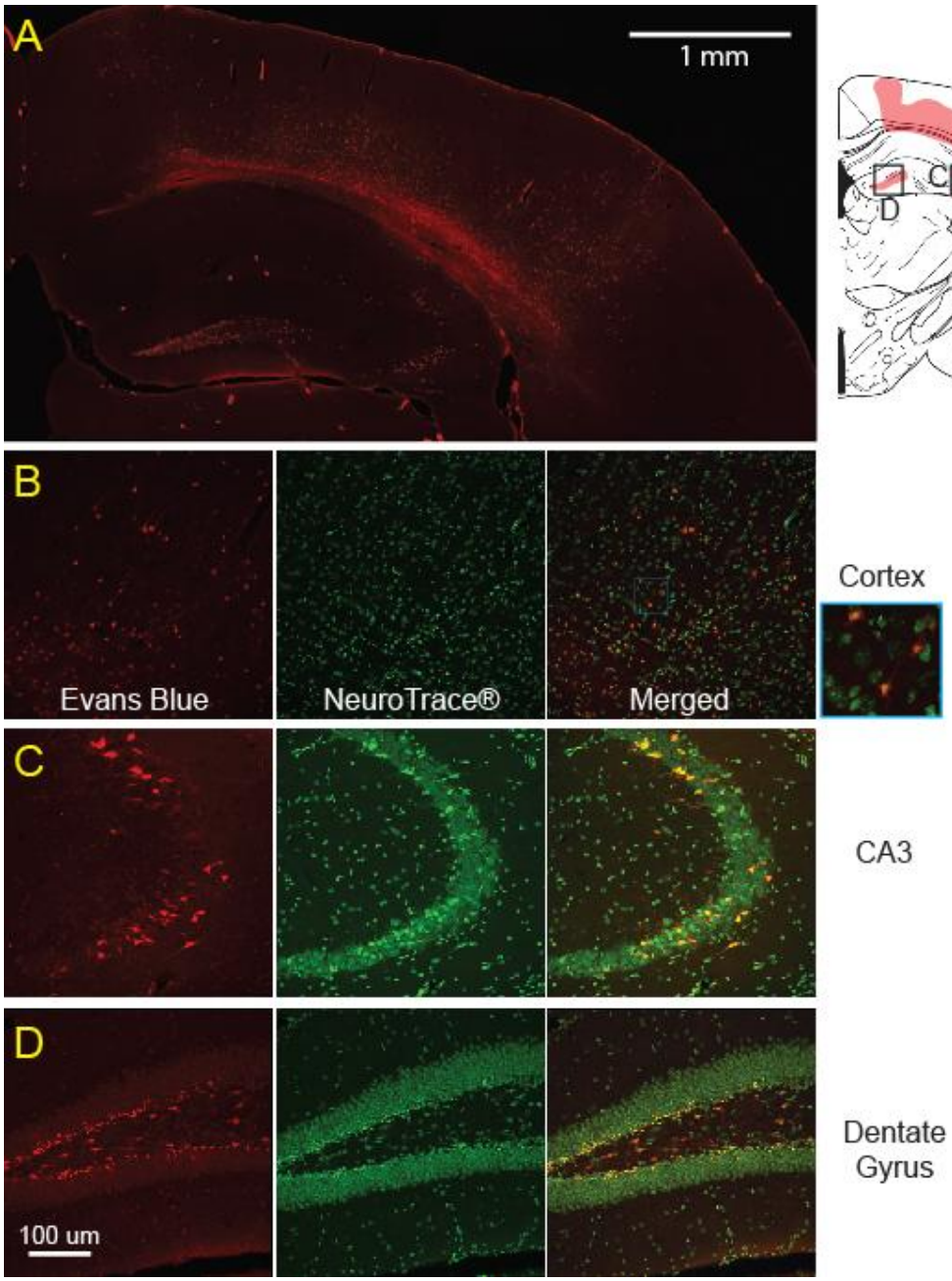

Figure 2.3. mCCI induces extravasation of the blood brain barrier (BBB) at the injured region.
The pattern of extravasation is shown and pictorially depicted (A). Co-labeling of EB and Neurotrace® for the cortex (B), CA3 (C) and dentate gyrus (D) show that the EB positive cells are mostly neurons.

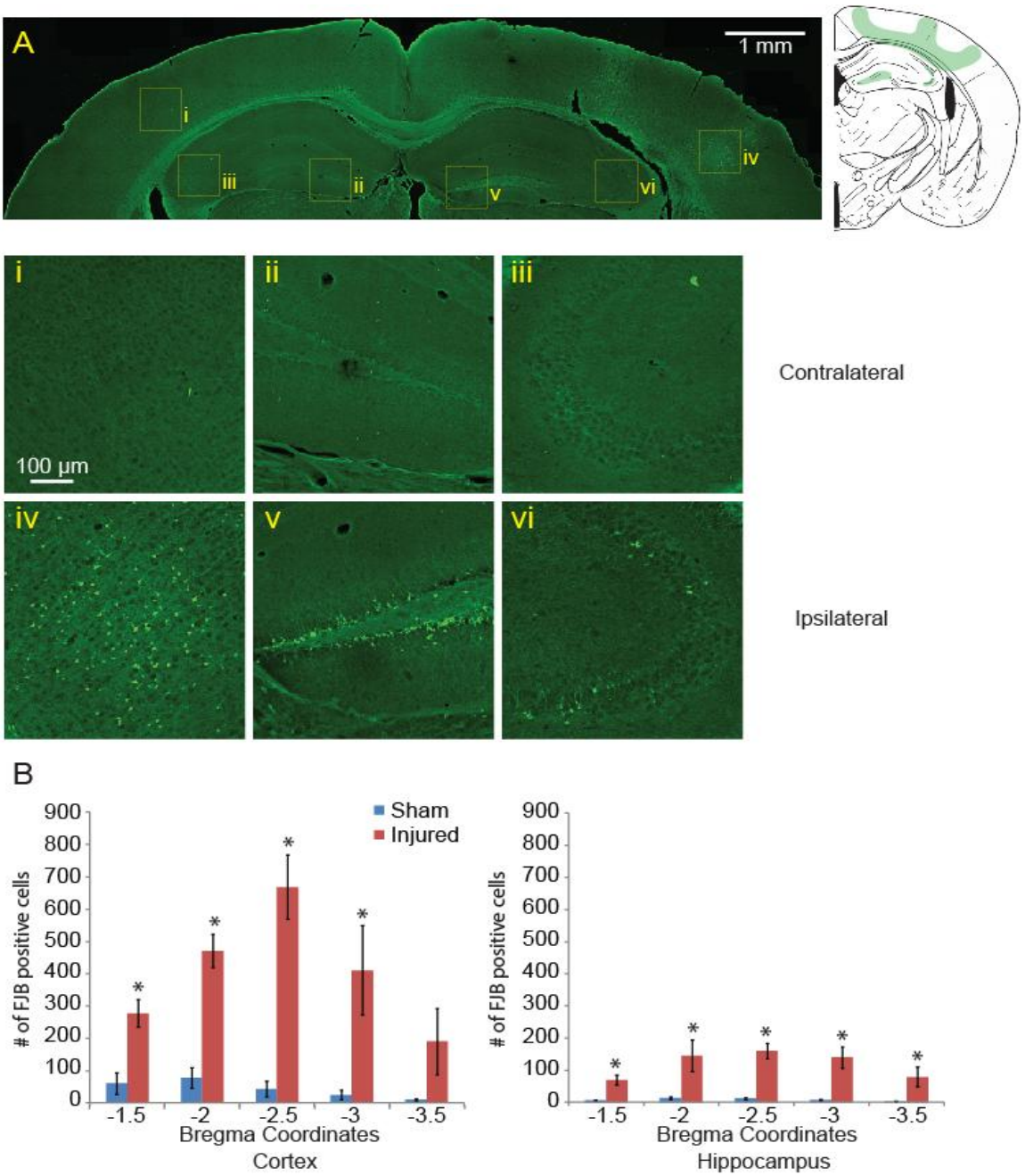

Figure 2.4. Degeneration at 24hr after injury shows a FJB staining pattern that was similar to the EB staining.

FJB positive cells in the cortex (iv), dentate gyrus (v), and CA3 (vi) on the ipsilateral side was not seen on the contralateral side (i, ii, iii, respectively) (A). (B) The number of FJB positive cells in injured animals was significantly increased compared to sham in both the cortical and hippocampal regions for bregma sections -1.5 to -3.0 (cortex $p<0.001$ for each section -1.5 to -3.0, for section -3.5 $p=0.0635$; hippocampus $p=0.0113$ for section 1.5, $p<0.001$ for sections -2.0 to -3.5; n=5 sham, n=10 injured).

RESULTS

mCCI induces blood brain barrier extravasation

The modification of the CCI technique produced little to no visible lesion and no visible hemorrhaging immediately after impact, but Evans Blue (EB) staining appeared throughout the lesion site (Figure 2.3A). In the cortex there was an approximate hemispherical pattern of EB staining in all animals, and there was a higher concentration of EB at the subcortical white matter directly below the impact site. No EB staining appeared in the region of cortex that was in direct contact with the impactor, consistent with no visible hemorrhage after injury. In the hippocampus, the dorsal CA3 region (stratum pyramidal) and the dentate gyrus (some staining seen in the granular but most staining occurred in the polymorphic layer) also showed EB staining. All animals subject to injury had EB loading in the dentate across all five bregma sections analyzed. However staining in the CA3 was only visible around bregma -1.5 and -2.0. No EB staining was seen in any of the sham animals (supplemental figure) or on the contralateral side.

At higher magnification, many of the cells in these regions were labeled positive for EB. Upon first inspection, it would seem likely that the EB positive cells were astrocytes due to the physical connection between astrocytes and vasculature (Abbott et al., 2006). However, triple labeling with glial fibrillary acidic protein (GFAP), Neurotrace™, and EB showed that across all regions of interest (cortex, dentate gyrus, and CA3), a majority of EB stained cells were neurons (Figure 2.3B-D). Together, these data demonstrate that EB-labeled albimun that extravasates from the injured vasculature was preferentially taken up by neurons.

mCCI induces neurodegeneration patterns that matches the EB patterns and persist for at least 8 days after injury

One day after injury, FJB staining showed a similar pattern to the EB staining (Figure 2.4A i-vi), with a hemispherical degeneration pattern reminiscent of the EB pattern. In comparison, the

cortical surface in direct contact with the impactor had no FJB staining. Elevated FJB staining in the subcortical white matter appeared directly below the impact site. In the hippocampus, similar to the EB staining patterns, there were FJB positive cells in CA3 regions (stratum pyramidal) in bregma sections -1.5 and -2.0 but not in subsequent sections (Figure2.4Avi). Staining in the dentate gyrus was apparent in all five bregma sections analyzed with the staining localized more to the polymorphic layer (Figure 2.4Av). While FJB is noted to stain degenerating neurons, it has been shown to co-label with astrocytes (Anderson et al., 2003). Therefore sections were triple labeled with GFAP, FJB, and a fluorescent nissl stain to determine which cell type(s) were FJB positive (Figure 2.5). All FJB positive cells were positive for the nissl stain and not GFAP. There was little to no FJB stained positive cells in the sham and on the contralateral side (Figure 2.4A i-iii). In the sections imaged across the lesion, most showed significant levels of FJB positive cells between sham and injured animals (Figure 2.4B). Sections -1.5 to -3.0 showed significant FJB positive cells for both the cortex and hippocampus (cortex $p<0.001$ for each section -1.5 to -3.0; hippocampus $p=0.0113$ for section 1.5, $p<0.001$ for sections -2.0 to -3.5). For section -3.5, the cortex trended towards significance at $p=0.0635$.

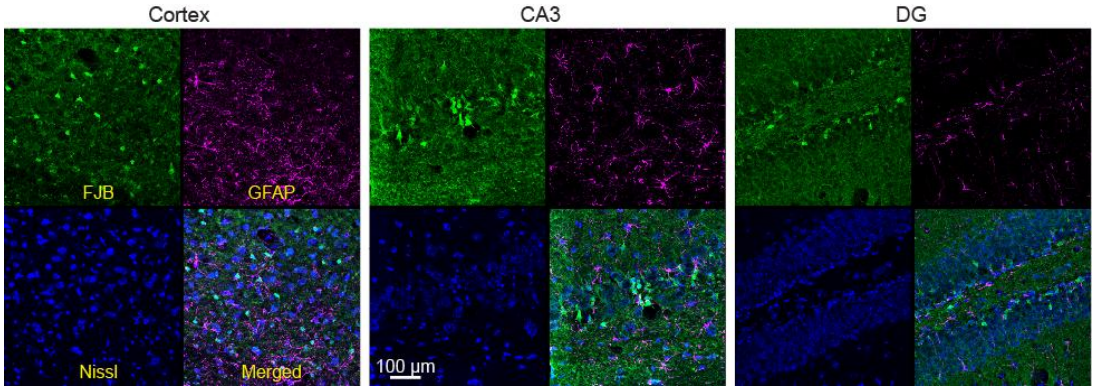

Figure 2.5. FJB, GFAP, Nissl triple label
In all regions examined – cortex, CA3, and dentate gyrus (DG) – the FJB colabeled with the fluorescent Nissl stain and not GFAP.

Neurodegeneration indicated with FluorJadeB (FJB) staining was sustained 8 days post injury, although reduced in number relative to 24 hour labeling. Although the level of positively stained cells in the cortex was reduced (Figure 2.6A), the pattern of FJB positive cells was still similar to that seen in at the 24hr time point. The number of FJB positive cells in injured brains remained significantly elevated compared to sham controls (for cortical degeneration, Figure 2.6Ai,ii,B, $p<0.001$ for all sections). Neuronal degeneration in the CA3 and the dentate gyrus was also significantly higher compared to sham (Figure 2.6Aiii,iv,C, bregma -1.5=0.0105, -2.0 p=0.0018, -2.5 p= 0.0102, -3.0 p=0.0058, -3.5 p=0.0338). Moreover, a new area of significant labeling appeared in the thalamus at this time point (Figure 2.6Av,vi,D, bregma -1.5 p=0.0024,-2.0 and -2.5 $p<0.001$, -3.0 p=.0081, -3.5 p=0.0323). However, a Nissl stain revealed no obvious neuronal loss in these regions (data not shown).

mCCI induces axonal injury in the subcortical white matter

To document the level of axonal injury in the subcortical white matter, tissue at the 24hr survival time were labeled for amyloid precursor protein (APP) (Figure 2.7A,B). A significant number of axonal varicosities were seen on the ipsilateral side in comparison to sham and the contralateral side ($p<0.001$ for all sections analyzed) (Figure 2.7Ai,ii,B). The number of varicosities tended to decrease in coronal sections located more distant from the center of the impact site. Abnormal axonal swellings were not observed in other areas. Further, APP expression was not elevated in other regions – cortex hippocampus, thalamus – in comparison to contralateral. The axonal varicosities present at 24hrs were no longer apparent at 8 days (data not shown).

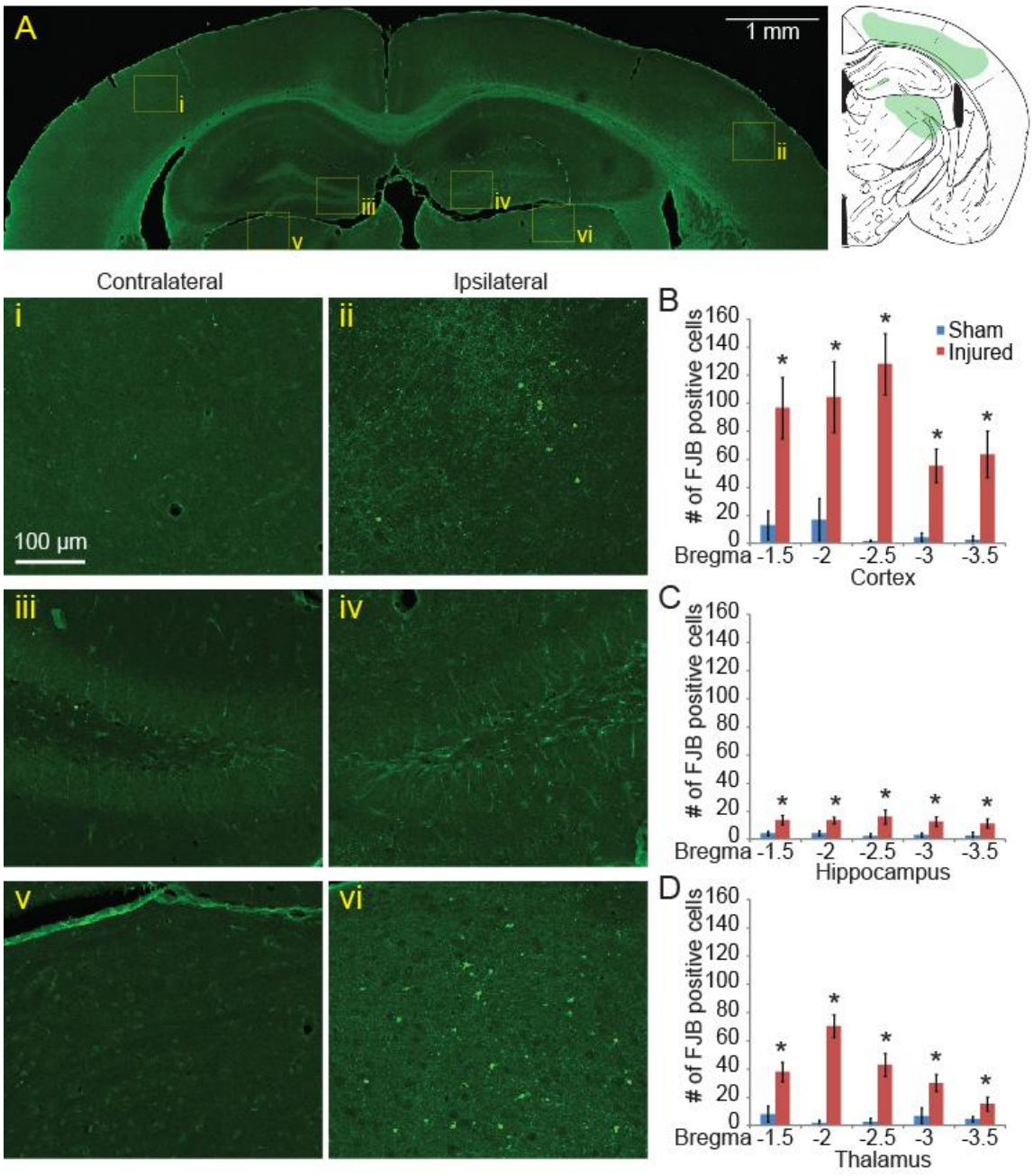

Figure 2.6. FJB 8 days after injury was diffuse and had decreasing level of degeneration. At this time point, FJB staining was located in the cortex (ii), dentate gyrus (iv), and thalamus (vi) A). Punctate staining in these regions could be due to debris from previously dying neurons. The contralateral regions did not show similar FJB staining (i, iii, v). (B) Degeneration in the cortex was still significantly elevated at 8 days compared to sham ($p<0.001$ for all sections). In the hippocampus, all sections show significant increase in FJB staining (bregma -1.5=0.0105, -2.0 p=0.0018, -2.5 p= 0.0102, -3.0 p=0.0058, -3.5 p=0.0338, n=4). In the thalamus, all sections showed significant levels of FJB staining (-1.5 p=0.0024,-2.0 and -2.5 $p<0.001$, -3.0 p=.0081, -3.5 p=0.0323). Samples sizes were n=5 for sham, n=11 for injured.

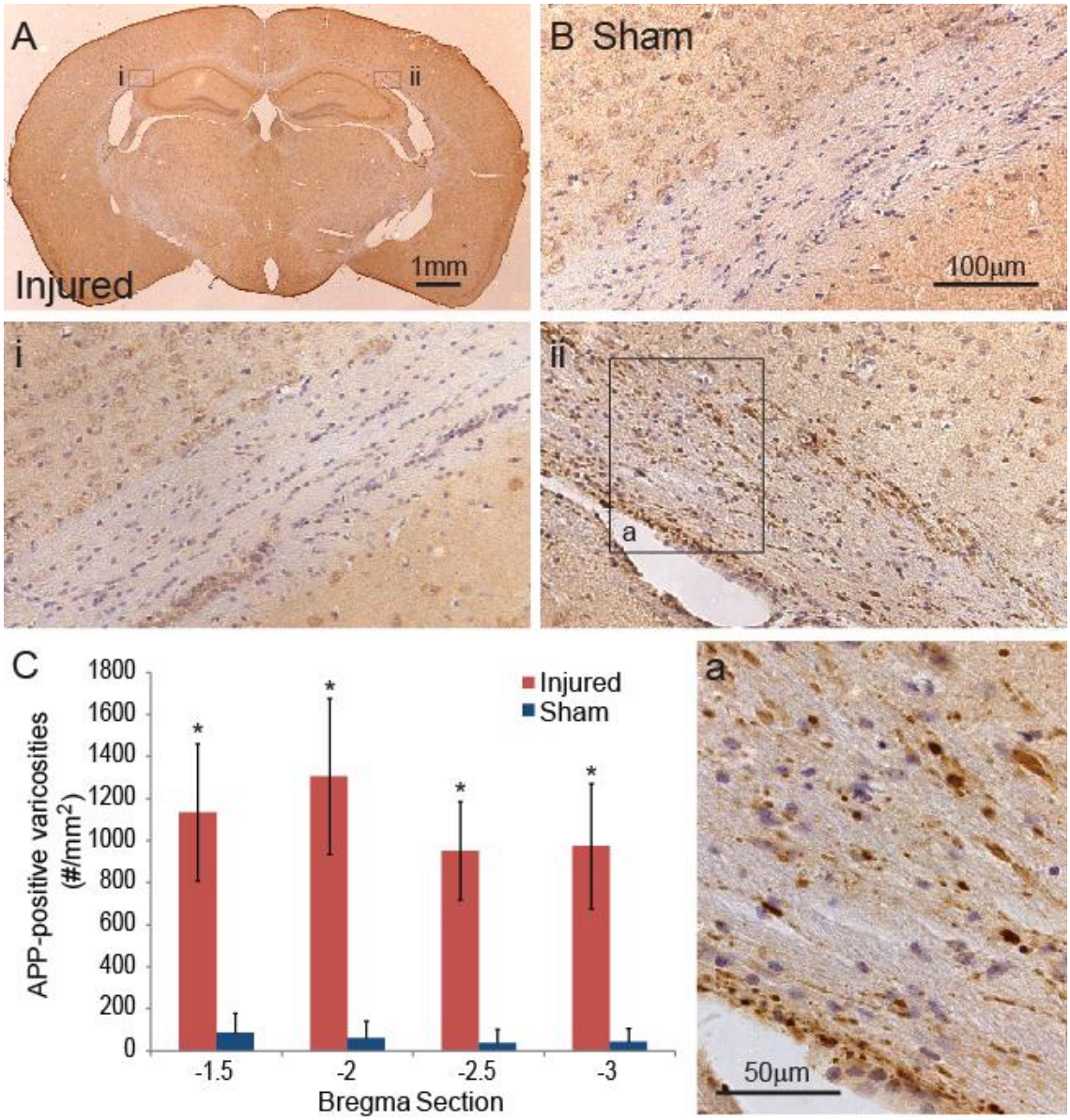

Figure 2.7. Axonal injury.
(A) APP staining was localized to the subcortical white matter on the ipsilateral side (i). Contralateral (ii) regions in of injured brains and sham brains (B) failed to have similar axonal pathologies. (C) Quantification of the axonal injuries show significant number of APP varicosities near and at the epicenter of impact ($p<0.001$ for all three bregma sections, n=5 sham, n=11 injured).

mCCI produces increase in gliosis that closely match EB and FJB patterns

On the cortex of the ipsilateral side, Iba-1 and GFAP staining patterns were also reminiscent of the EB and FJB staining patterns at 24hr and 8 day (Figure 2.8Ai,ii,iii,iv,v,vi), showing reactivity for both cell types in areas that also showed EB staining and neuronal degeneration. GFAP expression immediately under the impact site was less than the surrounding region, a pattern similar to that seen in EB and FJB. Increased GFAP expression in the cortex was more diffusely elevated but still showed similar patterning seen in FJB staining. It is important to note that there was a general increase in GFAP expression throughout the cortex, even at distal regions, compared to the contralateral side. GFAP expression in the hippocampus was also significantly elevated especially at and around the dentate gyrus (Fig 2.8Aiii,iv) and in the thalamus (Fig 2.8Av,vi). Across all five bregma sections imaged, the average GFAP expression was significantly elevated when compared with sham and the contralateral side (Figure 2.8B, $p<0.001$ between cortex, hippocampus, thalamus between sham and injured; $p<0.001$ between contralateral and ipsilateral for cortex and thalamus).

Similarly, staining for microglia with Iba-1 showed increased presence of microglia in the same regions that had elevated GFAP expression, FJB and EB labeling (Figure 2.9A). In the cortex, the region directly subject to impact showed increased microglia migration and the presence of some activated microglia. However, the regions surrounding the directly impact site showed a higher incidence of activated microglia (Figure 2.9E). Increased microglia presence was also found in the ipsilateral hippocampus and thalamus compared to the contralateral side (Figure 2.9F,G). There was no evidence of activated microglia or increased microglia presence on the contralateral side (Figure 2.9B-D).

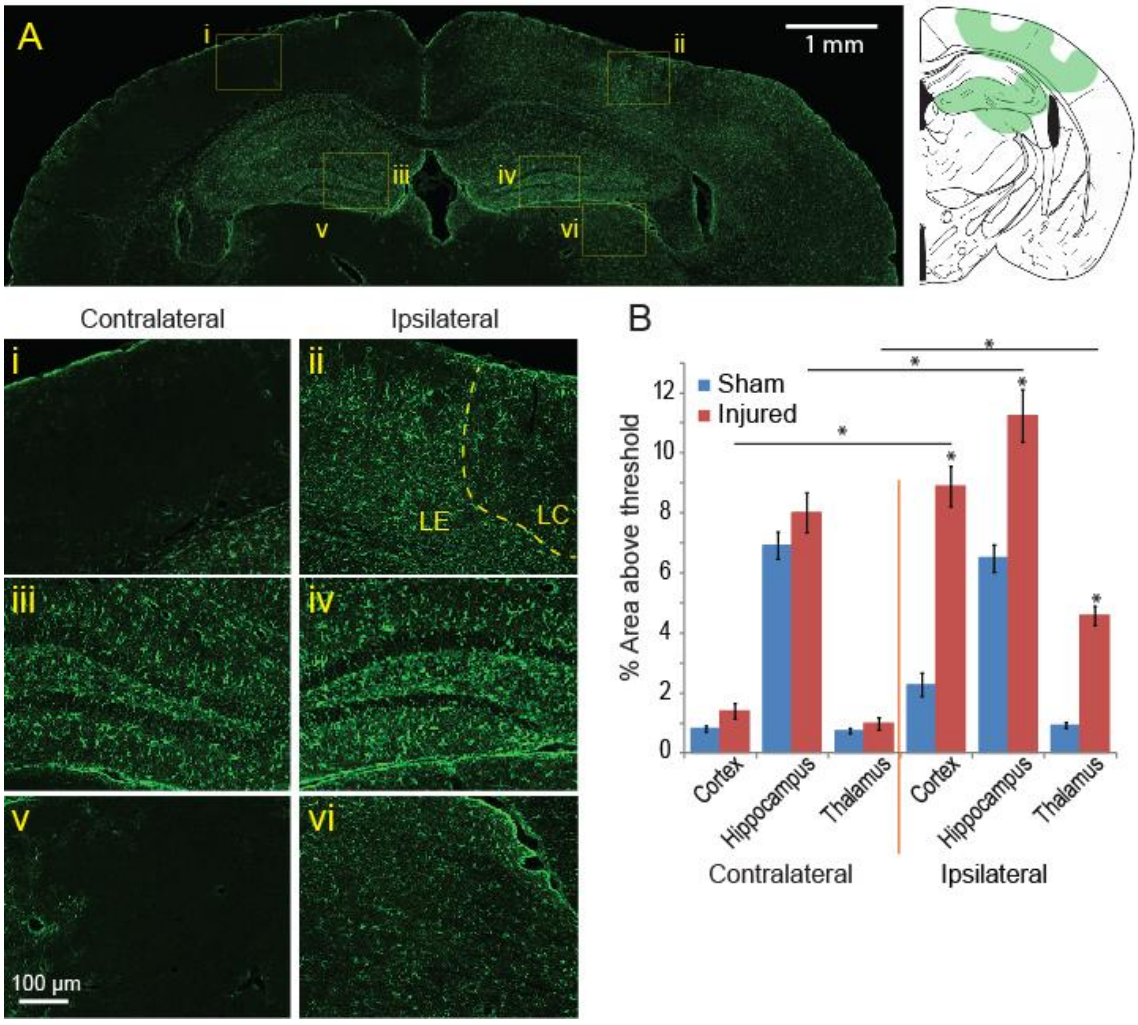

Figure 2.8. GFAP staining patterns were reminiscent of FJB degeneration pattern . (A)The GFAP staining pattern is shown and pictorially depicted. In the ipsilateral cortex, there was no prominent glial scar (ii). The lesion center (LC) also exhibited less GFAP expression than the lesion edge (LE). (i) The contralateral cortex did not have much GFAP staining. In the hippocampus, there was slight increase of GFAP expression in the ipsilateral compared to contralateral (iv versus iii), especially in the dentate gyrus. The thalamus also saw an increased GFAP expression (vi versus v). (B) Comparing the contralateral and ipsilateral GFAP expression averaged across all five sections was significant in the injured group ($p<0.001$ for each brain region); between sham and injured on the ipsilateral side, there was a significant increase for all three brain regions ($p<.0001$). Sample size n=5 sham, n=11 injured.

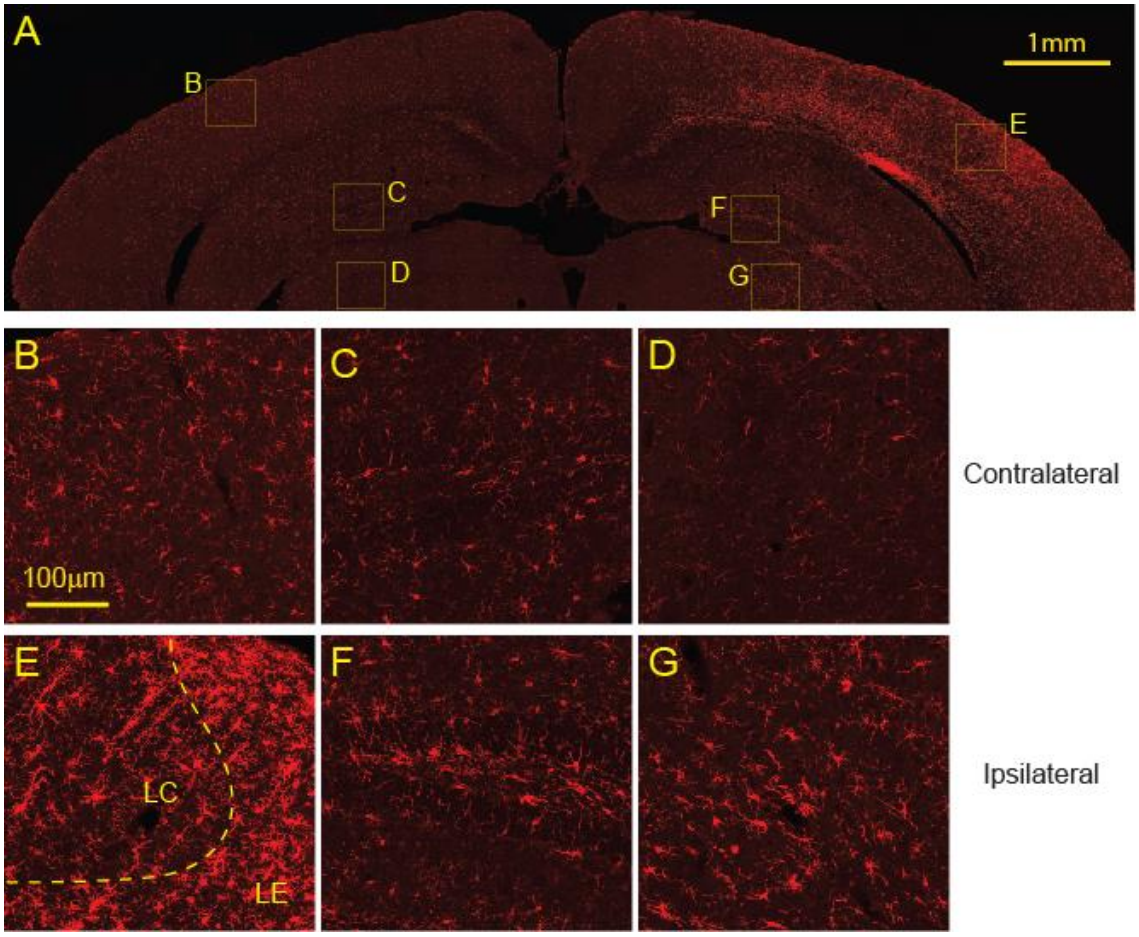

Figure 2.9. Microglia localized to site of injury .
(A) The ipsilateral side showed increased microglia migration, especially to regions that also showed FJB staining at 8 days. The ipsilateral cortex showed greater presence of activated microglia in the lesion edge (LE) compared to the lesion center (LC) (E). (B) The contralateral cortex showed minimal microglia presence and no activated microglia. The ipsilateral hippocampus (F) and thalamus (G) show increased microglia migration compared to contralateral (hippocampus (C), thalamus (D)) but both had less presence of activated microglia compared to the cortex.

mCCI produces slight behavioral deficits in motor dependent tasks but not in hippocampal dependent tasks

In all, mCCI produced very mild early behavioral deficits (Figure 2.10A). Injured mice showed vestibulomotor impairment after injury. A repeated measures ANOVA showed significantly lower fault and fall times on the rotarod compared to sham mice ($p=0.0009$, 0.0017 respectively, Figure 2.10B). The interaction between time and injury was not significant but was significant for

time alone ($p<0.0001$) showing that injured animals did not learn at a different rate than sham animals. At 4-5 days post injury, injured mice did not show a significant decreased preference for the displaced object than sham mice ($p=0.2345$, Figure 2.10C) in the hippocampus dependent behavioral task, SOR. Additionally, the CFC task administered 7-8 days post injury also failed to elicit significant behavioral difference between injured and sham mice ($p=0.2182$, Figure 2.10D). In all, mCCI produced early motor behavioral deficits.

DISCUSSION

In this chapter, we developed a model of mild TBI that was modeled on the estimated biomechanical conditions of mild TBI. Using an impact velocity range and an indentation depth that created tissue strain and strain rates in the hippocampus and cortex associated with concussion in humans, our modified CCI technique produced an injury that results in early and delayed neurodegeneration, axonal injury in the subcortical white matter, and glioreactivity. In comparison to CCI conditions commonly used in mice (2-6 m/s; 1 mm depth), the mCCI did not cause obvious tissue tears, primary hemorrhage at the impact site, or a necrotic lesion at the impact site. Although mCCI caused BBB extravasation indicated by EB dye extravasation, the EB labeling was not diffusely spread across the injured region. Rather EB labeling was confined to individual cells in the dorsal CA3 and the dentate gyrus (DG). Only the cortex, DG, and CA3 initially showed neuronal degeneration one day after injury, diminishing over the course of 8 days after injury. Delayed dorsolateral thalamic degeneration is prevalent in both forms of CCIs but with tCCI damage to this region as detected by silver staining and FJB was apparent by 24hrs (Hall et al., 2008); mCCI causes a greater delay in the development of thalamic damage. In terms of inflammation, both types of CCIs produce reactive astrocytes and microglia. With mCCI, regions of increased GFAP expression and microglia migration closely followed regions of neurodegeneration in the cortex, hippocampus, and thalamus. Mild tCCI too produced a gliotic

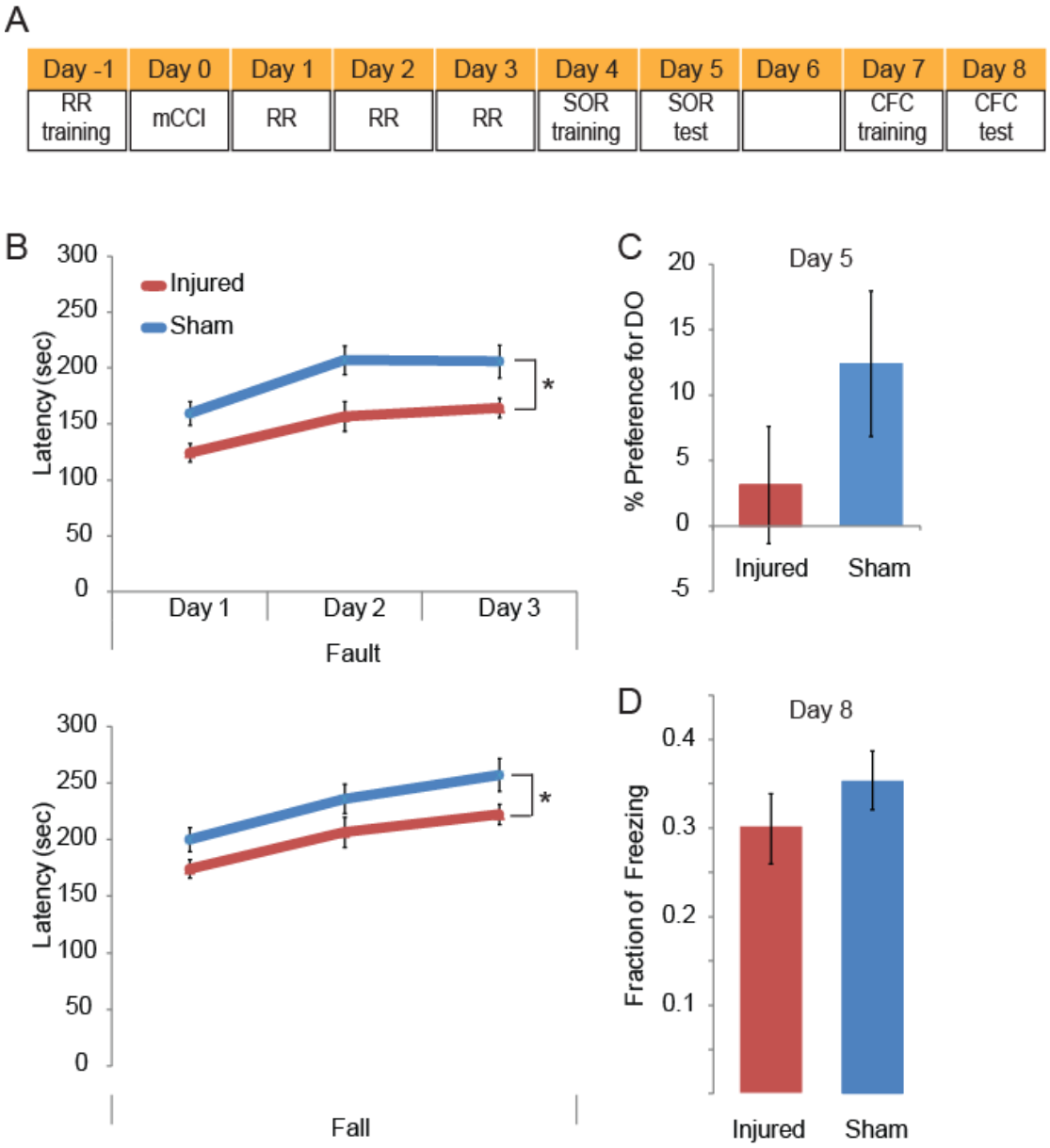

Figure 2.10. The results of behavioral testing.
Mild controlled cortical impact leads to a transient behavioral impairment. A behavioral testing paradigm to examine both cortical and hippocampal function after impact is shown in A. Rotarod (RR) training occurred the day before injury; RR was given on days 1-3 post injury. Spatial object recognition (SOR) was implemented on days 4 (training) and 5 (test day). Contextual fear conditioning (CFC) was given on day 7 (training) and 8 (test). The animals were perfused on day 8 after CFC. The rotarod results (B) indicate injured animals faulted at lower speeds with significantly lower fault and fall latency times as determine by a repeated measures ANOVA ($p=0.0009$ and 0.0017 respectively). In neither the SOR nor the CFC ($p=0.2345$, $p=0.2182$ respectively) did injured mice show significant level of altered behavior. Sample size n=17 sham, n=19 injured.

response that was limited to only the cortex (Baldwin and Scheff, 1996; Ekmark-Lewén et al., 2010; Hinkle et al., 1997) whereas for moderate/severe tCCI, astrogliosis was more widespread, encompassing the whole ipsilateral cortex, hippocampus and most of the thalamus (Chen et al., 2003). Axonal injury in the mCCI was localized to the subcortical white matter region below the impact site. In contrast tCCI studies showed APP varicosities in not only the corpus callosum but also had increased expression in the hippocampal commissure (Macdonald et al., 2007), the peripheral neocortex (Pleasant et al., 2011), the cortex and hippocampus (Ciallella et al., 2002). This difference between mCCI and tCCI APP staining is not unlike clinical studies comparing mild and severe TBI. In the clinical population, mild TBI and severe TBI patients displayed axonal injury in the same brain regions; the severe TBI patients more extensive axonal injury in these and other brain regions (Blumbergs et al., 1994, 1995).

Biomechanically, our review of the literature shows that our new CCI technique (mCCI) shares some similarities to FPI. Both mCCI and FPI have similar biomechanical loading rates, and these rates are in the range of human mTBI (Figure 2.1). Although both models produce direct cortical deformation requiring craniotomies, loading on the brain between the two models is very different. FPI produces variable loading on the dura as the fluid spreads unevenly and extensively across the surface of the ipsilateral hemisphere (Dixon et al., 1988) whereas the rigid indenter of a CCI provides reproducible injury patterns. There are two type of FPI: midline and lateral (Thompson et al., 2005). The midline FPI (MFPI) produces diffuse injuries. Low level MFPI often cause slight hemorrhages on the parieto-occipital cortex, corpus callosum, fimbria hippocampi, thalamus, and brain stem whereas high level injures produce similar but more extensive hemorrhaging patterns also encompassing the frontal, parietal, and occipital cortices (C. Edward Dixon et al., 1987; McIntosh et al., 1987). Neither low nor high MFPI injuries produce focal contusive injuries. Lateral FPI (LFPI) is more similar to mCCI as it produces focal injuries in addition to diffuse injuries. More severe lateral FPI injuries cause contusions (Goodman et al.,

1994); mild LFPI do not (Hylin et al., 2013; McIntosh et al., 1989). Mild LFPI produced BBB extravasation but the pattern was different than those of mCCI. Hemorrhage typically occupied the external capsule bordering the lateral ventricle from approximately the level of the caudate-putamen to the level of the subthalamic nucleus (McIntosh et al., 1989). There was minimal EB extravasation in the left cortical hemisphere. In one mild LPFI study, researchers noted no overt changes in neuronal density or dendritic damage, APP bulbs in the corpus callosum, and increased GFAP and Iba-1 staining in the corpus callosum and thalamus (Hylin et al., 2013). Another mild LFPI study (Spain et al., 2010) showed cell death only in the cortex at 24hrs which dropped to below sham by 72 hrs. There was no cell death in the thalamus at any time point and only a few animals showed hippocampal damage. 24hr staining of APP showed no significantly elevation of APP bulbs in any region although the cingulum showed increased bulbs at 4hrs and the thalamus at 6 weeks. Shultz et al (2011) showed activated microglia in the ipsilateral cortex and only saw significantly elevated GFAP expression in the cortical area directly below the impact region. While FPI model reliability between laboratories is poor as evidenced by the different resulting pathologies produced (Thompson et al., 2005), generally mild LPFI produces more focal damage with most of the damage concentrated in the cortex and less in the hippocampus and thalamus. While both mild FPI and mCCI produced axonal damage, increased gliosis, and neuronal cell loss, the largest difference between the two models is in the correlation of injury patterns between each of the histopathological stains. In mCCI, the regions of gliosis, degeneration, and BBB extravasations were very similar, something that has never been noted for mild FPI injuries.

With an ability to create cellular changes without more distinct hemorrhagic injury, this new CCI technique will allow us to extend our knowledge of tissue injury thresholds for the brain. Currently CCI type models and the direct cortical deformation (DCD) model from Shreiber et al (1997) are the only ones that can independently alter strain versus strain rate in the rodent. For the

cortex, strain, strain rate, and post-injury length of time have been shown to all affect cell death (Elkin and Morrison III, 2007). For the hippocampus, only strain and post-injury length of time and not strain rate, affect cell death (Cater et al., 2006). All three factors can be simulated with the mCCI to validate tissue thresholds found *in vitro* and determine if the regional anatomical vulnerabilities also occur *in vivo*. For instance, if neuronal degeneration in the hippocampus was not sensitive to strain rate, then a tCCI injury of 1.0mm impact depth should cause less injury to the hippocampus than an injury of 2.0mm impact depth. However tCCI produce greater histopathological and hippocampal dysfunction than mCCI suggesting that there other factors that affect injury thresholds that are not replicated *in vitro*. In this comparison of tCCI with mCCI loading conditions, the most striking difference is the presence of primary hemorrhage for the tCCI model. Although not explored directly in any biomechanical study, the presence of hemorrhage has been a focus of study in the past as a possible source that enhances neuronal degeneration (Alonso et al., 2011; Matz et al., 2001; Nadal et al., 1995; Sasaki and Dunn, 2001). Past studies found axonal injury thresholds to be 18% strain (Bain and Meaney, 2000) which was similar to the 17.2% strain threshold for vascular damage (Shreiber et al., 1997). mCCI seems to support this as the EB and FJB patterns were so similar.

mCCI can also be used to correlate biomechanics to biochemical changes. The concept of mechanoporation as it relates to strain and strain rate can be explored with mCCI and the results compared to in vitro studies. Cell cultures studies into mechanoporation, the process by which a traumatic insult produces sublethal pores or defects in the membrane, occurs within seconds to minutes of initial injury. The degree of mechanoporation being dependent on strain and strain rate (Cullen et al., 2011; Geddes et al., 2003). High strain rate loading causes cells to behave in a more rigid manner while at low strain rates cellular structural components are able to comply with even deformation. Authors concluded that mechanoporation studies could be used to determine the stress/strain concentrations in tissue. An *in vivo* model of TBI and

mechanoporation showed that neurons had immediate and prolonged membrane disruption due to uptake of pre and post injury dextran or HRP uptake (Farkas et al., 2006). However newer studies have shown that dextran and HRP uptake into neurons were due to NMDAR dependent endocytosis (Vaslin et al., 2007) and that this excitotoxic induced endocytosis could be used to deliver neuroprotective peptides (Vaslin et al., 2011) as a treatment for TBI. This may explain why Farkas et al showed only neurons being susceptible to mechanoporation as other cell types, not containing NMDARs, would not be subject to NMDAR induced endocytosis. Injection of the dextran dye pre and post injury as used by Farkas et al with this model, could help further define *in vivo* and validate *in vitro* functional tissue thresholds by comparing regions of dye labeled neurons and their stress/strain concentration.

Finally, the relative simplicity of the mCCI technique also suggests this technique would be useful in determining strain/strain rate thresholds following repeated TBI. Several studies with repeated TBI show the brain is much more susceptible in a subsequent injury, yet the exact mechanical threshold that changes over multiple injuries is not known (Laurer et al., 2001; Longhi et al., 2005). Recent studies using either a cortical impact or fluid percussion model show that repeated TBI will lead to changes that are observable with clinical imaging tools, ultrastructural tools including electron microscopy, and behavioral screening (Bennett et al., 2012; Shitaka et al., 2011; Shultz et al., 2011). Overall, repetitive TBI models show transient or no behavioral deficits, minimal histopathology with the first injury and significant behavioral dysfunction and prolonged histopathology; these features are similar to our modified CCI model described in this chapter. Therefore, this mCCI technique appears ideally positioned to expand our understanding of tissue injury thresholds for single and repeated TBI. The resulting thresholds that indicate the critical strain and strain rate combinations causing astrogliosis, microglia reactivity, BBB breakdown after repeated mechanical injuries will provide great insight into the potential mechanical vulnerability of the brain as it recovers from injury, leading to a much more

precise estimate of whether the mechanical tolerance of the brain over time changes after injury. Knowing these dynamic mechanical tolerances will lead to a more precise, injury-dependent prediction of vulnerability that would lead to better prediction of brain injury tolerance for head protection technologies. In addition, the evolving state of brain tolerance could inform us about new biochemical pathways that are activated over time after repeated injuries of the same mechanical magnitude, leading us into more precise measures of treating the injured brain after repeated injuries.

Chapter 3 *In vivo* imaging of stretch injury

ABSTRACT

Past *in vitro* work showed that astrocytes respond to mild stretch with an intercellular calcium wave (ICW) that spread far into the penumbra region. The mechanism of the ICW was dependent on the severity of injury, but was predominantly due to extracellular ATP activating purinergic receptors. However, astrocyte cultures are a poor model with which to study true astrocyte function. Cultured astrocytes have altered morphology and express different genes than astrocytes *in situ*, necessitating a validation of *in vitro* results *in vivo*. In this chapter, we adapted the mild CCI model that we created based on human mild TBI biomechanics to allow for real time in vivo imaging during injury. With the micro CCI model, we found that astrocytes produce a sustained ICW originating from the site of impact. This response was greatly reduced with application of apyrase, a nucleotidase, but not with flufenamic acid, a gap junction blocker. Due to limitations of the setup, we were not able to test multiple injury levels. However, the results suggest that astrocytes do respond to mechanical injury with a calcium wave similar to that *in vitro* and at the injury level tested, the mechanism of the wave was also from extracellular ATP.

INTRODUCTION

Astrocyte excitability operates via changes in intracellular calcium levels (Agulhon et al., 2012; Verkhratsky et al., 2012; Zorec et al., 2012). Past work *in vitro* shows that calcium waves propagate through the astrocytic syncytium. Based on these results, the hypothesis arose that calcium could be the mechanism where astrocytes convey information through long distances (Agulhon et al., 2008).

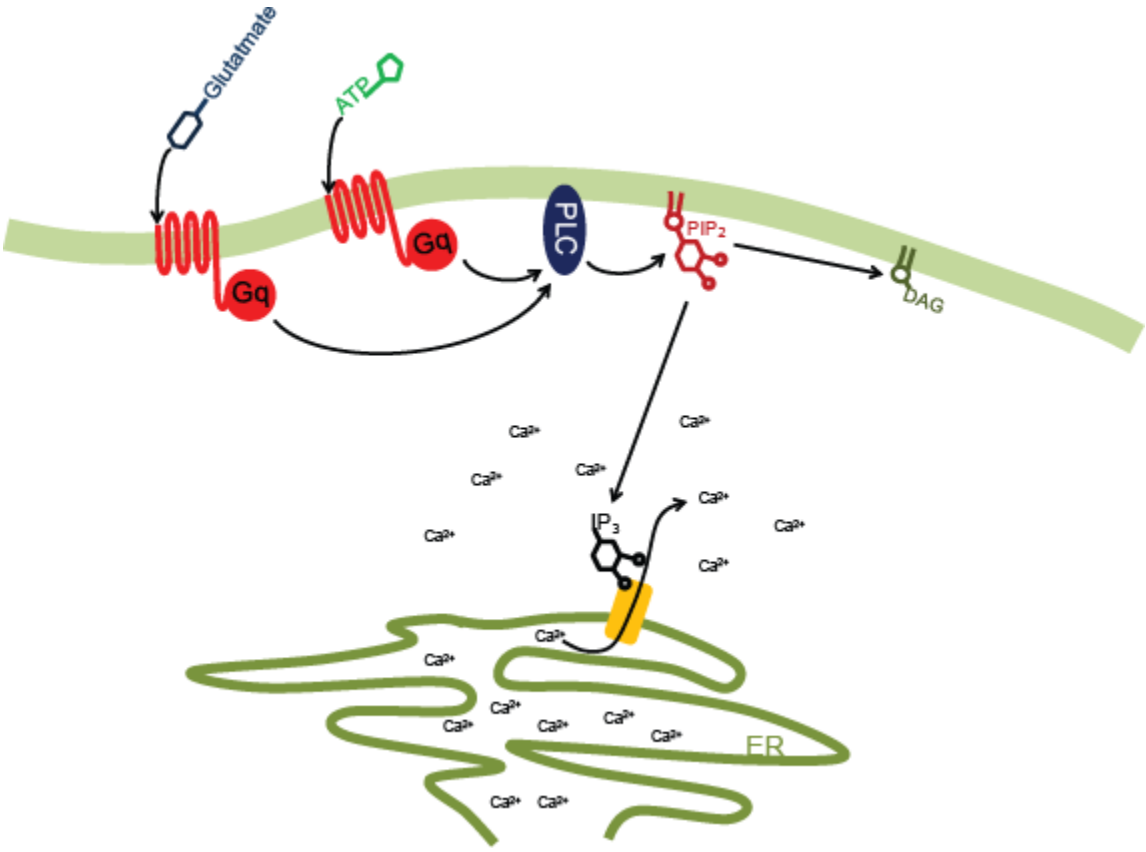

Figure 3.1. The PLC/IP_3 pathway
Once activated, GqGPCR activates PLC which hydrolyzes PIP_2 into DAG and IP_3. IP_3 activates IP_3 receptors on the endoplasmic reticulum (ER) causing calcium to be released from the internal stores.

The most widely accepted pathway for intracellular calcium increase in astrocytes is through the phospholipase C (PLC)/ inositol 1,4,5 –triphosphate (IP_3).pathway (Agulhon et al., 2008; Zorec et al., 2012). Gq G protein coupled receptor (GPCR) activation causes PLC to hydrolyze the membrane bound lipid phosphatidylinositol 4,5 –bisphosphate (PIP_2) into IP_3 and diacylglycerol (DAG) (Figure 3.1). IP_3 activates IP_3R on the endoplasmic reticulum (ER) causing calcium release. (Fiacco and McCarthy, 2006; Scemes, 2000; Scemes and Giaume, 2006). Once triggered, the intracellular calcium can cause intracellular calcium levels to rise in neighboring astrocytes producing intercellular calcium waves (ICW) (Scemes and Giaume, 2006).

The pathway for ICW transmission is noted to occur through two possible ways (Agulhon et al., 2008). The first is through "*de novo*" generation, where intracellular calcium increase in the cell causes extracellular release of a signaling molecule that can activate the GqGPCR on nearby cells. In most cases, this extracellular molecule is adenosine triphosphate (ATP) (Agulhon et al., 2008; Bowser and Khakh, 2007; Scemes, 2000). The second pathway is through transmission of IP_3 through gap junctions, based on extensive *in vitro* work. Although intracellular calcium increases occur readily *in vitro*, the relative incidence of ICW occurring under physiological conditions *in vivo* occurs (e.g., Kuga, et al., 2011; Ding et al., 2013) but less frequently (Agulhon et al., 2008).

Perhaps the most significant for astrocytic ICWs is in mediating pathological states. Using 2-photon imaging, Ding et al (2009) showed that after induction of ischemia through photothrombsis, astrocytes in the ischemic region displayed highly synchronous calcium oscillations that were blunted with the application of 2-methyl-6-(phenylethynyl)-pryidine (MPEP), a mGluR5 antagonist, and CGP54626, a $GABA_BR$ antagonist. The induction of status epilepticus (SE) through application of pilocarpine was able to cause acute and prolonged calcium waves *in vivo* which were reduced with the application of MPEP (Ding et al., 2007). In both cases, blocking the calcium waves *in vivo* led to neuroprotection. In a cortical spreading

depression (CSD) model, injection of KCl to trigger CSD also triggered astrocytic calcium waves which propagated farther than did the CSD wave itself (Peters et al., 2003).

These studies showed that astrocytic ICWs are elicited in a disease state and that blocking these waves are neuroprotective. Until now, there was no meaningful evaluation of the role for astrocytic ICWs in recovery after TBI. Mechanical stimulation of a single astrocyte in culture can cause an outward propagation of ICW that extends beyond neighboring cells (Charles et al., 1991; Scemes and Giaume, 2006). Astrocyte cultures undergoing stretch display a large sustained increase in intracellular calcium due to release of calcium from ER stores (Rzigalinski et al., 1998). Even though calcium levels returned back to the basal levels, subsequent glutamate induced calcium responses were inhibited. Astrocytes injured by a rapid, transient strain that simulates mild TBI caused ICWs to spread into the penumbra region and the mechanism of calcium propagation depended on the level of injury (Choo et al., 2013; Miller, 2009). The blockade of intercellular wave mechanisms provided neuroprotection in organotypic hippocampal slices. Inhibiting the same pathway that produce ICWs through pretreatment of purinergic receptor P_2Y_1 receptors (P2Y1R) also produced reduced neuronal cell death and improved behavior after a controlled cortical impact (CCI) injury in mice (Choo et al., 2013).

However, astrocyte cultures serve as a poor model for studying astrocytic functions (Agulhon et al., 2008; Lange et al., 2012). Gene profiles between astrocytes in culture and *in vivo* are dissimilar; cultured astrocyte express genes that are not expressed *in vivo* (Agulhon et al., 2008). Cultured astrocytes also express different synaptic proteins (which are involved in exocytosis of messenger molecules) from *in situ* and vice versa (Wilhelm et al., 2004). Culturing conditions can also influence gene and receptor expression, contributing to significant differences in experimental result between labs (Lange et al., 2012).

In this chapter, we investigated if the mechanically induced calcium waves found *in vitro* could be replicated in an *in vivo* model of injury. Using a 2-photon system to image the pia layer

of an anesthetized mouse, we created a mechanical device that was capable of imparting an impact to the cortex. We recorded the acute increase in cytosolic calcium within the astrocytes after injury, characterized the extent of injury, and also tested to see if the mechanism of the calcium waves *in vivo* was similar to mechanisms observed in past *in vitro* research.

METHODS AND MATERIALS

Cortical Craniotomy and Dye Loading

Mice (C57Bl6, Jackson) were prepared for *in vivo* imaging as previously described (Tian et al., 2006). Briefly, mice were anaesthetized with an intraperitoneal (IP) injection of 1.5 g/kg urethane (Sigma Aldrich, St. Louis, MO). A head plate containing a window for the exposed cortex was cemented to the skull with Vetbond™. A 1.8-mm craniotomy was produced on the left hemisphere, midway between bregma and lambda. The dura was gently removed, being careful not to damage the underlying cortex. The exposed cortex was incubated with 0.65mM of fluo-4-AM (Invitrogen, Grand Island, NY) diluted in 20% pluronic in dimethyl sulphoxide (DMSO) with artificial cerebrospinal fluid (ACSF) for 1.5 hours. Fluo-4 was rinsed with ACSF and was incubated for an additional 30 min to allow for de-esterification. The cortex was continuously irrigated with artificial CSF to prevent drying. This loading protocol preferentially labels astrocytes with Fluo-4 up to a depth of ~150 mm beneath the surface of the cortex (Figure 3.2; Tian et al., 2006). 100μM Sulforhodamine 101(SR101, Invitrogen, Grand Island, NY) was topically applied for 5min just prior to setup of the mice on the microscope. SR101 specifically loads astroctyes *in vivo* (Nimmerjahn et al., 2004) and was used in our preparations to detect astrocytes.

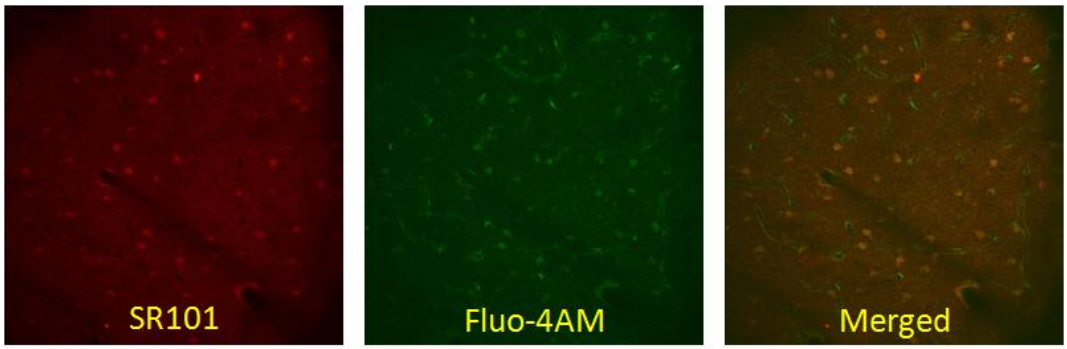

Figure 3.2. Astrocytes loaded with SR101 and Fluo-4AM.
40× objective. The cells labeled with Fluo-4AM co-labeled with SR101 demonstrating that the cell type of interest were astrocytes.

Adaptation of *In Vivo* Models for Imaging

To see if a mechanically induced intercellular calcium waves occurred *in vivo*, we modified an animal TBI model to fit under a 2-photon microscope. Of all the injury models available, only the CCI satisfied our needs. The impactor size and impact depth was reduced so that a non-hemorrhagic injury was produced in the cortex as well as fit under the objective. The craniotomy size used in the *in vivo* imaging protocol was also much smaller than that used in a typical CCI injury. As the same solenoid model was used to actuate the micro CCI as used in the mCCI, both models used similar impact speed.

microCCI injury

Lateral Impact: After the dye was loaded and rinsed away, half the cortex was coverslipped, and 1.5% low temperature agarose was injected between the coverslip and the cortex to minimize motion artifact during *in vivo* imaging. The agar covering the half of the cortex that was not covered by a glass coverslip was cut away and removed. Once mice were mounted in the stage of the microscope system the impactor, metal conical shaped tip of 1.0mm and 2.0mm in diameter was put into position into with a 10× objective. The metal tip was driven by a solenoid (SoftShift, Ledex, USA). With the impactor in the extended position, the tip was lowered until it made

contact with the cortex at the agar interface (Figure 3.3). Once the impactor was retracted, the impactor was lowered in by the desired impact depth.

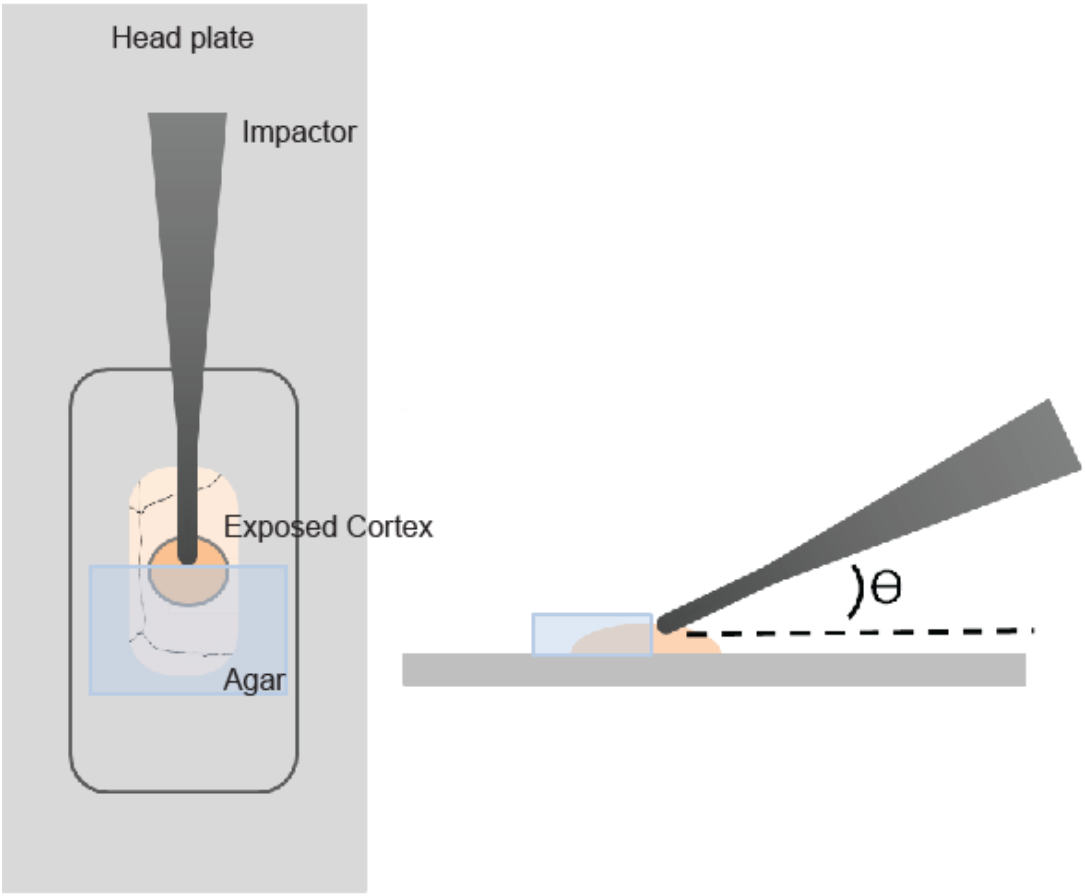

Figure 3.3. Lateral microCCI setup.
Glassslip covered agar filled half the exposed cortex. The angle of impactor ranged between 15° - 30° from hortizontal.

Vertical Impact: The craniotomy and the dye loading protocol remained the same. In the vertical setup, agar was not used. A silicone membrane (Sylgard 184 + 186 mix; Dow Corning, Midland, MI) between 0.1-0.15mm thick was used to cover the entire cortex. Cortical impacts were delivered using a custom-built impactor, with a tip diameter of 200 mm. The impact depth (~200-300m) was determined by the length of the custom impactor. The 10× objective was used to position the impactor in the middle of the craniotomy (Figure 3.4). After collecting the data, the

impactor tip was lowered and a z stack of the cortex in the deformed position was used to determine impact depth.

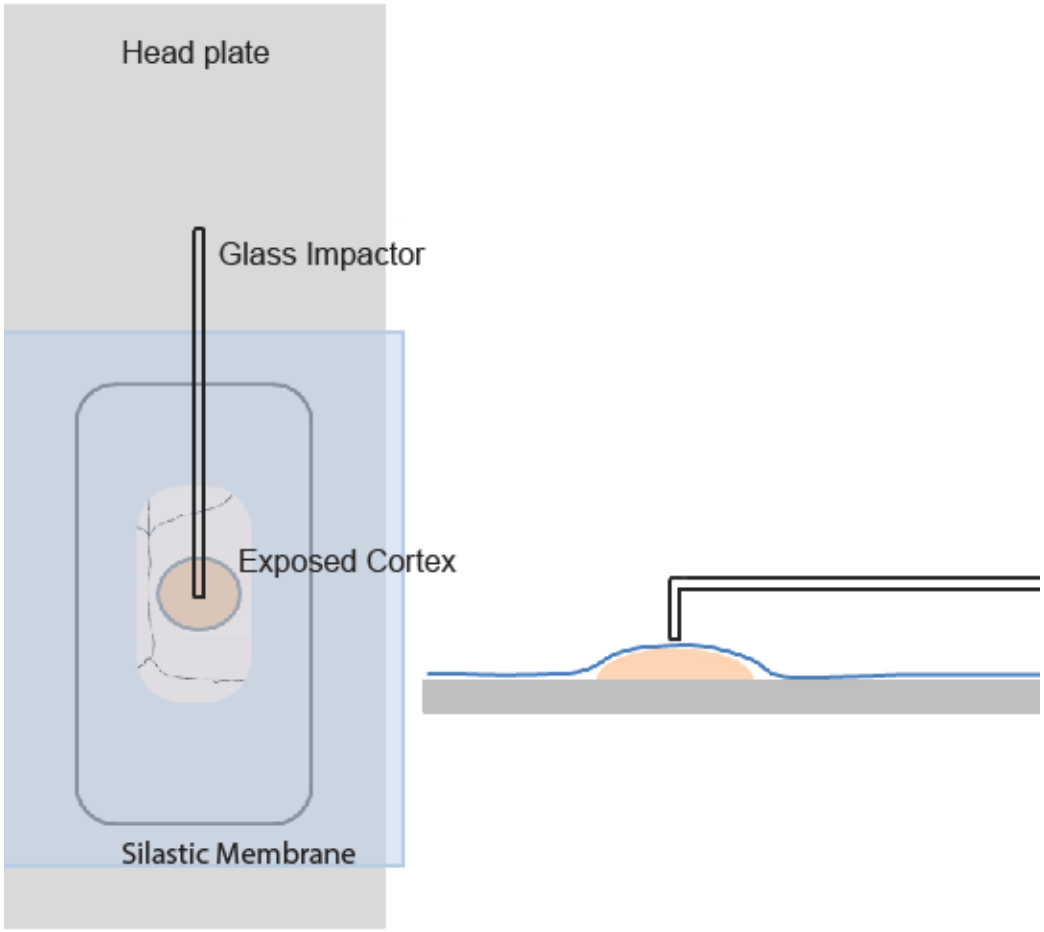

Figure 3.4 Vertical impact setup.
A custom made impactor tip impacts the cortex in a vertical downward direction. A thin silicone membrane covers the cortex to prevent the impactor tip from piercing the brain as well as to disperse the mechanical force across a wider surface area.

In vivo Imaging

Mice were mounted in a *in vivo* 2-photon imaging system (Prairie Technologies), and images were acquired at 3s intervals using a 40× water-immersion infra-red objective with 820nm excitation wavelength. A three second time lapse between each image was used to reduce the

amount of photobleaching. We were able to image up to 200μm into the cortex with fluo4-AM. Imaging of calcium responses with and without impact were taken at around 50-80μm below the pial surface.

Statistical Analysis

All statistical tests were carried out using JMP10. The variance between groups was first tested for normality (Shapiro-Wilks test) and then equality (Bartlett test). When the variance between groups was not similar, the two sample t test was used, otherwise a one way analysis of variance (ANOVA) was used.

RESULTS

Development of the microCCI Model

The depth of impact was limited by the working distance of the objective used. Initially, the impactor was oriented at a 15° to 30° angle from horizontal using a metal conical tip. Two different tip diameters were used, 1mm and 2mm. The original setup (Figure 3.3) was configured to image half the impacted area and half of the penumbra region. However this setup in many of test preparations caused contusions or knocked the imaging out of focus.

The lateral impact model was able to show increased calcium activity in astrocytes after impact (Figure 3.5). However the consistency was low and the spread of the calcium wave was poor. Many times, the plane of interest was knocked out of focus and did not return. This could be due to the impactor deforming the agarose, causing it to press on the cortex. Hemorrhaging was also an issue with this model. Many of the impacts caused small contusions to the cortex, potentially due to the large lateral distance the impactor needed to travel with respect to the downward distance (as the angle of the impactor was small), causing greater lateral deformation than vertical.

To ensure that the poor calcium response was not due to the injury model and preparation, we next pursued a vertical impact (Figure 3.4). However, the severity of the impact was limited

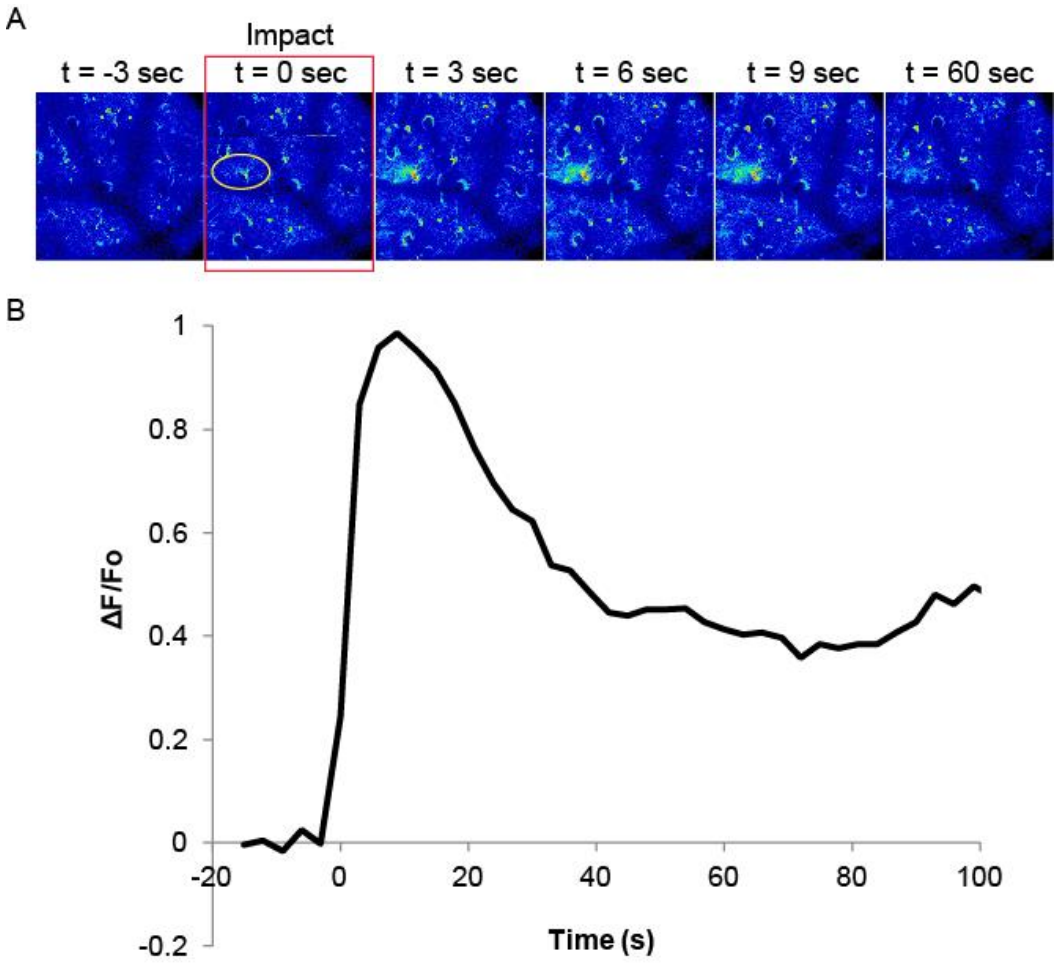

Figure 3.5. Lateral micro CCI induced a calcium wave in astrocytes immediately after impact.
(A) 40× time-lapse images of the calcium wave after impact and (B) the graphed response of the highlighted region.

by the short working distance of the objective, as well as the impactor material. Based on the data from the lateral impacts, response time of the calcium wave *in vivo* occurred acutely and dissipated quickly. Therefore the impactor could not be moved in and out of the field of view during the time of interest. Pulled micropipettes were used for their near optically transparent properties as well as their malleability when heated. The same solenoid from the lateral impact model was used to actuate the tip in a downward motion. The impactor was visible with the 10×

objective which allowed the impactor to be positioned as close to the center of the craniotomy field as possible (Figure 3.6). At the 40× objective however, the impactor was not visible which allowed for unobstructive view of the dye loaded cells and subsequent impact response (Figure 3.6).

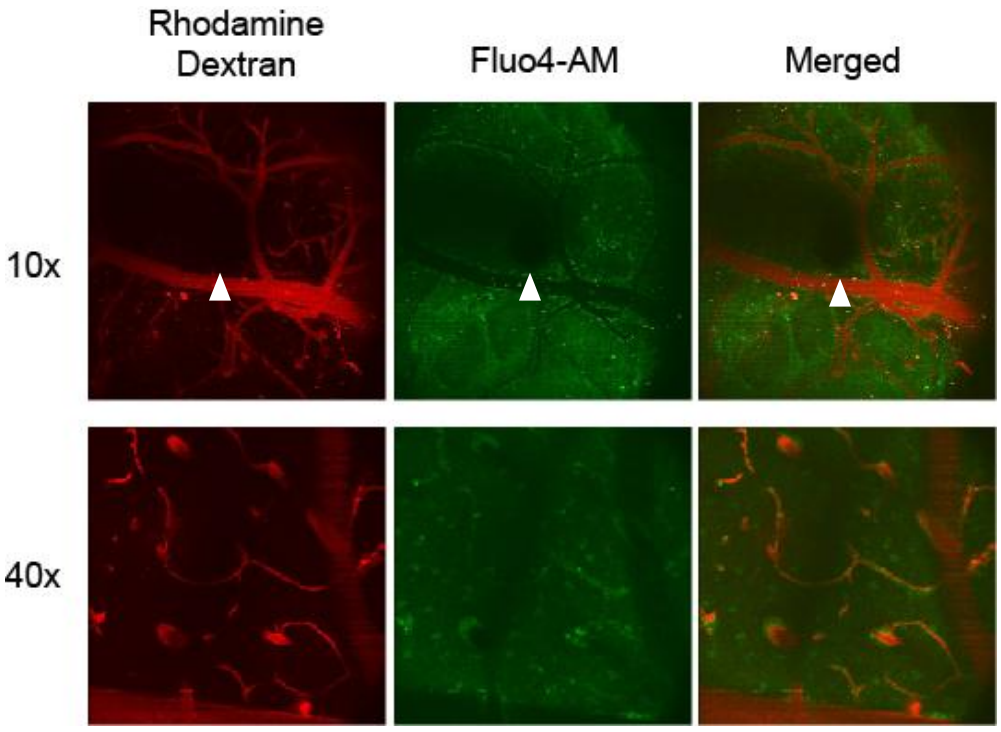

Figure 3.6. 2-photon images of the *in vivo* preparation with the vertical impactor in position. (A) Under the 10× objective the vertical impactor was visible which allowed for the impactor to be positioned in the middle of the cortex. In this preparation, rhodamine dextran was injected into the tail to delineate the vasculature. Fluo4-AM was loaded topically to measure calcium loading in the cell. The white arrow depicts the location of the impactor tip. (B) 40× objective of the region directly below the impactor. With this objective the impactor was no longer visible.

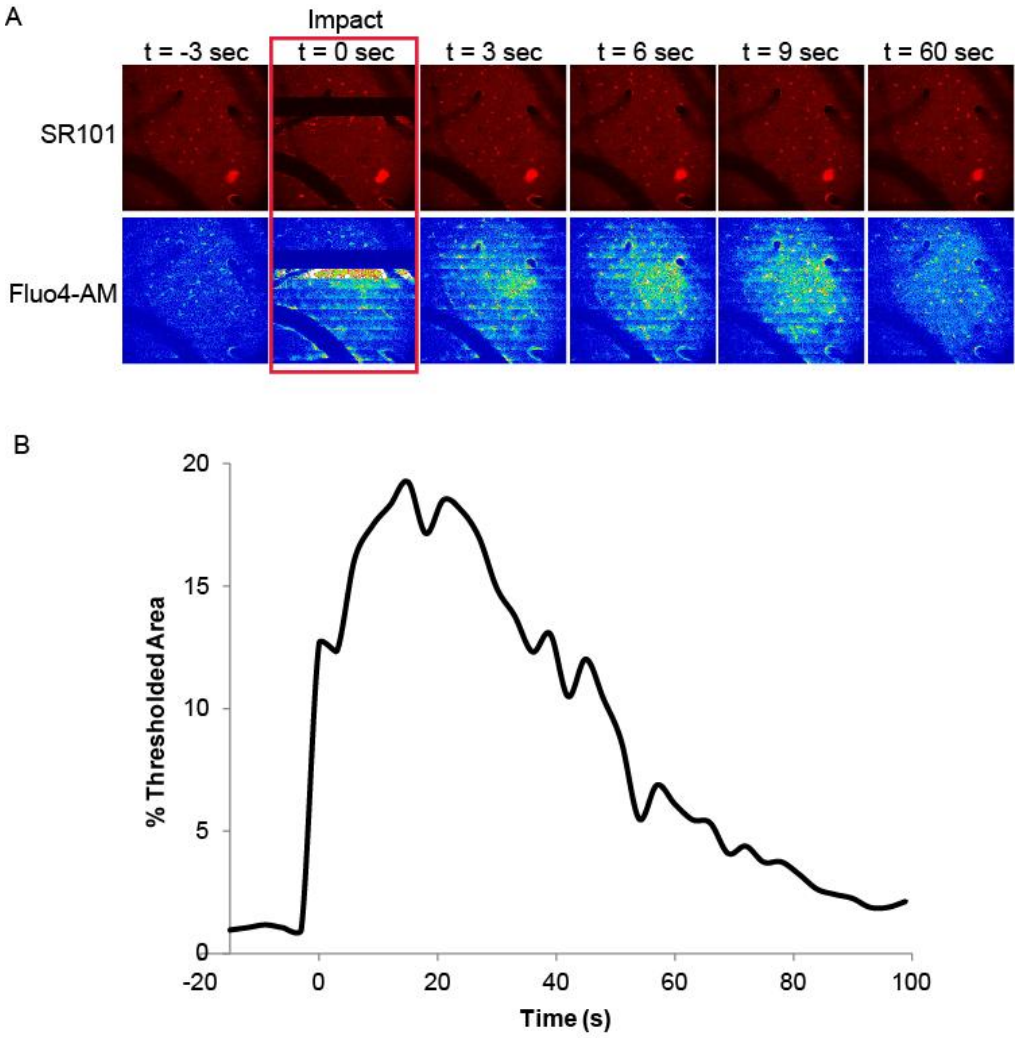

Figure 3.7. Vertical micro CCI induced a strong calcium response immediately after impact. (A) 40× time-lapse images with SR101 showing labeled astrocytes and Fluo4-AM of the calcium wave. The lines in the time-lapse dye loaded images are due to perfusion of the brain and motion of the animal. (B) The impact region shows sustained area of intracellular calcium increase after injury.

Injury Induced Calcium Wave

A mechanical impact was able to induce an intracellular calcium wave in astrocytes *in vivo* (Figure 3.7A). The calcium wave originated from the impact site and extended radially outward. Due to the fluctuation of the surface of the cortex from vascular perfusion and animal motion, there were small image plane changes with cells coming in and out of focus. Unlike the lateral

injury model, the vertical method did not employ the use of low melting agar to help reduce motion artifacts. A comparison in time lapse imaging between a vertical impact (Figure 3.7A) to the lateral impact (Figure 3.5A) shows noticeable lines that run across the image at each time snapshot. To measure the spread of the ICW, the normalized change in fluorescence ($\Delta F/F_o$) was thresholded above 0.54. Plotting the thresholded area against time (Figure 3.7B) gave us an idea on how fast and long the calcium wave lasted.

The Mechanism of Injury Evoked ICW in Astrocytes is Through Extracellular ATP

Next we tested for the mechanism by which the mechanically induced ICW occurs. *In vitro* results showed that the mechanism for ICWs depended on the injury level, extracellular ATP was the dominant pathway for all injury levels tested (Choo et al., 2013; Miller, 2009). Apyrase, a nucleotidase, breaks down ATP and ADP into adenosine. Flufenamic Acid (FFA) is a gap channel blocker. Mice were topically treated with each drug prior to injury. FFA treated injury calcium response was similar in the spread and decay as the untreated animal (Figure 3.8A, B). In contrast, apyrase treatment reduced the spread of the calcium wave. Both the untreated and FFA treated mice displayed similar and significant increases in thresholded area post injury compared to sham animals (Figure 3.9). Apyrase treated injured animals had peak thresholds that were similar to sham treated and untreated animals. This suggests that the dominant mechanism for mechanically induced ICWs is through extracellular ATPs. We also tried pretreating with either pyridoxalphosphate-6-azophenyl-2', 4'-disulfonic acid (PPADS) or suramin, two broad P2 receptors (P2R). However PPADS reacted to the 2-photon laser and artificially increased the fluorescence over time (data not shown) and suramin complicated the surgery. Animals pretreated with suramin would undergo spontaneous bleeding at the craniotomy site, precluding imaging at the injury site.

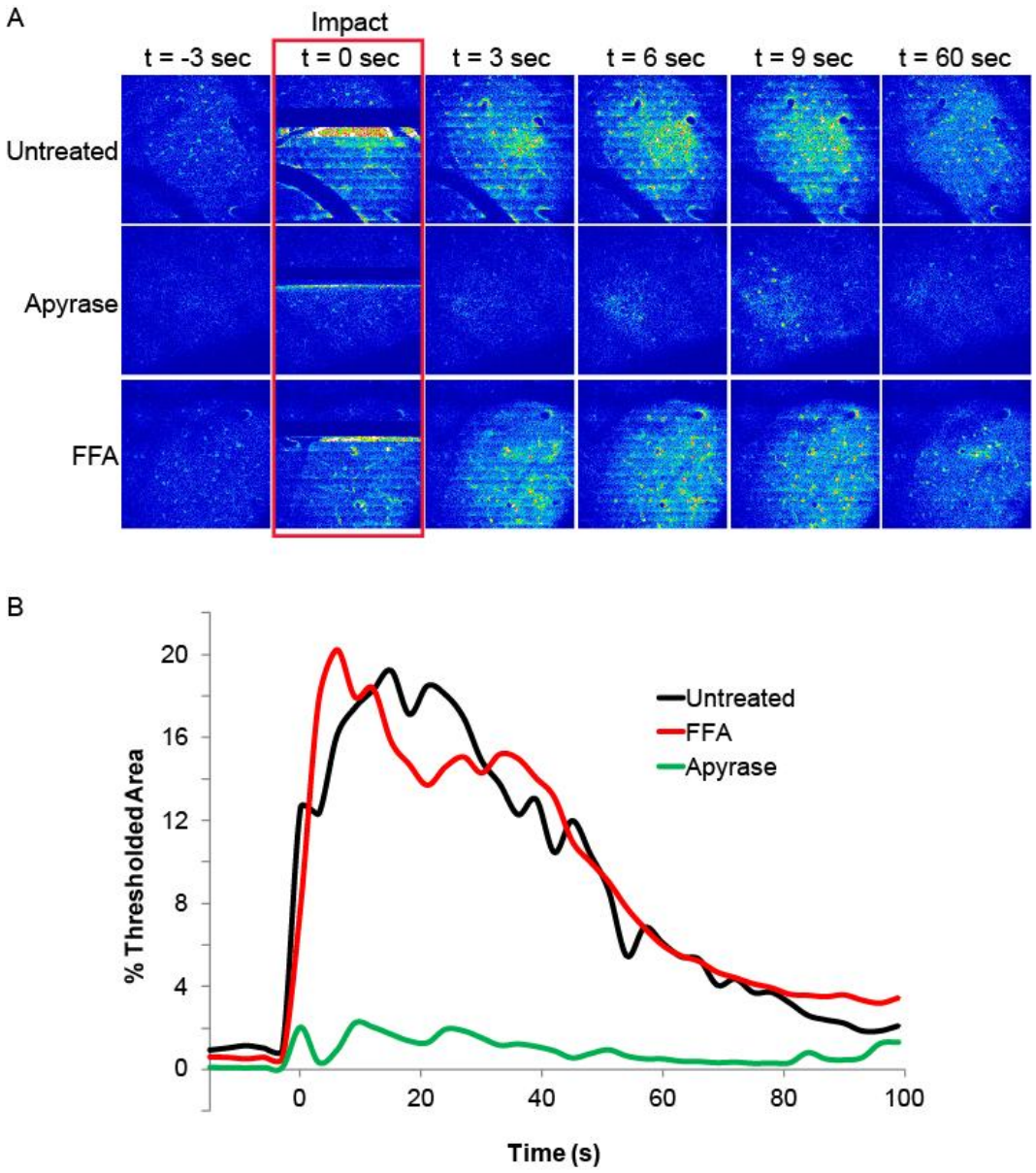

Figure 3.8. Stretch induced calcium wave was attenuated with apyrase.
Topical application of flufenamic acid (FFA) was not able to attenuate the calcium response after injury. Apryase was able to reduce the level of injury induced fluorescence. Time-lapse imaging shown in (A) and responses graphed in (B).

DISCUSSION

Past *in vitro* research showed ICWs being elicited from astrocytes in culture immediately after injury, spreading from the injured to the penumbra region. The strains in culture ranged from 5% to 25% strain (Choo et al., 2013; Miller, 2009). The mechanism for ICW transmission in the penumbra region was dependent on the injury level. At 5% strain the predominate mechanism was extracellular ATP through activation of P2 receptors, at 15% strain caused ICW to occur through both gap junctions and P2 receptors, and at 25% strain mGluR and P2 receptors but not gap junction caused ICWs. Due to the differences between astrocytes in culture and astrocytes *in vivo* (Agulhon et al., 2008; Lange et al., 2012), we needed to determine if the *in vitro* injury response can be replicated *in vivo*.

Toward this goal, we developed a method to image the acute response of a mechanical impact on cortical astrocytes and study its mechanisms *in vivo*. Initially we tried a lateral impact approach. This method allowed us to injure and retract the impactor so as not to interfere with imaging. This method also covered the imaging side of the craniotomy with a low melting temperature agarose to help reduce the artifact motion seen in the 2-photon images. The impact depth with the lateral model could also be easily controlled. While ICWs were seen with this model, consistency and hemorrhaging were major issues. In the vertical injury model, we used a custom formed micropipette glass as the new impactor. The glass micropipette was optically transparent at high magnification but not at low magnification which allowed the tip to be properly positioned before testing. Immediately after vertical injury impact, a calcium wave was propagated from the site of injury into the surrounding region. The spread of the ICW could be blunted by pre- treatment with apryase, but not FFA, suggesting that the main mode of ICW transmission is through extracellular ATP activation.

A limiting factor in this vivo study was the severity of the injury produced by the microCCI. The impact severity was limited by two things: the working distance of the objective and the need to remain below the threshold for blood brain barrier (BBB) breakdown. The impact depth in the vertical injury model was set by the length of the pipette which could be no longer than the 2mm working distance of the objective, making the actual impacting depth the 2mm minus the width of the impact depth and the height of the walls of the custom made mouse head plate. The second limiting factor was that all impacts needed to be below the thresholded for BBB compromise of around 17.2% (Shreiber, 1998; Shreiber et al., 1997). The opaque nature of blood blocks any fluorescent excitation or emission of the fluorophores.

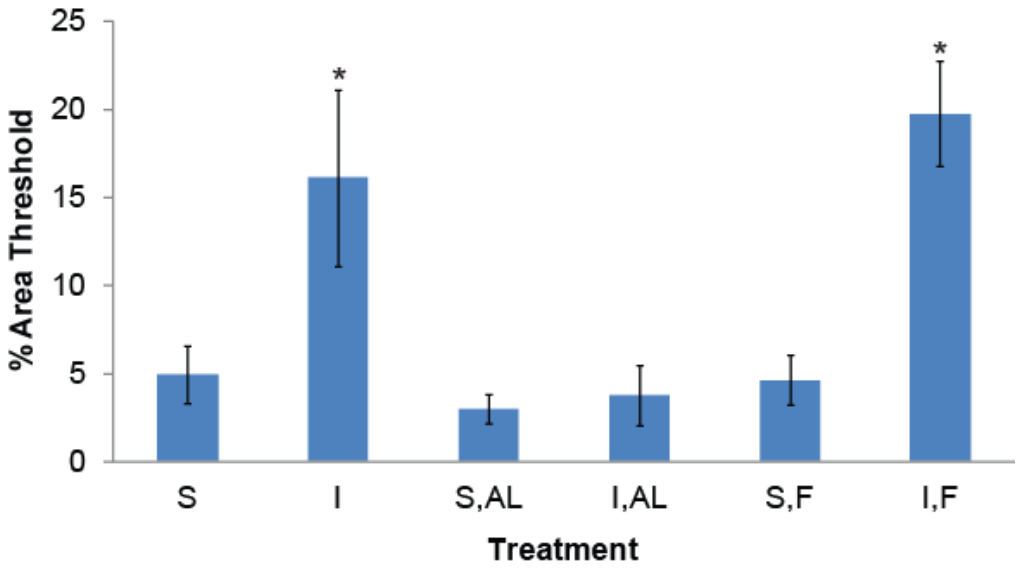

Figure 3.9. Peak thresholded area after impact.
Untreated and FFA injured mice had significant greater response area than their respective shams (*, $p<0.05$, S=Sham, I= Injured, AL= Apyrase, F=Flufenamic Acid).

These two limiting factors place some perspective on the strains produced by the micro impactor. As FFA was not able to reduce the level of calcium signaling *in vivo* but apyrase was, this suggests that the peak strain was below 15%. It is possible that gap junctions is not the

predominate pathway of calcium waves *in vivo* impact regardless of strain. To help answer this question, a finite element analysis of the micro impact could determine the strain and strain rates the micro impact had on the cortex.

It is important to note the difference in the regions of interest between the *in vitro* and *in vivo* studies. *In vitro* studies conducted by Miller (2009) focused on understanding the ICWs in the penumbra region. They note that the response in the injured stretch region was different, on average lower, but more variable than the calcium response in the penumbra region. In this study, we focused on the site of injury. With the lateral impact model, we imaged the penumbra region however the response that we created with the impact was small and did not easily spread to nearby cells. However, by focusing on the site of impact, we were able to detect strong ICWs from astrocytes in response to mechanical trauma.

While we showed that extracellular ATP was responsible for the bulk of the ICWs, we have not shown which P2 receptors – P2X or P2Y – were responsible. *In vitro* results suggest P2Y receptors, which are GqGPCRs, as the more likely culprits (Miller, 2009; Morrison et al., 2011), however P2X receptors have been implicated in inflammation and apoptosis of both astrocytes and microglia (Franke et al., 2012), and may possibly explain gliosis after TBI. Furthermore, higher levels of extracellular ATP can also activate P2X7R which can lead to influx of extracellular calcium into the cell (James and Butt, 2002). We have also not shown if any glutamatergic receptors might have a role in the ICW transmission *in vivo*. Despite the limitations of the small impacted strains, we have shown that the *in vivo* astrocytic syncytium responds to a mechanical force with an ICW that propagates from the site of injury outward and the main mechanism is extracellular ATP.

Chapter 4 Inhibited IP3 signaling in astrocytes *in vivo* after TBI leads to partial alteration of neurological deficits and changes in glial reactivity

ABSTRACT

Intracellular calcium alterations in astrocytes are a major mechanism for controlling a broad number of astrocyte functions that include trophic factor and neurotransmitter release, hypertrophy, gliovascular coupling, and neuronal metabolic support. The phospholipase C (PLC)/inosital 1,4,5 triphosphate (IP_3) pathway is a key pathway for communicating calcium signaling across the astrocyte syncytium *in vivo*, yet the role of this pathway in controlling outcome after traumatic brain injury (TBI) is unknown. In this chapter, we tested directly if actively reducing the IP_3 signaling within astrocytes *in vivo* led to any alteration in either behavioral or histological outcome after TBI. We used the controlled cortical impact (CCI) model and examined if the effect of astrocyte specific IP_3 signaling was different following either mild or moderate TBI. We used a transgenic mouse line engineered to expressed venus tagged IP_3 phosphatase (VIPP) directly in astrocytes of mature animals, using a tet.On system. In a moderate CCI injury that include primary contusion and surrounding gliosis, VIPP animals showed worse behavioral outcome in the watermaze eight days after injury. Moreover, the extent of reactive astrocytes was reduced in VIPP animals compared to littermate wildtypes. After mild CCI injury, VIPP animals displayed transient behavioral impairment. Although *in vivo* 2 photon imaging showed that VIPP animals showed a reduction of the immediate spread of intercellular calcium waves from the injury site, this did not lead to an improvement of behavioral deficits after injury over wildtype. There was also no corresponding change in neuronal degeneration one day after injury. Eight days after mild injury, astrocyte reactivity was significantly increased in the cortex of VIPP animals compared to littermate wildtypes. This difference was seen in the ipislateral hippocampus or thalamus. Together, these data show that IP_3 signaling within astrocytes

contributes partly to outcome over the spectrum of mild to moderate TBI *in vivo*, potentially as a mediator in recovery of deficits at more severe levels of injury and as a contributor to early impairment after mild TBI.

INTRODUCTION

Astrocytes, the predominate glial cell type and distinguished by the expression of glial fibrillary acidic protein (GFAP) (Agulhon et al., 2008), are responsible for a variety of functions ranging from the regulation of blood flow to influencing synaptic transmission (Oberheim et al., 2006). Although not electrically excitable, astrocytes express a number of G protein coupled receptors (GPCR) and use calcium as the predominant medium for signaling (Agulhon et al., 2008; Zorec et al., 2012). The widely accepted mechanism for intracellular calcium increases in astrocytes is through the phospholipase C (PLC)/inosital 1,4,5 triphosphate (IP_3) pathway (Agulhon et al., 2008). Gq GPCR activation causes PLC to hydrolyze phosphatidylinositol 4,5 bisphosphate (PIP) into diacylglycerol (DAG) and IP_3. IP_3 activates IP_3 receptors (IP_3R) causing the release of calcium from the endoplasmic reticulum (ER) stores (Refer to chapter 3 figure 3.1).

Although the existence of physiologic intercellular calcium waves (ICWs) in astrocytes *in vivo* is under debate, it is known that calcium waves in astrocytes occur in a number of pathophysiologic states that include epilepsy, cortical spreading depression (Fiacco and McCarthy, 2006), and local ischemia (Ding et al., 2009). Recently, the incidence and progression of intercellular calcium waves in astrocytes after traumatic brain injury (TBI) was also demonstrated. The data showed ICWs contributing to both neuronal circuit dynamics and glial reactivity in the region surrounding the primary mechanical injury (Choo et al., 2013; Miller, 2009).

A primary candidate for mediating the communication of astrocyte intercellular waves *in vivo* is the IP_3 signaling cascade. In astrocyte cultures, stretch injury causes immediate (5-30min) and sustained (24 – 48hrs) increases in IP_3 (Floyd et al., 2001); inhibiting PLC activity with neomycin or U73122 reduced the level of reactive astrocytes after biaxial stretch (Floyd et al., 2004) and also prevented depletion of intracellular calcium stores (Weber et al., 2001).

Alternatively, blocking a key upstream activator of the IP_3 signaling cascade (metabotropic glutamate receptors; mGluRs) also reduced stretch induced astrocytic intracellular calcium levels *in vitro* as well as prevented depletion of ER calcium stores (Chen et al., 2004). Both of these pharmacological approaches have shown efficacy when used in experimental TBI models (Golding and Vink, 1994) (Lyeth et al., 2001), but neither approach provides a direct examination of how the IP_3 signaling within astrocytes specifically contributes to outcome after TBI.

In this chapter, we studied the effect of reducing IP_3 signaling in astrocytes on injury recovery. Unlike prior studies that used the application of drugs, we used transgenic mice overexpressing a venus tagged IP_3 phosphatase (VIPP) gene specifically in cells that expressed GFAP (Figure 4.1). As a result, this transgenic tool allowed us to directly test for the role of IP_3 signaling in astrocytes on the outcome after TBI. Our results show that IP_3 signaling contributes in a complex manner over the spectrum of TBI. It is important for recovery after more severe forms of TBI, possibly hinders recovery after mild TBI, and contributes to alteration in glial reactivity.

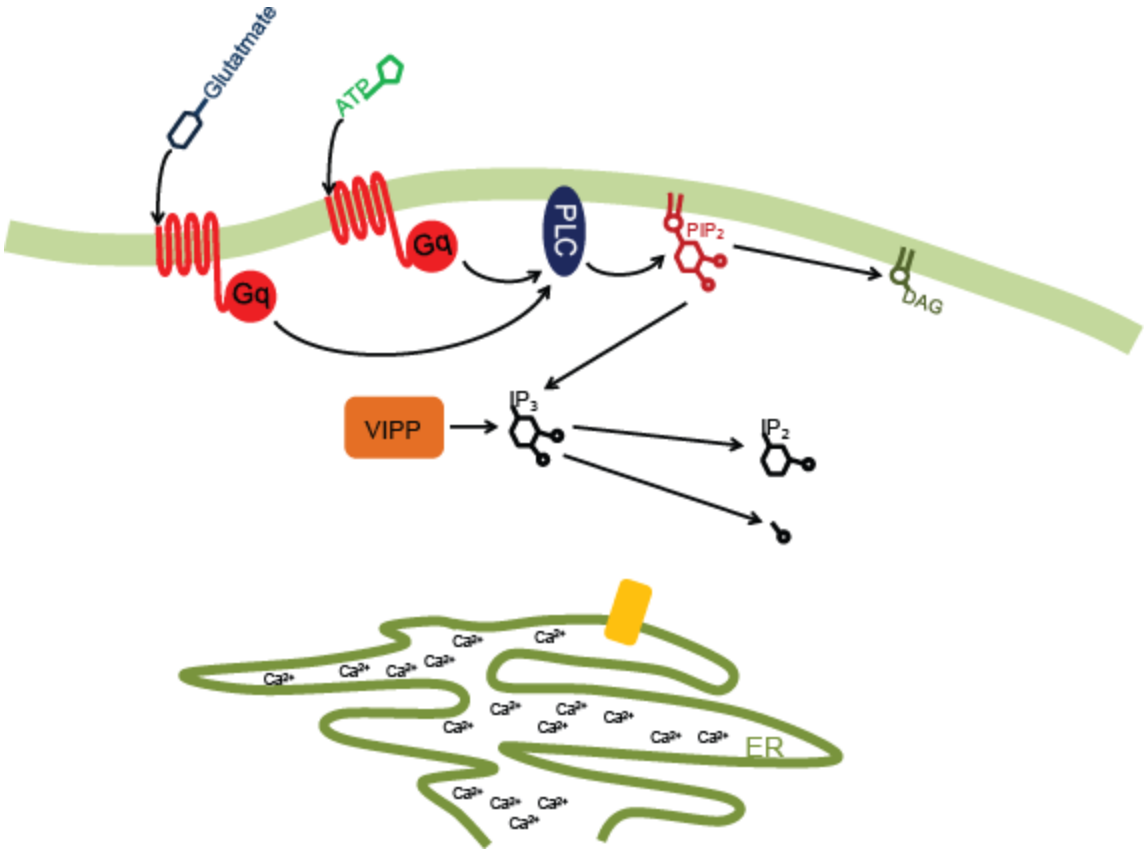

Figure 4.1. VIPP prevents IP3 induced calcium release from internal stores.
VIPP catalyzes the reaction of IP_3 into IP_2 (1-phosphatidyl-1D-myo-inositol 4-phosphate) and a phosphate. IP_2 is unable to activate IP_3R, thereby preventing the release of calcium from the ER. (ER = endoplasmic reticulum).

MATERIALS AND METHODS

VIPP mice were exposed to two different injury levels using the same type of direct cortical deformation injury model – controlled cortical impact (CCI). For producing moderate injuries, we used a 6m/s impact velocity and an impact depth of 1mm to create a primary hemorrhagic contusion that formed a large necrotic lesion 8 days after injury. For studying mild injuries, we used an impact velocity of 0.43m/s and an impact depth of 2mm to create areas of blood-brain

barrier breakdown, early neuronal degeneration in the cortex and hippocampus, but no primary contusion or secondary tissue loss.

We evaluated both the histological and behavioral impairments across these two distinct TBI injury levels. We developed a separate set of behavioral tasks that allowed us to examine cortical and hippocampal function in the mild TBI group. The injury and behavior schedule is shown in Table 4.1. For the more moderate CCI group, the neurological severity score (NSS) and the Morris water maze (MWM) was used. For the mild CCI group, a three day rotarod protocol was followed by spatial object recognition (SOR), and then by contextual fear conditioning (FC).

Table 4.1. Behavioral Schedule

	Day -1	**Day 0**	**Day 1**	**Day 2**	**Day 3**	**Day 4**	**Day 5**	**Day 6**	**Day 7**	**Day 8**
CCI		NSS	NSS	NSS		NSS MWM	MWM	MWM	NSS MWM	Probe
mCCI	RR training		RR	RR	RR	SOR	SOR		FC	FC

VIPP Breeding

VIPP animals were bred and raised as first described in Halassa (2009). Animals were bred under 12hr light/dark cycles. Pups were weaned at 3 weeks of age and genotyped. Details of producing GFAP.tTA and tetO.VIPP lines are described elsewhere (Halassa, 2009). These lines were maintained in a heterozygous state and backcrossed onto a C57B16/J genetic background (Jackson Laboratories, Bar Harbor, ME). Bigenic offspring of these two lines (VIPP), and their wildtype littermates, were maintained on 40 mg/kg doxycycline (dox) containing food (Bioserv, Frenchtown, NJ). They were switched to a regular diet to allow full transgene expression in the VIPP animals for a minimum of 2 weeks prior to use. A portion of the bigenic animals were kept on dox for the duration of the experiments, serving as an additional comparison group to both the

VIPP and littermate wildtype mice. Due to the potential effect progesterone has on the recovery of brain injury (Feeser and Loria, 2011; Shakeri et al., 2013), only male mice were used.

2-photon imaging and injury

The protocol for in vivo 2-photon imaging during impact was the same as described in chapter 3. Please refer back for details.

Cortical Impact Brain Injury

All animal procedures were approved by University of Pennsylvania's Institutional Animal Care and Use Committee (IACUC). VIPP and littermate wildtype (WT) mice were divided into the following groups:

Table 4.2 Experimental Groups – Numbers indicate the numbers of animals in each group

	Injury			**Sham**		
	CCI	mCCI		CCI	mCCI	
	8 day	24hr	8 day		24hr	8 day
VIPP	14	5	14	11	4	13
on Dox	12	4	11	15	NA	10
WT littermates	26	6	14	27	5	13
on Dox	26	NA	16	25	NA	13

On the day of injury, mice were anaesthetized with isoflurane (5% induction, 2% maintenance) and placed in a stereotaxic frame. A 4-mm craniotomy was produced on the left hemisphere, midway between bregma and lambda. The moderate CCI injury was produced using a pneumatic driven device (Smith 1995, Dixon 1991). The impact speed was 5.8-6.0 m/s with a rounded, brass cylindrical impactor tip 3mm in diameter. Mild controlled cortical impact (mCCI) brain injuries were produced using an impactor speed of 0.43 m/s and a cortical impact depth of 2mm. The injury device consists of a solenoid (SoftShift 2EPM, Ledex, Vandalia, OH) attached to a linear potentiometer (Omega LP803-1, Stamford, CT). A custom Matlab (Mathworks, Natick, MA) program actuated the solenoid and collected the potentiometer readings. The solenoid-potentiometer was positioned in place with a custom built adjustable angle attached to a digital

linear stage. The angle of the impactor was measured and set with a digital angle meter to 20° from vertical. The 4 mm diameter hemispherical impactor tip was made of Sylgard® 184 (Dow Corning, Midland, MI). After either injury, the cranial exposure was sutured close, and the animals were placed in a warmed cage to recover until ambulatory.

Histology

Mice were anaesthetized with an overdose of sodium pentobarbital. Animals were transcardially perfused with 30 ml of ice-cold phosphate buffered saline (PBS) (pH 7.4) and then 40 ml of freshly hydrolysed ice-cold 4% paraformaldehyde. Brains were harvested, post-fixed overnight in 4% paraformaldehyde at 4°C and then cryoprotected in 24% sucrose. Tissue was mounted in Tissue-Tek® (Fisher Scientific, Hampton, NH) and was frozen in isopentane cooled with dry ice. Tissue was cryosectioned at 20 µm. Sections were taken 500µm apart starting from bregma -1.5 to -3.5.

For fluoro-jade® B (FJB; Millipore, Billerica, MA) labeling, sections were rehydrated in graded ethanols (100%, 95%, 80% 70%; 2 min each) followed by distilled water. Sections were then incubated in a solution of 0.06% potassium permanganate on a rotating stage for 20 minutes, rinsed in distilled water for 2 minutes, and placed in a 0.0005% FJB solution (5mL of a 0.01% stock solution of FJB to 95 mL of 0.1% acetic acid). After 30 minutes in the FJB staining solution, the sections were rinsed with three changes of distilled water for 1 min per change. Excess water was drained onto a paper towel, and the sections were air dried in an oven at 37° for 30 min. The dried sections were cleared by immersion in xylene for at least 2 minutes before coverslipping with permount (Fisher Scientific, Hampton, NH). The sections were viewed with a Leica SP5 confocal microscope (Leica, Germany).

To stain for astrocytes and microglia, sections were rehydrated in 1×PBS (3times 5min each) and then incubated with 10% normal goat serum for 30 minutes with 0.1% triton-X. The

sections were incubated overnight at room temperature in polyclonal anti-GFAP (1:500; Neuromics, Edina, MN) or anti-Iba-1 (1:1000; Wako, Richmond, VA). After rinsing with 1×PBS, sections were then incubated with Alexa 546 conjugated secondary for 1hr at room temperature. Sections were mounted with ProLong Gold antifade (Invitrogen, Grand Island, NY).

To measure the fraction of tissue spared, the total volume of twelve to fourteen sections across the span of the lesion on the ipsilateral side were divided by the volume of the contralateral side. Because the ipsilateral side of the brain showed shrinkage, traditional lesion volume was determined as percent tissue spared.

Behavior Tests

Rotarod :The rotarod protocol was adapted from Oliveira et al (2011). In short, the rotarod apparatus (Med Associates Inc, St. Albans, VT) has a 3.2 cm diameter rotating rod raised 16.5 cm above a platform and divided into five sections for testing multiple mice simultaneously. The rotarod gradually increases its rotation speed from 4 to 40 rpm over the course of 5 min. Latency to first fault (defined as the mouse riding with the platform in a single rotation) as well as fall time was recorded. Mice were trained on the rotarod at 4 rpm for sixty seconds twenty-four hours before injury. Three trials a day were given during three consecutive days with an inter-trial interval of 1 h. Each trial started at the same time every day and ended when mice fell or when mice ran for 300 sec.

Spatial Object Recognition: The spatial object recognition (SOR) protocol was adapted from Oliveira et al (2010). In short, the experimental apparatus consisted of a gray rectangular open field (60 cm × 50cm × 26 cm) with a visual cue placed on the arena wall. Prior to training, mice were handled for 1 minute a day for 3 days. During the training day, mice received four 10 minutes training sessions. Between sessions, mice were placed back in their home cage for three minutes. During the first session, mice were habituated to the gray rectangular open field in the

absence of objects, but with an internal cue on one of the four walls. During the next three sessions, mice were placed in the same box but now with two distinct objects - a glass bottle (100mL volume) and a metal tower (1.5625 in^2). Any mouse that successfully climbed either object was removed from behavioral analysis. Mice were allowed to freely explore the environment and the objects for 10 minutes. After 24 hours, mice were placed back in the rectangular environment for the testing phase. The two objects were again present, but one of the two objects was now displaced to a novel spatial location. Mice were again allowed to freely explore the environment and the objects for 10 minutes. Time spent exploring the displaced and non-displaced objects was measured. Exploration was analyzed during both the training and testing phases. The identity of the objects, as well as the spatial location in which the objects were located, was balanced between subjects. The response to spatial change was assessed by comparing the mean time the mice spent exploring the objects (when mice were facing and sniffing the objects within close proximity and/or touching them) belonging to each category (displaced and non-displaced) in the test session minus the mean time spent in contact with the same object category in the last training session. A positive value indicates recognition of the spatial change.

Contextual Fear Conditioning: In the contextual fear conditioning (CFC) test, mice were placed in a testing chamber (Coulbourn, Whitehall, PA) on training day for 3 minutes. Two minutes and twenty-eight seconds into the three minute period, mice were given a single 2 seconds long, 1.5mA shock. Twenty four hours later, mice were place in the same testing chamber and their percent freezing was calculated across the course of 5 minutes.

Morris Water Maze: The Morris water maze (MWM) was used to test spatial learning and memory as a measure of hippocampal functionality (D'Hooge and De Deyn, 2001; Vorhees and Williams, 2006). The maze was conducted over the course of 5 days with the first day of MWM occurring 4 days after injury. On each of the first four days of watermaze testing, mice were

expected to find a hidden platform in four trials from each of the four directions (N, S, E, W). The order of the starting direction was altered each day so as not to accustom the animals to the procedure. The time required for each mouse to find the platform is the latency time. The four trials on each day were averaged. A mouse that could not find the platform in 90 sec was given latency time of 90 sec and then led to the platform by hand. Each mouse was required to stay on the platform for 15sec before being picked up so they may learn that getting on and staying on the platform was required for exiting the maze. The probe trail was conducted on the fifth day (Day 8 post injury). The platform was removed and the mouse allowed to swim for 30 seconds. The memory score was determined based on Smith et al (1991).

Neurological Severity Score: The neurological severity score (NSS) was used to assess motor function and reflex at specific time points after injury: 1hr, 4hrs, 1day, 2days, 4 days, and 7days. The NSS used here was composed of 10 tasks (Flierl et al., 2009). Each failed task received a score of 1 for a total of 10 for failing all ten tasks. The tasks are listed in Table 4.3.

Table 4.3 Neurological Severity Score Task List

Task	Description
Exit circle	The ability to exit a 30cm diameter circle within 3min
Mono/Hemiparesis	Paresis of upper and or lower limb on the contralateral side
Straight walk	Ability to walk in a straight path when placed on the floor
Startle reflex	Measures innate reflex. Mouse will bounce in response to a loud noise
Seeking behavior	Physiological behavior as a sign of "interest" in the environment
Beam balancing	Ability to balance on a 7mm wide beam for at least 10sec
Round stick balancing	Ability to balance on a round 5mm diameter stick for at least 10 sec
Beam walk: 3cm	Ability to walk across a 30cm long beam
Beam walk: 2cm	Ability to walk across a 30cm long beam
Beam walk: 1cm	Ability to walk across a 30cm long beam. Most difficult of the three beams

Statistical Analysis

All statistical tests were carried out using JMP10 (SAS Institute, Cary, NC). The variance among groups was first tested for normality (Shapiro-Wilks test) and then equality (Bartlett test). When the variance among groups was not similar, the two sample t test was used; otherwise a one way analysis of variance (ANOVA) was used. A two way ANOVA was used to look for significance between genotype and injury. A repeated measures ANOVA was used in the rotarod and watermaze behavioral tests.

RESULTS

VIPP mice show worse behavioral deficits after moderate cortical impact injury

A minimum of two weeks before any procedures, mice were taken off the dox diet to allow the transgene to fully express (Halassa, 2009). Moreover, the normal grooming behavior and general activity of the VIPP mice did not differ from their WT counterparts, nor did this behavior different between VIPP animals maintained on a dox diet.

Following moderate cortical impact injury, both VIPP mice and littermate wildtype mice showed no difference in performing the NSS tasks, but did show significant differences with their surgical sham counterparts ($p<.0001$). VIPP and WT littermates sham animals showed no difference in performance suggesting that in these simple neurological scoring tasks, the transgene does not affect baseline NSS behavior. In addition, there was no significant difference in NSS scores between VIPP and WT on dox injured and sham animals from their off dox counterparts suggesting that dox did not measurably affect NSS outcome (Figure 4.2). At the one hour time point after injury, all injured groups had averaged an NSS score of 8 (VIPP injured 7.9±0.4, VIPP on dox injured 7.8±0.3, VIPP sham 1.6±0.3. VIPP on dox sham 2.0±0.4, WT injured 8.2±0.2, WT on dox injured 7.6±0.2, WT sham 1.5±0.2, WT on dox sham 1.0±0.2). Almost all animals maintained their startle reflex and most animals in the injured group

maintained seeking behavior. Sham animals performed almost all tasks. The most difficult task was the round stick balancing; almost all mice failed to accomplish this task.

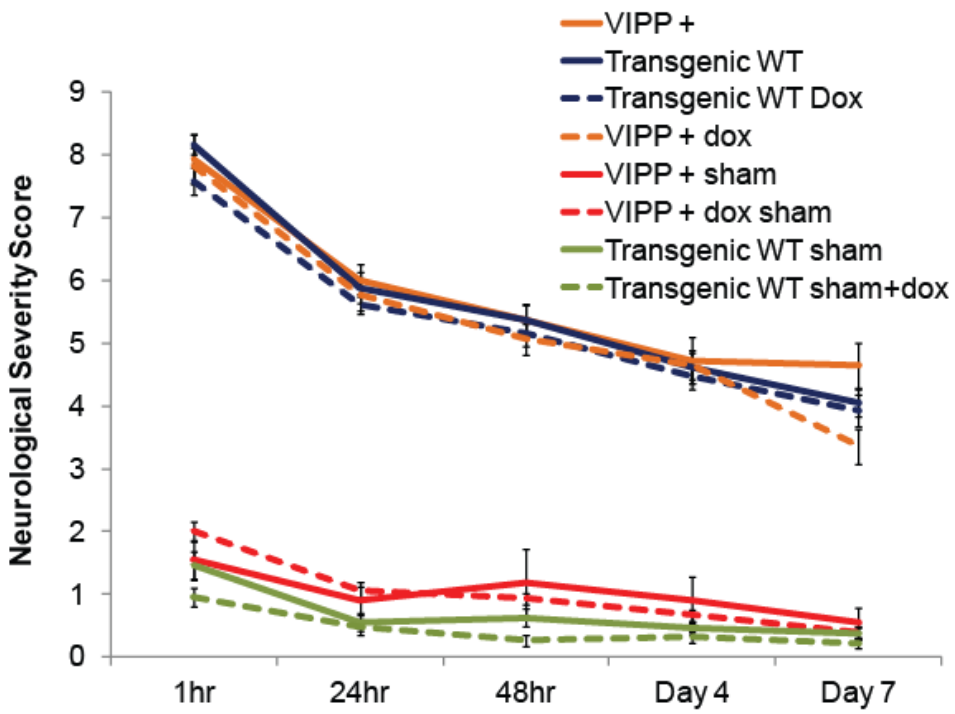

Figure 4.2. VIPP did not affect NSS behavior.
NSS behavior did not vary across genotype for either sham or injured groups. All injured groups were significantly different from sham groups ($p<0.0001$). There was no effect from genotype or genotype×injury. Data are expressed as Media ± Standard Error of the Mean (S.E.M.).

The impact of IP_3 signaling through astrocytes became apparent when measuring animal performance in the Morris water maze. In the MWM, sham groups performed similarly across all four days (Figure 4.3). There was no significant difference between VIPP and WT littermate shams. In the injured groups, the initial performances were similar. On average the animals had a latency of around 70 sec (VIPP injured 72.7±4.6 sec, WT injured 69 ±3.1 sec, VIPP on dox injured 66.5 ±4.7 sec, WT on dox injured 65.8 ±4.5 sec). Over the course of the four days, all sham groups displayed similar learning behavior and the injured groups showed similar learning

behavior. A repeated measures ANOVA comparing the off dox groups (VIPP injured, WT injured, VIPP sham, WT sham; all off dox) showed significance between subjects with injury ($p<0.0001$) but not with genotype ($p=0.0697$) or genotype×injury ($p=0.1492$). Within subjects, there was significance with time ($p<0.0001$) and time×injury ($p=0.0165$) but not with time×genotype ($p=0.4016$) or time×genotype×injury ($p=0.1820$). Together these results suggest that the expression of the transgene alone had little to no effect MWM behavior and that the bulk of effects came from injury. However, when we compare the MWM performance on the first day (Day 4) with each of the subsequent days, we see that the performance at Day 7 compared to Day 4 showed a significant effect from injury ($p=0.0288$) as well that of the interaction between genotype and injury ($p=0.0412$). This suggested that by the last day of the watermaze, VIPP expressing injured animals performed significantly different from WT injured.

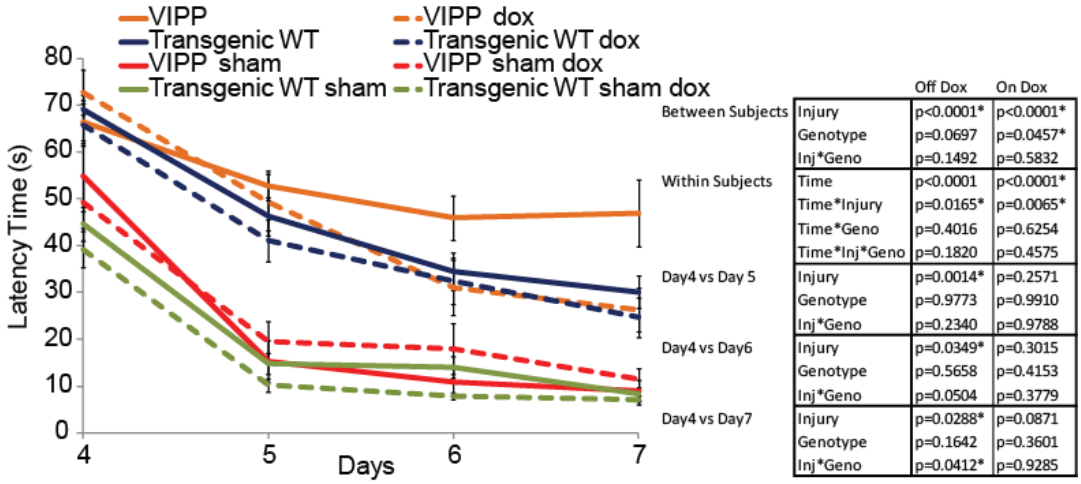

		Off Dox	On Dox
Between Subjects	Injury	p<0.0001*	p<0.0001*
	Genotype	p=0.0697	p=0.0457*
	Inj*Geno	p=0.1492	p=0.5832
Within Subjects	Time	p<0.0001	p<0.0001*
	Time*Injury	p=0.0165*	p=0.0065*
	Time*Geno	p=0.4016	p=0.6254
	Time*Inj*Geno	p=0.1820	p=0.4575
Day4 vs Day 5	Injury	p=0.0014*	p=0.2571
	Genotype	p=0.9773	p=0.9910
	Inj*Geno	p=0.2340	p=0.9788
Day4 vs Day6	Injury	p=0.0349*	p=0.3015
	Genotype	p=0.5658	p=0.4153
	Inj*Geno	p=0.0504	p=0.3779
Day4 vs Day7	Injury	p=0.0288*	p=0.0871
	Genotype	p=0.1642	p=0.3601
	Inj*Geno	p=0.0412*	p=0.9285

Figure 4.3. VIPP negatively affected MWM performance.
VIPP did not affect MWM latency scores until the last day. A repeated measures ANOVA was not significant except for injury between and within subjects. A repeated measures ANOVA comparing Day 7 latency to Day 4 latency times showed a significant interaction between genotype and injury. Data are expressed as Media ± S.E.M.

The on dox groups (VIPP on dox injured, WT on dox injured, VIPP on dox sham, WT on dox sham) in a repeated measures ANOVA between subjects showed significance due to injury ($p<0.0001$) and genotype ($p=0.0457$) but had no significance in the interaction (genotype×injury, $p=0.582$). Within subjects, the repeated measures ANOVA showed injury contributed significantly to behavioral changes over time (time×injury, $p=0.0065$) but not genotype (time×genotype, $p=0.6254$) or the interaction of all three (time×genotype×injury, $p=4575$). These results suggest that while the transgene on dox may have differed in behavior from WT on dox, their behavioral over time with and without injury did not differ.

In examining the probe trial on day 8, we saw VIPP injured animals performing significantly worse, averaging a memory score of 14±3.0 compared to the WT littermates' average of 45±5.1. A two way ANOVA test showed significant interaction between genotype and injury ($p=0.0155$) (Figure 4.4A). The VIPP on dox injured animals averaged a much higher memory score at 63.7±9.2, almost near sham memory scores. In contrast WT on dox injured only averaged 46.5±8.2. The similar performance between WT injured and WT injured on dox suggested that dox did not significantly alter behavioral performance and likely did not contribute to the improved performance to the VIPP injured on dox. The similar swim speeds between the injured groups (VIPP injured 16.9±1.5 cm/s, WT injured 16.42±0.6 cm/s, VIPP on dox injured 17.4±1.0 cm/s, WT on dox injured 17.9±0.7 cm/s, Figure 4.4B) suggested that the improved memory score of VIPP on dox injured group cannot be attributed to faster swim speeds. It is possible that the improved probe trial performance of the VIPP on dox injured group may potentially be due to elevated leaky transgene expression (Figure 4.5) as a result of increased GFAP expression after injury potentially driving increased VIPP expression (the VIPP transgene is driven off the GFAP promoter). VIPP on dox injured high memory scores compared to the other injured groups also could possibly be due to these mice relying on other memory paradigms

(taxonomy, or procedural; (Crawley, 2007)) rather than spatial memory to find their way to the platform location.

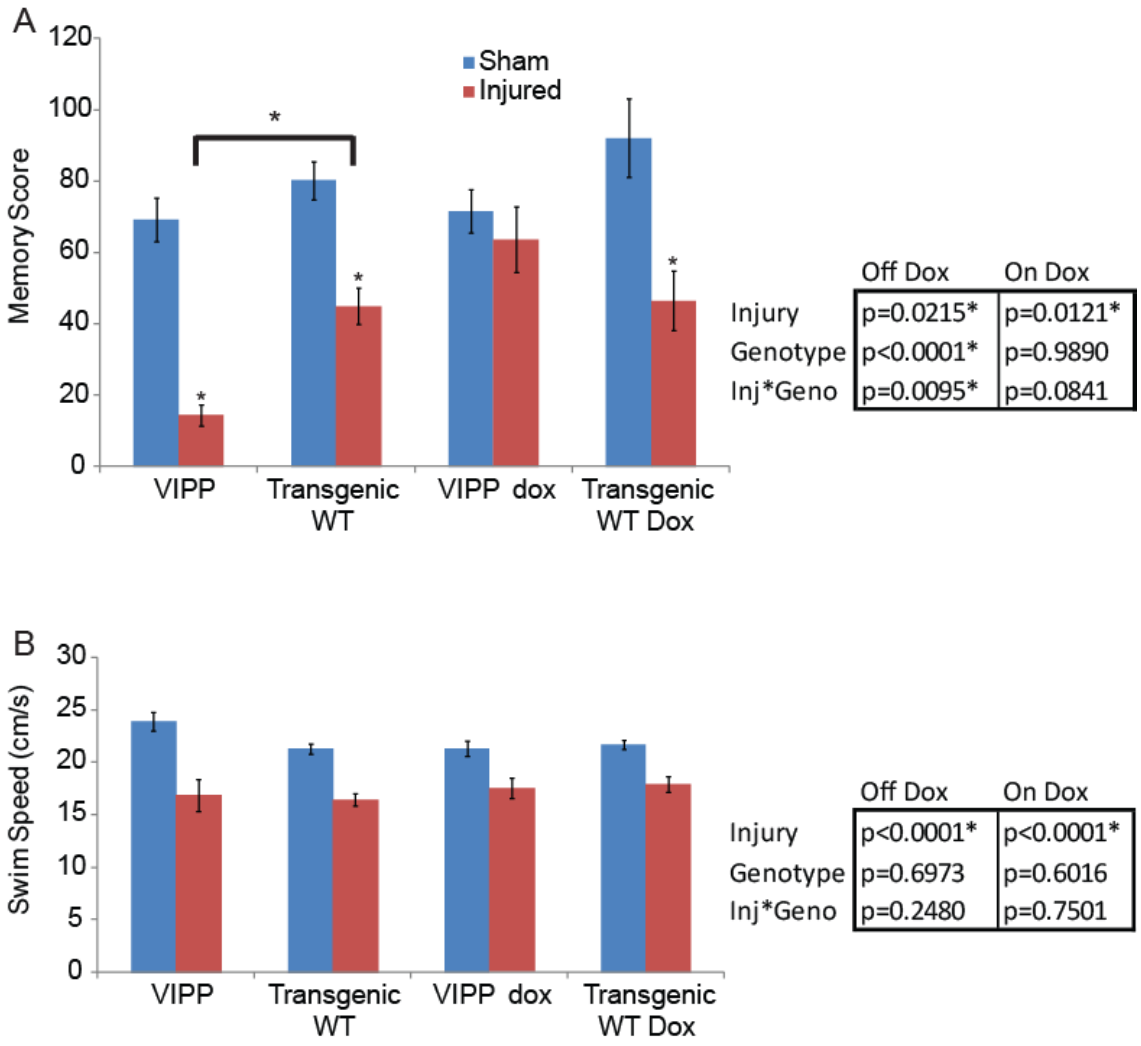

Figure 4.4 VIPP mice had decreased probe trial performance.
(A)VIPP mice performed significantly lower memory score on probe trial than either the transgenic WT or VIPP on dox animals. The WT and VIPP injured mice performed significantly worse than sham animals ($p<0.0001$). (B) Swim speeds were not different between genotype but were different between injured and sham ($p<0.0001$). Data are expressed as Media ± S.E.M.

Summarizing the behavioral results from the NSS and the watermaze showed that the overexpression of the IP_3 phosphatase did not affect baseline behavior. Blunting IP_3 signaling

after injury decreased spatial learning and memory. The difference in both the latency times at day 7 and the lower probe scores a day 8 suggested contrary to *in vitro* and *in vivo* neomycin studies, inhibition of IP_3 signaling to blunt calcium signaling in astrocytes impedes the recovery of brain injury in spatial learning and memory.

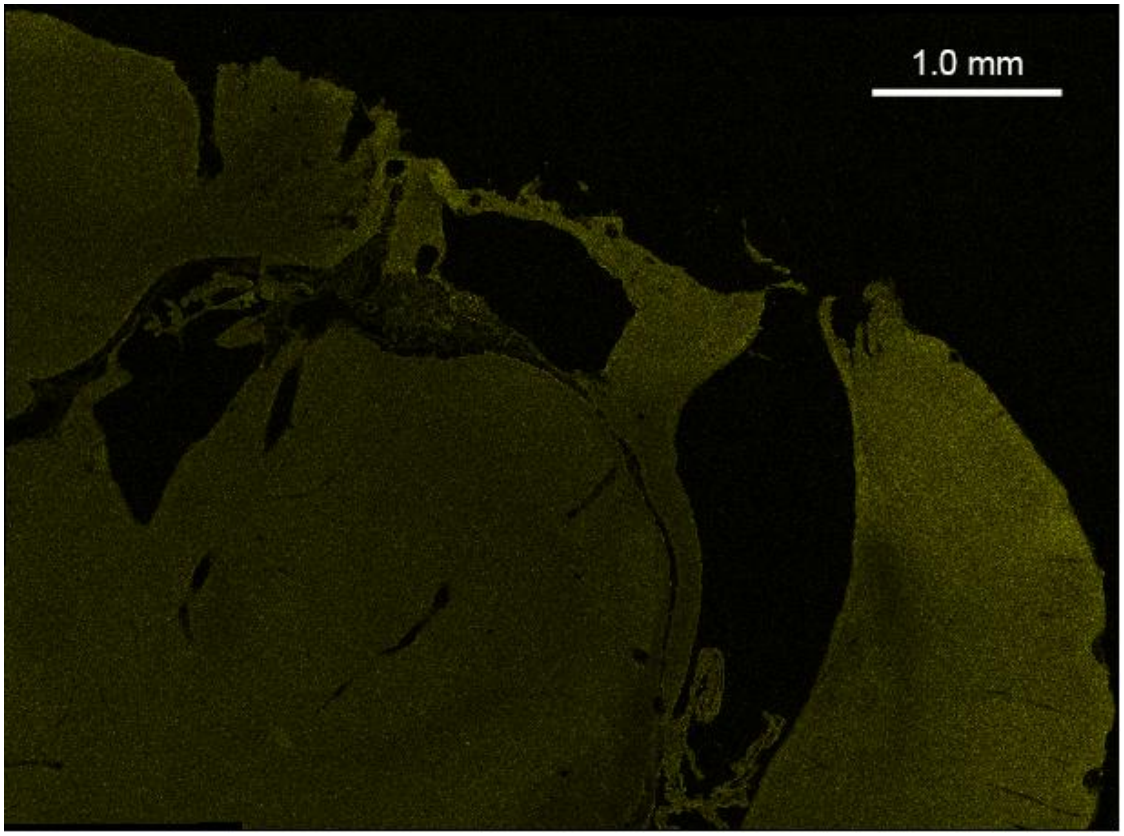

Figure 4.5. Expression of venus fluorescent protein in CCI injured VIPP on dox mice. The regions adjacent to the lesion (in the cortex and hippocampal remanants) showed presence of venus fluorescent protein suggesting leaky transgene expression occured in the on dox animals subject to CCI.

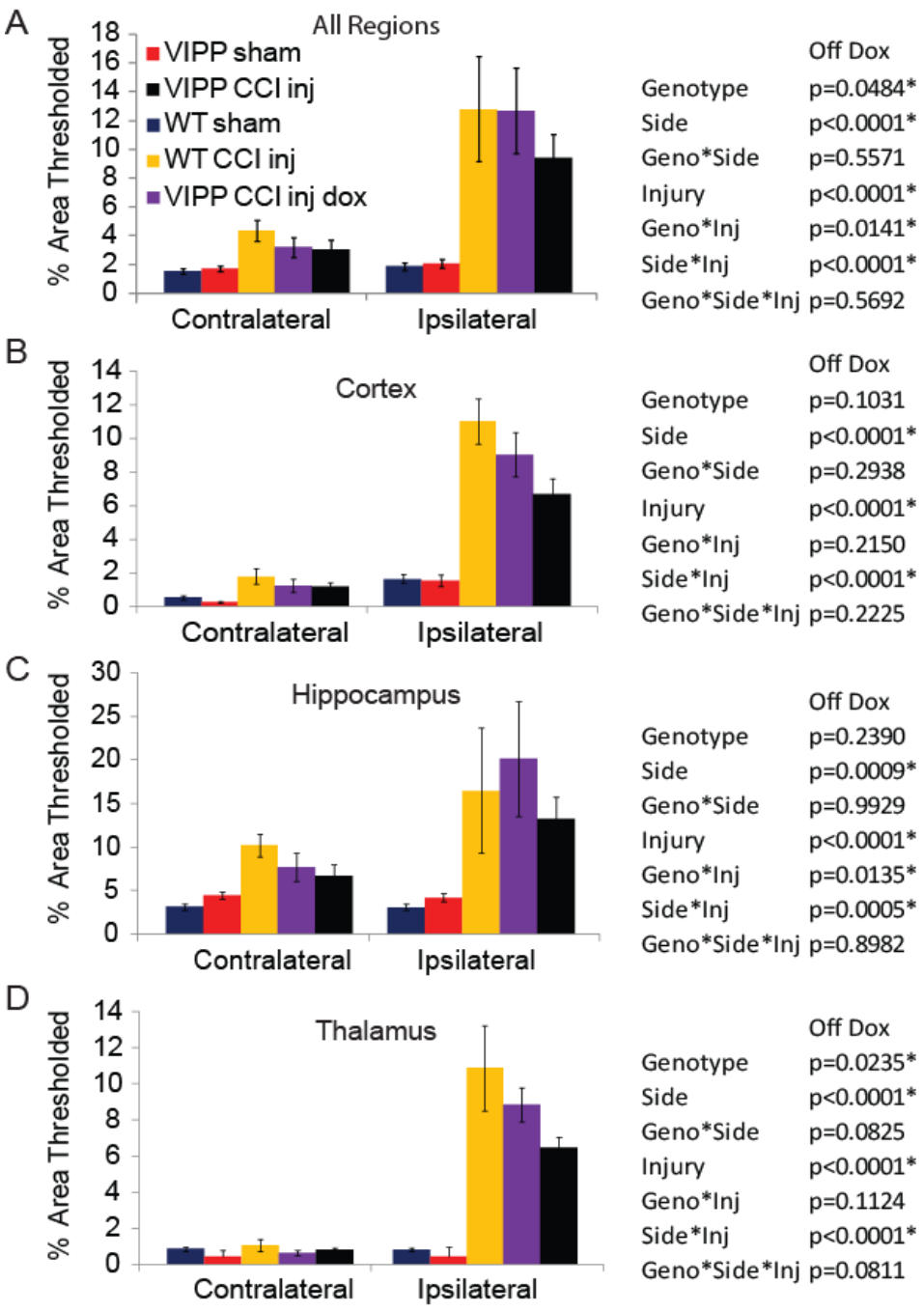

Figure 4.6. GFAP expression after CCI
VIPP animals showed significantly less GFAP expression than the WT CCI injured animals. The GFAP expression averaged across all regions (A), the cortex (B), the hippocampus (C), and the thalamus (D) all show that injury significantly increased GFAP expression in the ipsilateral compared to contralateral. CCI injured VIPP mice had reduced GFAP expression compared to WT (geno×inj) in the hippocampus and when averaging all regions together.

Astrocyte specific IP_3 signaling does not influence either cortical lesion size or the extent of astrocyte reactivity after moderate cortical impact injury

One indicator of damage is the amount of tissue loss that appears in the injured hemisphere after CCI. The lesion volumes among all three CCI injured groups were not significantly different (Figure 4.7). VIPP injured mice had slightly but not significantly increased tissue sparing compared to WT or VIPP on dox injured mice.

Comparing the results of a whole model ANOVA analysis yielded the following results: VIPP mice overall had lower GFAP expression than the WT counterparts. There was regional differences in GFAP expression; the hippocampus overall had the highest levels of GFAP expression across all regions and conditions compared to the cortex and thalamus. This trend was not different between VIPP and WT mice. Injury significantly increased GFAP expression. VIPP mice also had significantly reduced GFAP expression when injured (genotype×injury). Different brain regions also responded differently to injury (region×injury) but VIPP mice had similar trends in GFAP expression across the different brain region as WT mice after injury (genotype×region×injury).

Comparing only the results of the cortex showed that the contralateral and the ipsilateral GFAP expression were significantly different (region, region×injury) and that VIPP mice showed similar GFAP expression trends between contralateral and ipsilateral (genotype, genotype×region), with and without injury (genotype×injury, genotype×region×injury). Post hoc analysis using Tukey's honest significant difference (HSD), showed that

Analysis of the hippocampus showed that the contralateral and the ipsilateral regions had different GFAP expression after injury (region, region×injury). Similar to the cortex, the hippocampus had increased GFAP expression after injury (injury, region×injury). Unlike the cortex, the presence of the transgene significantly decreased GFAP expression after injury (genotype×injury).

Across all animal groups, we observed a significant increase in the extent of astrocyte reactivity in the ipsilateral hemisphere compared to surgical sham samples ($p<0.0001$). As expected, VIPP animals maintained on dox had similar levels of GFAP expression after moderate CCI injury when compared to WT injured counterparts. However, we saw no significant interaction between genotype and injury using linear regression analysis testing (Figure 4.6). In CCI injured animals, there was significantly greater GFAP expression on the contralateral hippocampus compared to sham animals ($p<0.01$) potentially suggesting that VIPP reduced the spread of the injury into the contralateral side.

In summary, these data on moderate cortical impact show the suppressing IP3 signaling within astrocytes leads to an enhancement in neurobehavioral impairment measured in the Morris water maze and a related deficit in the probe trial. However, neither of these was accompanied by significant changes in the tissue spared or changes in astrocyte reactivity measured 8 days after injury. With these changes after moderate cortical impact injury recorded, we next examined if there were significantly different effects of IP3 signaling in astrocytes after mild CCI injury.

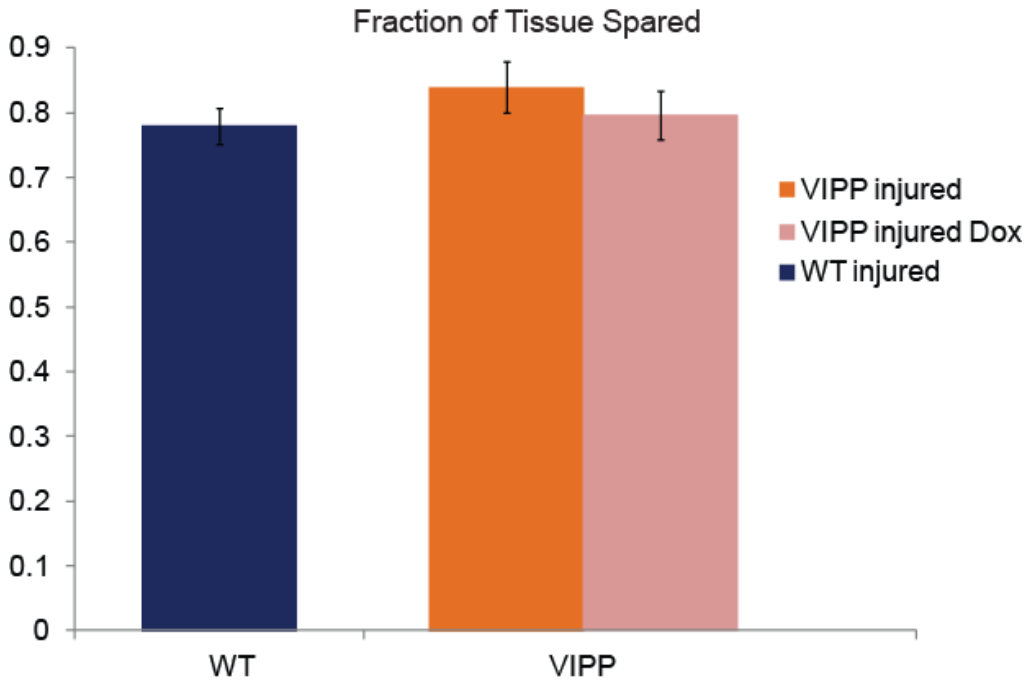

Figure 4.7. Lesion Volume. The fraction of spared tissue on the ipsilateral side compared to the contralateral side was not different between the injured groups. Data are expressed as Media ± S.E.M.

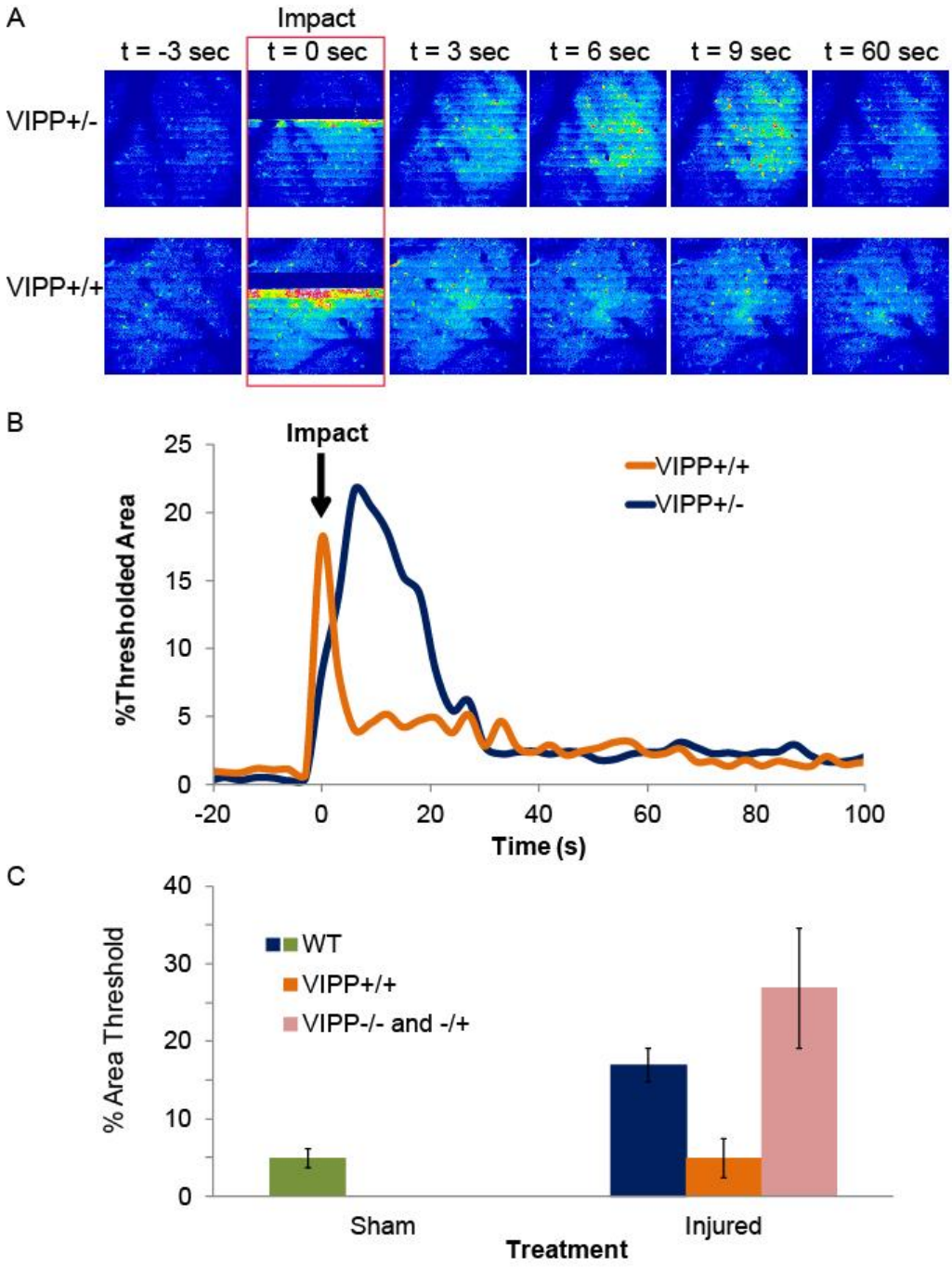

Figure 4.8. Expression of VIPP reduced mechanically induced intercellular calcium waves in astrocytes.
Mechanical injury produced a more robust response in VIPP single gene animal (VIPP+/-) compared to the bigenic animal (VIPP+/+) (A). The percent thresholded area of the cortical calcium response is plotted in (B). (C) The percent thresholded area of a VIPP bigenic animal had significantly reduced calcium response after impact compared to VIPP single gene and WT animals (*, $p<0.05$ compared to WT injured). Data are expressed as Media ± S.E.M.

Suppression of IP_3 signaling in astrocytes limits injury induced intercellular calcium waves

Previous work shows that a focused impact to the cortex will cause a propagation of intercellular waves in vivo through the astrocyte syncytium. This in vivo impact model to the superficial cortical layers does not cause any bleeding, and the mechanical conditions are similar to the mild CCI injury technique we developed previous (see chapter 2). Therefore, we used this model to study the role of IP3 astrocyte signaling in propagating mechanically induce intercellular waves in vivo after injury. VIPP and WT littermates were injured using the micro CCI technique (see chapter 3). Compared to single gene VIPP mice, bigenic VIPP (VIPP+/+) mice showed a reduction in the spread of the intercellular calcium wave throughout the astrocyte network after injury (Figure 4.8A). Immediately after impact, the VIPP bigenic calcium response was smaller and decayed faster than the VIPP single gene (Figure 4.8B). The peak thresholded area after impact was significantly greater in WT mice and in the single gene mice than in bigenic VIPP mice (Figure 4.8C, $p<0.05$ compared to WT injured).

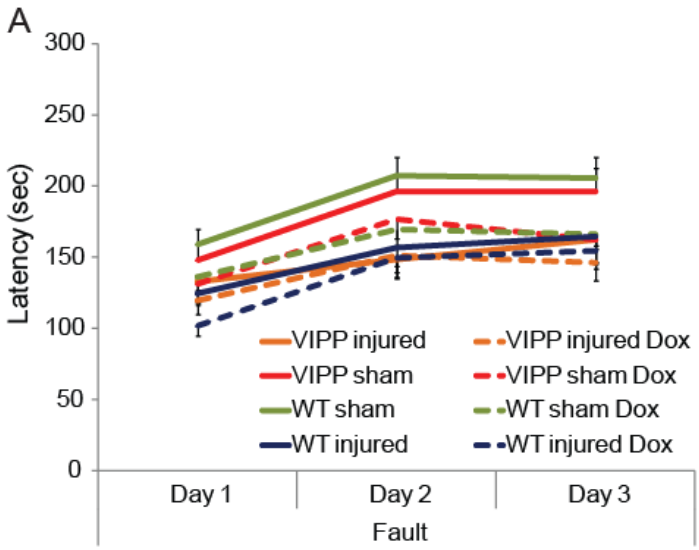

	WT	Fault
Between Subjects	Injury	p=0.0045*
Within Subjects	Time	p<0.0001*
	Time*Inj	p=0.5888
	VIPP	
Between Subjects	Injury	p=0.0363*
Within Subjects	Time	p=0.0037*
	Time*Inj	p=0.1323
	VIPP vs WT	
Between Subjects	Genotype	p=0.5695
	Injury	p=0.0005*
	Geno*Inj	p=0.6246
Within Subjects	Time	p<0.0001*
	Time*Geno	p=0.7425
	Time*Inj	p=0.1009
	Time*Geno*Inj	p=0.7675

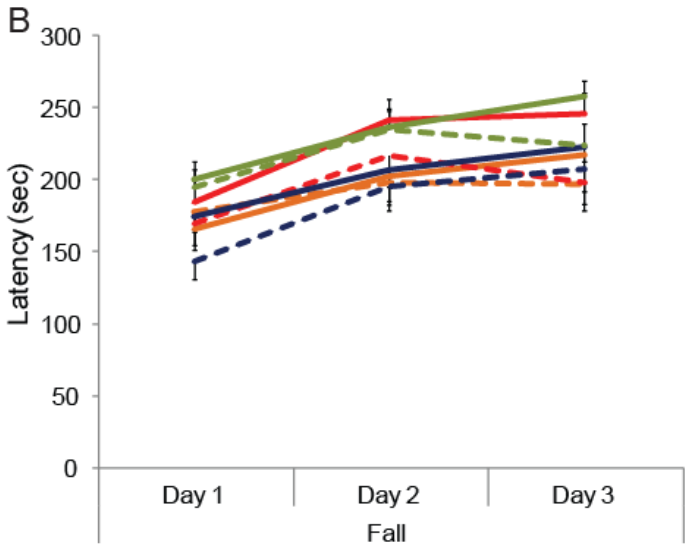

	WT	Fall
Between Subjects	Injury	p=0.0284*
Within Subjects	Time	p<0.0001*
	Time*Inj	p=0.8285
	VIPP	
Between Subjects	Injury	p=0.1492
Within Subjects	Time	p=0.0002*
	Time*Inj	p=0.3992
	VIPP vs WT	
Between Subjects	Genotype	p=0.5486
	Injury	p=0.0120*
	Geno*Inj	p=0.9545
Within Subjects	Time	p<0.0001*
	Time*Geno	p=0.4669
	Time*Inj	p=0.6130
	Time*Geno*Inj	p=0.6247

Figure 4.9. VIPP had a mild effect on rotarod behavior.
There was a significant difference in the performance of injured mice. However a lack of significant interaction between genotype and injury suggested that the transgene did not alter post injury behavior on the rotarod. The VIPP on dox injured mice did not perform significantly different from the WT injured mice across all three days for both fall and fault parameters. WT injured mice performed significantly worse compared to sham in both fault and fall parameters whereas VIPP injured mice did not show a deficit compared to VIPP sham mice in the fall parameter. No significant interaction was observed between genotype and injury in a linear regression test. Data are expressed as Media ± S.E.M.

Reduction in astrocyte IP_3 signaling leads to a modest, but not significant, reduction in some behavioral deficits after mCCI Injury

For the initial rotarod testing over the first three days after injury, WT littermate injured animals displayed significantly time to fault for all three days (Figure 4.9A). A repeated measure ANOVA showed no significant interaction between genotype and injury or between genotype, injury, and time. There was a significant deficit in behavior due to the injury ($p=0.0005$ off Dox, $p=0.04285$ on Dox) and with time ($p<0.0001$ for both off and on Dox groups) suggesting that over the course of the three days, all animals improved their rotarod performance. In the fall parameter of the rotarod (Figure 4.9B), a repeated measures ANOVA showed an effect due to injury ($p=0.0005$) in the off Dox groups but not in the on Dox groups ($p=0.1037$). Both off and on Dox groups had a significant effect from time ($p<0.0001$ for both off and on Dox groups) suggesting that all groups improved fall latency scores over the three days. As expected, VIPP animals maintained on dox injured had both fault and fall times that were not significantly different from WT injured across all three days of testing. VIPP sham animals had shorter but not significant fault and fall times than WT sham suggesting that genotype did not affect motor coordination and memory, similar to NSS sham results.

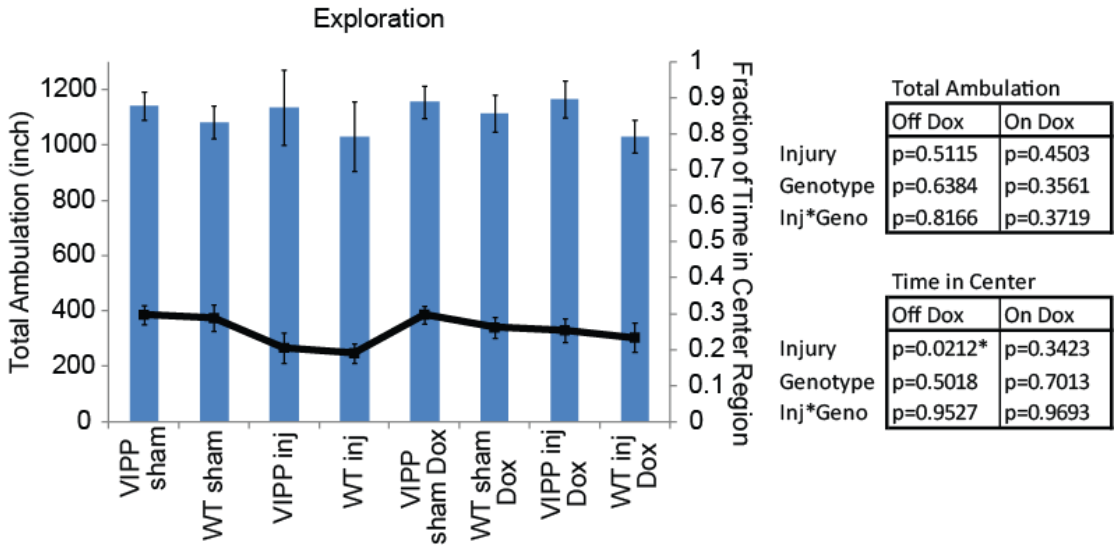

Figure 4.10. Behavior during session 1 of SOR.
All groups had similar total ambulation distances. Off dox injured animals spent significantly more time on average than off dox sham animals in the periphery (p=0.0212) but on dox injured and sham groups spent a similar amount of time in the center; there was no effect of genotype on exploratory behavior. Data are expressed as Media ± S.E.M.

In the first session of the SOR test, mice were allowed to explore the empty test arena to acclimate them to the testing environment. Examining their exploratory behavior in an open arena during these 10 minutes can shed light on their levels of anxiety (Bailey and Crawley, 2009). During this training session, all animals – sham or injured – show similar ambulation distances (Figure 4.10). There were no differences in any of the groups in the total amount of distance traveled in the box suggesting that neither injury nor transgene expression affected basic motor function. However, injured mice spent significantly less time in the center region than sham mice (p=0.0212), suggesting that injury increased anxiety levels in mice. There was no effect of genotype in these parameters.

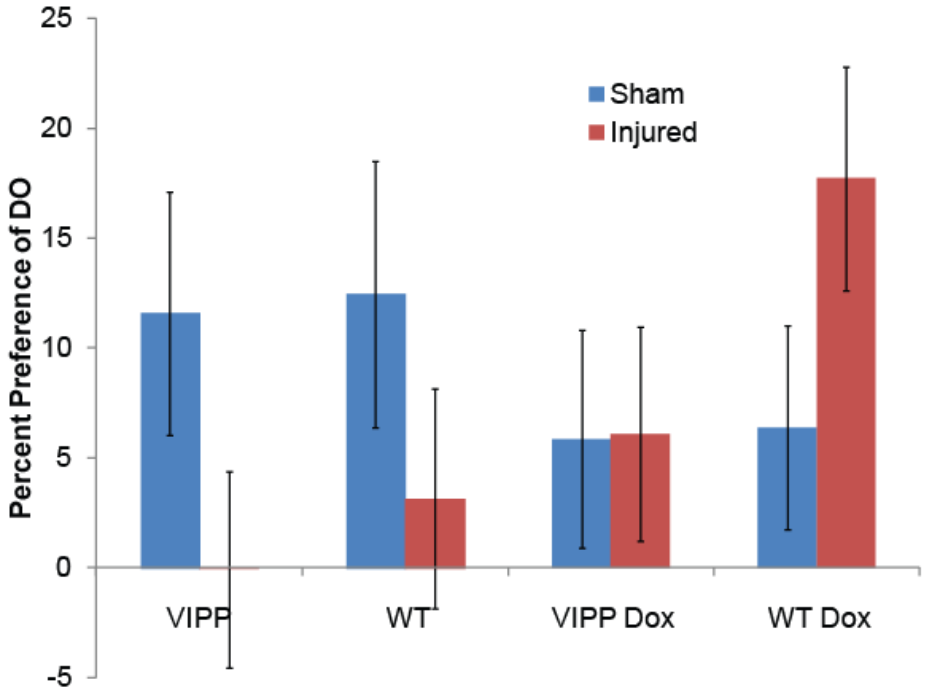

Figure 4.11. VIPP did not affect preference for the displace object in SOR.
The transgenic WT nor the VIPP sham animals did not have significant preference for the displace object more than injure animals. The VIPP on dox injured animals had similar percent preference as the injured transgenic WT. Data are expressed as Media ± S.E.M.

Behavior and interaction with the objects in the SOR test were measured in session 4, with the expectation that no and the test session to determine the effect of injury and genotype on spatial memory. There was no significant behavioral difference between injured and sham for any of the groups (Figure 4.11) in a one way ANOVA.

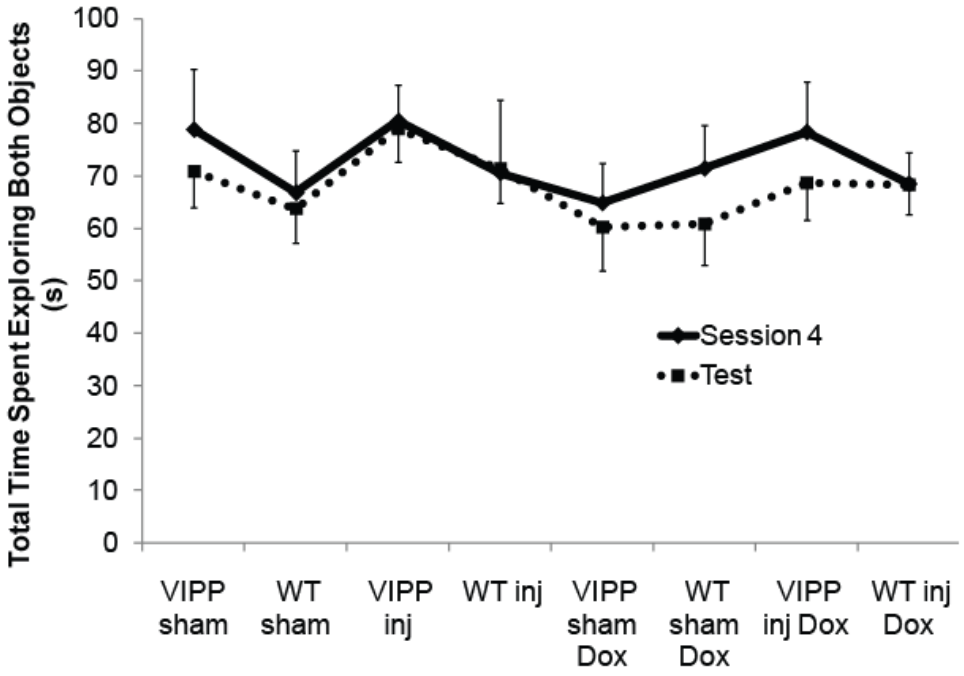

Figure 4.12. Time exploring SOR objects in session 4 and test session.
Animals in all groups had similar total exploration times. Injury or genotype had no affect on the animal exploration behavior. The amount of time spent exploring both objects for session 4 also did not greatly differ 24hrs later when one of the objects was displaced, during the test session. Data are expressed as Media ± S.E.M.

A two way ANOVA showed significant effect of injury ($p=0.0474$). VIPP injured animals tended to perform worse than the VIPP dox and WT littermates. Although not significant, VIPP injured on average had almost no preference for the displaced object compared to either WT or VIPP on dox injured. The time spent exploring both objects in the area were approximately the same for all groups for both sessions (Figure 4.12). The difference in displaced object preference was not due to decreased interest in the objects in either session 4 or test session. These results in combination with the CCI injury suggested that the outcome for blocking IP3 signaling in astrocytes is regions specific: worsen outcome in the hippocampus and little effect in the cortex.

In CFC, all groups tested had similar freeze fraction (Figure 4.13). This suggests that neither injury nor genotype had an effect on this hippocampal dependent task on day 8 post injury. There is evidence in the literature that contextual fear condition and other fear conditioning tests are a ventral hippocampal function and spatial tasks are more dorsal (Bannerman et al., 2003; Biedenkapp and Rudy, 2009; Fanselow and Dong, 2010; Richmond et al., 1999; Rudy and Matus-Amat, 2005). None of the mCCI mice showed damage in the ventral portion of the hippocampus supporting the lack of behavioral effect from CFC.

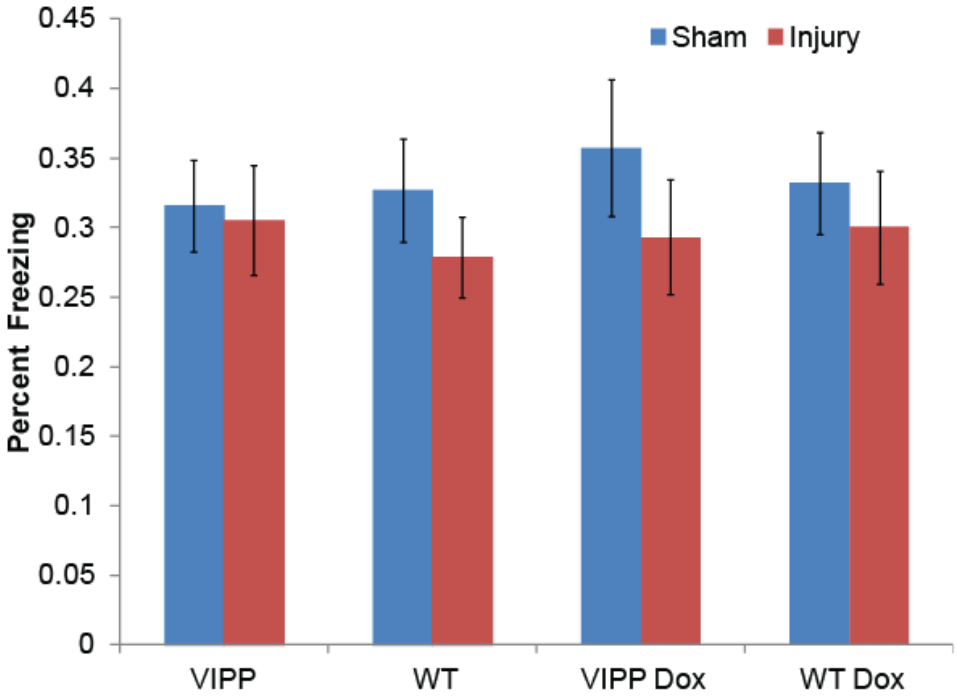

Figure 4.13. Overall freeze fraction in CFC.
All the groups, sham and injured, had similar freezing fractions. Neither injury nor genotype had an effect on contextual fear conditioning. Data are expressed as Media ± S.E.M.

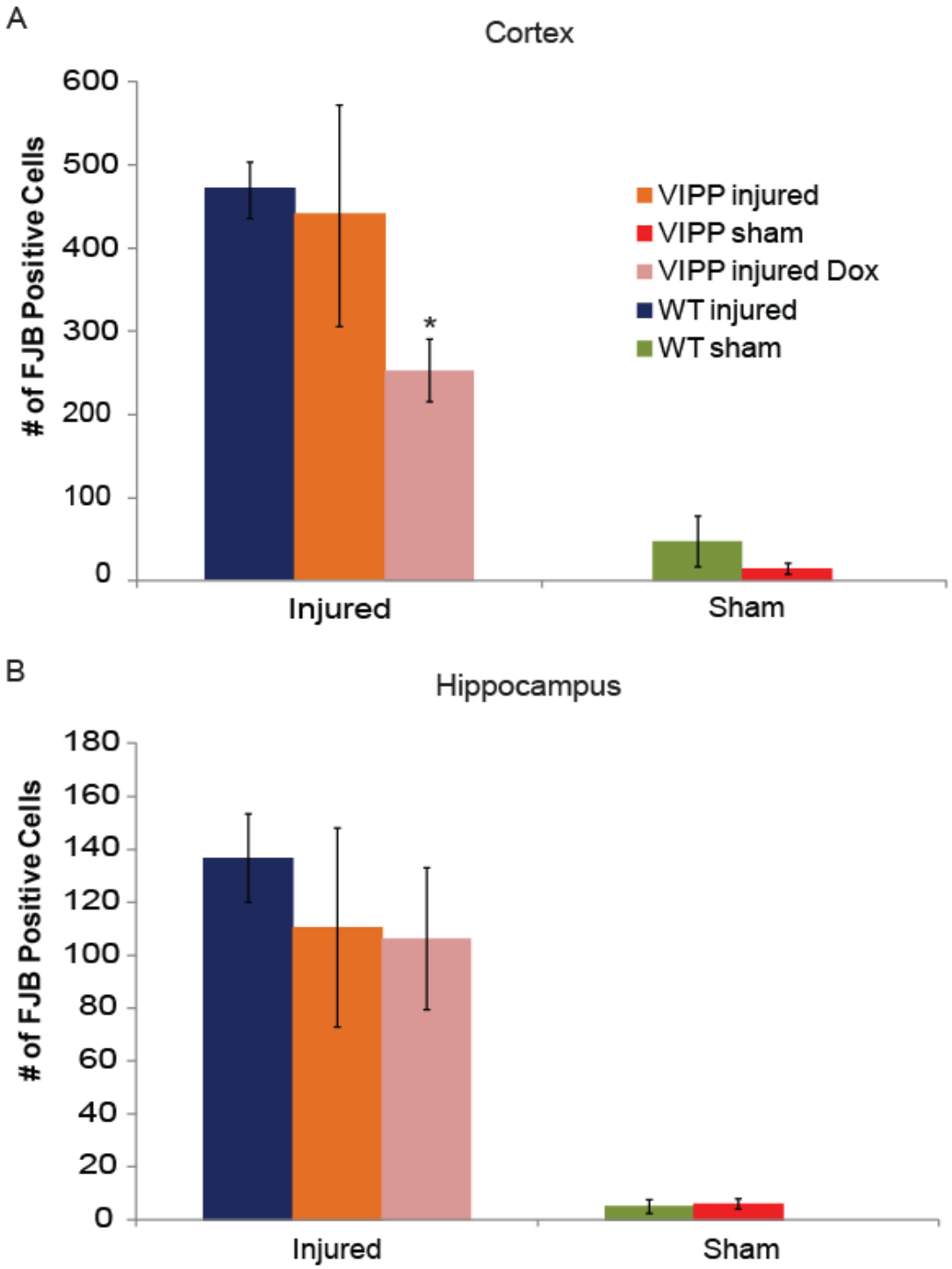

Figure 4.14. Neurodegeneration at 24 hours.
Injured animals had a significant greater number of FJB positive cells than sham animals in both the cortex (A, $p<0.0001$) and the hippocampus (B, $p<0.0001$). There was no effect of genotype. The VIPP injured on dox group also had significantly lowered FJB positive cells in the cortex compared to WT injured ($p=0.0016$). Data are expressed as Media ± S.E.M.

Reducing astrocyte IP_3 signaling does not significantly alter neuronal degeneration but does change astrocyte reactivity after mild cortical impact injury

Acute neuronal degeneration indicated with FJB staining at the 24hr time point showed all injured groups showed significantly elevated number of FJB positive cells ($p<0.0001$) relative to surgical sham animals. Moreover, the VIPP injured on dox group had significantly less FJB positive cells in the cortex ($p=0.0015$). However, we observed no difference in the level of degenerating neurons between WT and VIPP injured animals in either the cortical or hippocampal regions (Figure 4.14). In the hippocampus, the number of FJB positive cells in VIPP on dox did not differ from the other injured groups. In off dox sham mice, the venus fluorescent protein was slight but visible (Figure 4.15). On dox VIPP animals had lower baseline venus fluorescent expression than off dox sham however there was elevated fluorescent protein expression in cortex of on dox mCCI injured animals but not in the hippocampus (Figure 4.16).

GFAP expression at 8 days

In the cortex, mCCI induced greater GFAP expression in VIPP injured mice than WT injured ($p=0.0263$) in a linear regression test for significant interaction between genotype and injury. This suggested that blunting IP_3 signaling in astrocytes may have different consequences when depending on the injury severity. We saw no significant difference on astrocyte reactivity in either the hippocampus or thalamus of the injured hemisphere between VIPP and WT animal groups.

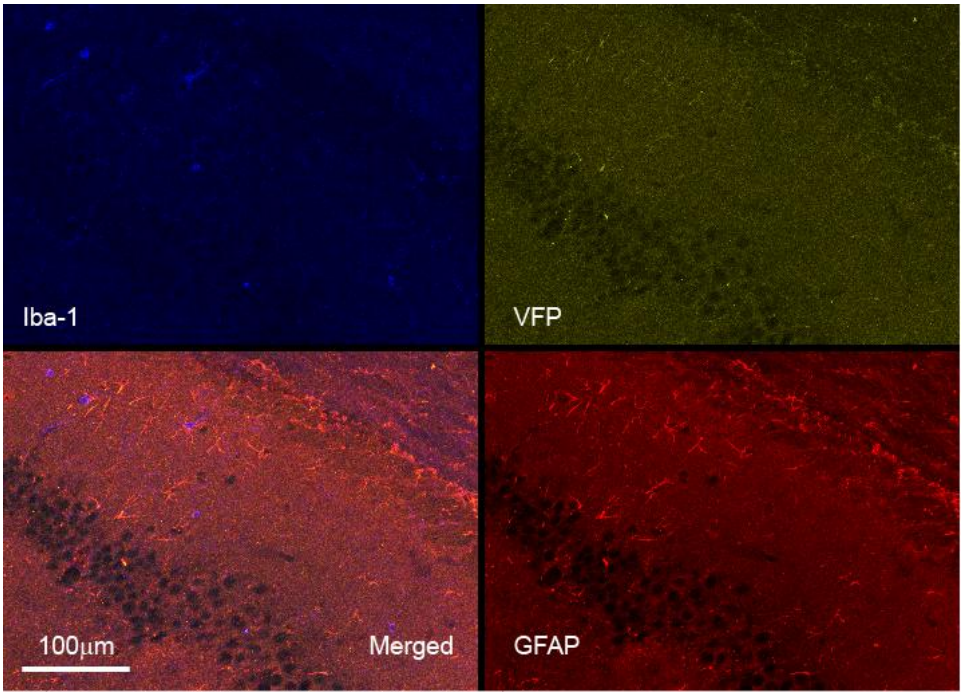

Figure 4.15. Sham VIPP mice showing baseline VIPP expression.
Baseline VIPP expression is very low. GFAP merged with VFP expression. VFP = venus fluorescent protein.

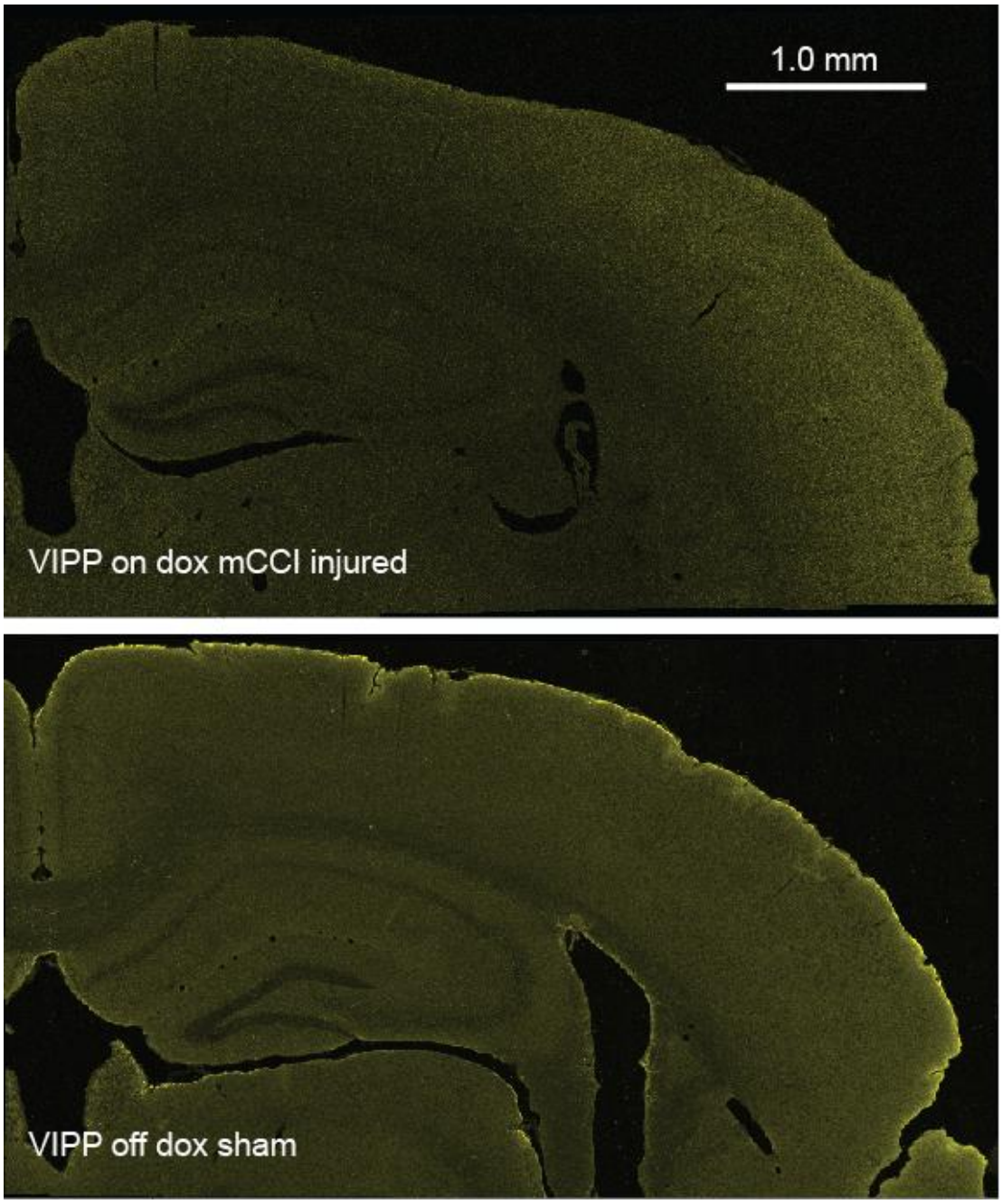

Figure 4.16. VIPP expression in on dox mice subjected to mCCI injury compared to sham off dox.

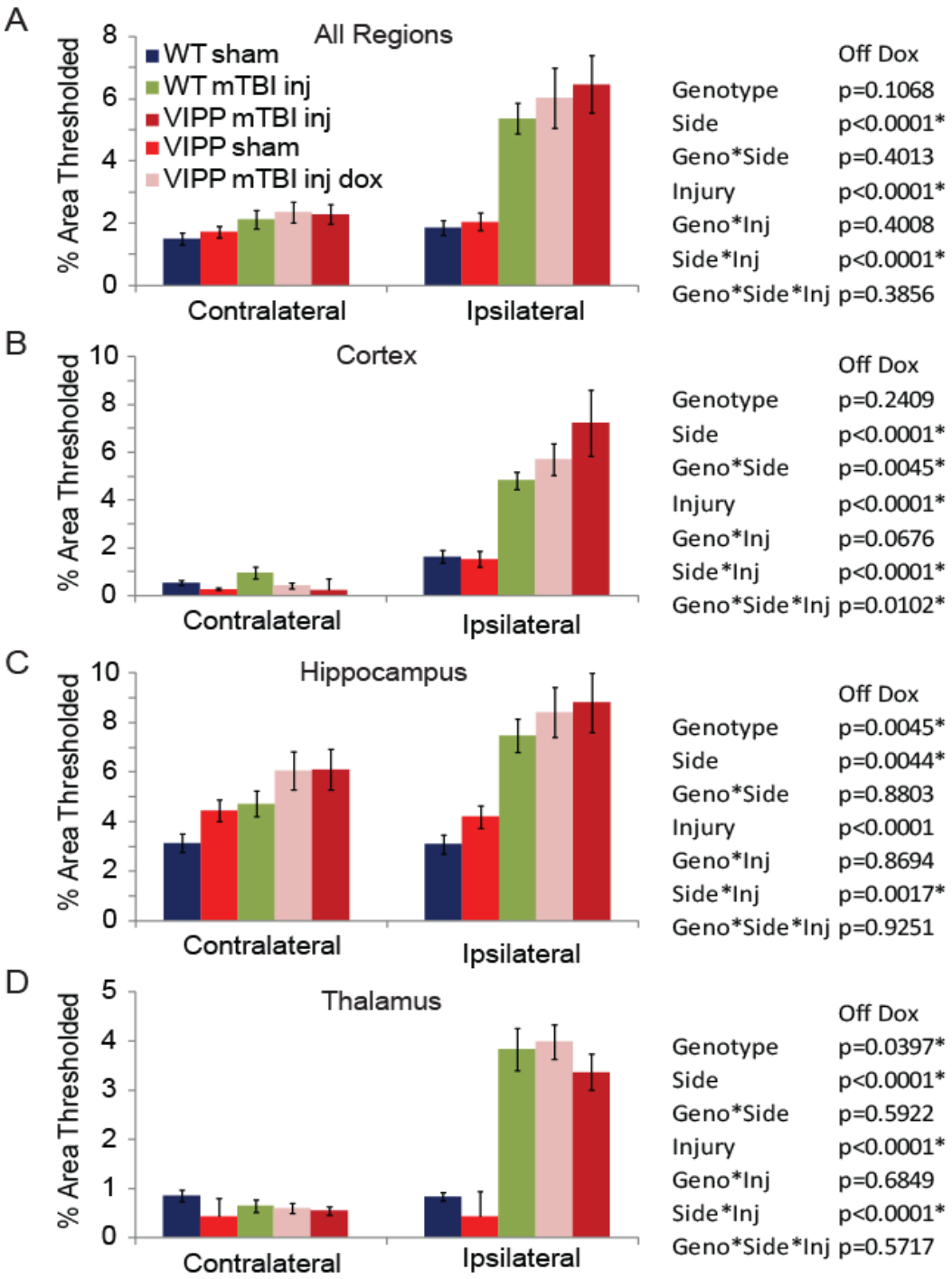

Figure 4.17. GFAP expression in mCCI.
VIPP on dox mice did not have significantly different GFAP expression from WT injured mice for all brain regions and both injury types. mCCI injured VIPP mice had greater GFAP expression in the cortex (p=0.0263) but similar levels in the hippocampus and thalamus. Contralateral sham and injured regions were not different for each group with the exception of the hippocampus. Data are expressed as Media ± S.E.M.

DISCUSSION

In this study, we evaluated the role of IP_3 signaling within astrocytes on both the behavioral and histological outcome after controlled cortical impact brain injury. In moderate cortical impact injury, we observed that suppressing IP_3 signaling in astrocytes led to a significantly worse hippocampal deficit eight days after injury, but without any overt change in the extent of astrocyte reactivity in the injured hemisphere. CCI injured VIPP mice did have reduced, but not significant, GFAP expression compared to WT. In contrast, with mild cortical impact injury, we demonstrated that IP_3 signaling reduction in astrocytes was enough to block the immediate propagation of an intercellular calcium wave through astrocytes, but this led only to a modest reduction in cortical and hippocampal dysfunction over the first 8 days after injury. Furthermore, the GFAP expression in the cortex was significantly increased in VIPP injured over WT injured.

VIPP on dox animals had better memory retention on WT littermates potentially due to noted neuroprotective effects of minocycline and doxycycline (Elewa et al., 2006; Jantzie et al., 2005; Siopi et al., 2012a, 2012b). It is also possible that the VIPP on dox effects could be due to leaky transgene expression (Figure 4.8). If this is the case, then this suggests that the level of IP_3 reduction is important. The swim speed for the injured groups were significantly worse compared to sham ($p<0.0001$) but there was no effect from genotype. This suggested that VIPP affected memory and spatial navigation but not motor recovery. This was supported by NSS results. The lack of effect on motor recovery could be due to the magnitude of injury to the motor cortex from the CCI. Too much of the motor cortex on the ipsilateral side could have been damaged and prevented any effect the transgene could have.

It is possible that dox had a neuroprotective effect on injury in this model as tetracyclines have been shown to be neuroprotective after a brain injury (Elewa et al., 2006; Jantzie et al., 2005;

Siopi et al., 2012b). It is also possible that the leaky expression in on dox animals may have affected cell death outcome, or a combination of both dox and leaky VIPP expression.

Overall, these *in vivo* results demonstrate that suppressing IP_3 signaling in astrocytes after TBI produce differential outcomes up to one week after injury depending on injury severity. *In vitro* results showed that increasing strains alter the mechanism for astrocytic calcium signaling. The greater the strain, the more pathways that are involved in the propagation of the calcium wave (Choo et al., 2013). Neary et al (2003) showed that extracellular signal-regulated protein kinase (ERK) activation in astrocytes depended on level of strain as well as strain rate. Increasing strain and strain rate independently increase ERK activation. Cullen et al (2007) also showed that astrogliosis to be dependent on strain rate. The difference between GFAP expression of mCCI and CCI supported these in vitro findings. The mCCI with the higher strains but lower strain rates did not produce the same level of astrogliosis as CCI, with the higher strain rate but lower strain. However, Cater et al (2006) showed that organotypic hippocampal slices was susceptible to strain and not strain rate. The CCI parameters used in the study produced a much higher strain rate but much less strain in the hippocampus than mCCI. Yet CCI injured VIPP mice had significantly worse water maze performance whereas mCCI injured animals did not show significant behavioral difference (WT or VIPP) compared to sham. Based on the Cater et al study, the injured animals in the mCCI should have much experience more hippocampal damage than CCI histologically as well as functionally. This discrepancy between hippocampal *in vitro* and *in vivo* results suggested that either organotypic cultures cannot accurately determine tissue tolerances or more likely, that the presence of blood and blood products have a large effect on neuronal survival that cannot be accounted *in vitro*. It also highlights the importance of accurately modeling injury biomechanics.

IP_3 signaling is responsible for a number of functions and one of the reasons for our mixed outcome could be due to these other functions. One in particular is microvascular control.

After CCI injury, there is decreased localized cerebral blood flow (lCBF) in the injured region (Kochanek et al., 1995). Calcium increases in astrocytic endfeet cause vasoconstriction and dilation (Mulligan and MacVicar, 2004). It is possible that VIPP reduce calcium increases in endfeet limiting astrocytic control of vasculature. If VIPP asrtrocytes have reduced capacity to control vasculature, there may be increased cerebral blood flow dysregulation causing greater dysfunction of neuronal activity. Other downstream effects of IP_3 signaling are also currently not well understood and it may be possible that the effects of inhibiting IP3 are differentially countered by downstream pathways depending on injury severity. We also cannot ignore the possibility that while we showed that VIPP mice subject to micro CCI injury reduced intracellular calcium in asrocytes, it is possible the with the level of injury produced by mCCI and CCI, VIPP may have failed to reduced the calcium levels in the manner seen with micro CCI.

While the outcome of our VIPP studies may not support past *in vitro* findings, comparisions to other in vivo studies also show differing trends. *In vivo* studies with PLC inhibitor, Neomycin, showed pretreated fluid percussion injury (FPI) rats showed improved bioenergetic, magnesium level, and motor function compared to saline treated (Golding and Vink, 1994). Similarly VIPP was able to preserve some motor function in mCCI injured mice. This suggests that reducing IP3 was partially successful in preserving cortical function but that reducing the levels of DAG is also important. Levels of DAG have been shown to be increased after TBI. Furthermore, DAG can activate protein kinase C (PKC) which can influence receptor activity and enhance further calcium influx into the cell (Weber, 2012). Increased DAG levels also induce vesicle ATP release independent of PKC activity (Mungenast, 2011). If VIPP were able to reduce the initial intracellular astrocytic calcium rise in both CCI and mCCI injured mice, it is possible that high levels of DAG could cause subsequent influx of extracellular calcium into the cell. If this did occur, then VIPP would only delay neuronal degeneration.

However, drugs are receptor specific and not cell type specific. Neomycin and U73122 cannot preferentially target and blunt astrocytic PLC activity. The VIPP transgene was specifically targeted to astrocytes and the use of transgenic animals can help to discern the contribution of astrocytic IP_3 calcium signaling on recovery after TBI. The discrepancy in results between using neomycin and in this study could be due from a combined effect of blocking IP_3 signaling in both astrocytes and neurons.

Solely targeting astrocytic calcium may still be a potential therapeutic treatment. An in vitro BAPTA-AM loading protocol was able to specifically load astrocytes and doing so reduced cell death at 24hrs (Choo et al., 2013). However, BAPTA-AM chelates calcium and effectively attenuates the effect of pathways other than ER store release of calcium. VIPP can only block IP_3 induced calcium and is unable to block other sources of calcium. Neuroprotection from BAPTA-AM treated cultures suggests that ER store calcium release may not be the predominant pathway to ICW in astrocytes after a moderate to severe injury. Additionally, blocking only IP_3 in astrocytes can potentially worsen outcome by further increasing the biochemical in-balance in the cell after TBI.

Future studies with VIPP should look at long-term effects. For our studies we are careful to not consider or speculate longer term effects with VIPP. At 7 days NSS, the three injured groups were starting to show deviation. At day 7 watermaze, VIPP showed differences from the other two injured groups. The probe trial on day 8 showed VIPP mice had significantly reduced capacity for spatial memory. It is of interest to note that across the three days on rotarod, the gap in performance between VIPP sham and injured increased, although the repeated measure ANOVA was not significant. These results potentially suggest that VIPP in astrocytes produce long term effects and may not be seen in a short 8 day survival study.

Chapter 5 Inhibited astrocytic vesicular release and the effect on TBI

ABSTRACT

Research into gliotransmission has shown that astrocyte release of adenosine triphosphate (ATP) and glutamate can affect neuronal signaling. In TBI, overactivation of ionotropic glutamate receptor, N-methyl-D-asapartate receptor (NMDAR), has been a major mechanism leading to neurodegeneration. Astrocytes have been hypothesized to contribute to this excitotoxic environment through stretch induced release of ATP and glutamate. dnSNARE have inhibited vesicular release and have been shown to improve outcome in ischemic and sleep deprivation models. In the CCI injured mice, dnSNARE mice did not improve the neurological severity score but did improve watermaze outcome on day 7. The rate of spatial learning across time was also significantly improved compared to WT injured. In mild CCI injured mice, dnSNARE prevented motor deficits seen in WT injured but failed to provide any improvement in the more hippocampal based tasks. A caveat to this study is that dnSNARE mice do show a reduced surface expression of NMDARs. The reduced surface expression in NMDARs in the dnSNARE could be the main mechanism of neuroprotection although the histopathology did not support this theory. dnSNARE injured animals have decreased GFAP expression in both models, an effect typically attributed to inhibited purinergic signaling. The level of neuronal cell death was also not significantly decreased in dnSNARE mice, an effect that is prevalent in NMDAR inhibition pre and immediately post injury.

INTRODUCTION

Research from the past two decades have shown that astrocytes can modulate the neuronal network through the release of gliotransmitters such as glutamate (Parpura et al., 1994) and adenosine triphosphate (ATP) (Newman, 2003) through a calcium dependent process called gliotransmission (Agulhon et al., 2012). Gliotransmitters can be released through a number of different mechanisms, one of which is exocytosis. Formation of soluble N-ethylmaleimide-sensitive fusion protein attachment protein receptor (SNARE) complex allows the docking and fusion of vesicles to the plasma membrane and is the main pathway of regulated exocytosis (Halassa, 2009). Calcium dependent glutamate and ATP release is dependent on exocytosis through the SNARE complex mediating vesicular release (Zorec et al., 2012). Inhibiting this process prevents gliotransmission (Pascual et al., 2005).

Why is gliotransmission so important? Gliotransmission has been shown to strengthen and weaken neuronal signaling through modulation of receptors on both pre and post synapses (Perea et al., 2009). In pathophysiology, abnormal glial calcium excitability has been linked to a number of neurological disorders (Agulhon et al., 2012). Astrocyte calcium transients in a mouse model of Alzheimer's displayed increased frequency, longer duration, and traveled longer distances than wildtype (WT) littermates (Kuchibhotla et al., 2009). Increased calcium waves were also noted in an ischemic model (Ding et al., 2009), cortical spreading depression (CSD) model (Peters et al., 2003), and in status epilpeticus (Ding et al., 2007).

These data together suggest that the release of extracellular ATP and or glutamate from astrocytes due to injury can potentially cause excitotoxic signaling on neurons. After stretch injury, astrocytes respond with a far reaching calcium wave that spreads into the penumbra region. The intercellular calcium rise also induces a release of ATP and glutamate from astrocytes through vesicular release which may contribute to the excitotoxic environment after stretch.

Inhibition of purinergic receptors have been shown to be neuroprotective *in vitro* and *in vivo* (Choo et al., 2013). Blocking purinergic signaling in vivo, of which astrocytes are a major source, has been shown to improve outcome after moderate TBI (Choo et al., 2013). Similarly, blocking the calcium increase specifically in astrocytes with BAPTA-AM, is also neuroprotective *in vitro* stretch injured cultures (Choo et al., 2013; Miller, 2009). Blocking the predominant pathways that cause intracellular calcium waves (ICW) through P2Y1R antagonism with MRS2179 was able to reduce cell death with pre and post injury treatment of injured organotypic hippocampal slices (Choo et al., 2013; Miller, 2009). Treatment of organotypic slices with apyrase, to degrade extracellular ATP into adenosine was also equally neuroprotective (Choo et al., 2013; Miller, 2009). Together, these data suggest that astrocytes can have significant effects on the resulting changes in neurons after traumatic brain injury (TBI).

To test the specific contribution of gliotransmitters on cognitive and histological impairments after TBI, we used a transgenic animal specifically designed to inhibit vesicular release from brain astrocytes. If the contribution of purinergic signaling from astrocytes after TBI be a major source of excitotoxic factors, dnSNARE mice would ideally be more resistant to injury and behavioral changes after TBI. dnSNARE mice have already shown to provide neuroprotection in a ischemia brain injury model (Hines and Haydon, 2013) and status epilepticus model (Clasadonte et al., 2013). Given the potential change in mechanisms of cognitive deficits and neuronal death across the TBI severity spectrum, we studies two different levels of TBI severity using the controlled cortical impact (CCI) model of TBI. Our results demonstrate that gliotransmission can affect outcome after both mild and more severe TBI, and the improvement in outcome when vesicular release from astrocytes is suppressed indicates an important new direction in designing therapies.

MATERIALS AND METHODS

dnSNARE mice were exposed to two different injury levels using the same type of direct cortical deformation injury model, CCI. At the higher end, using a 6m/s impact velocity with an impact depth of 1mm, a contusion was induced and by 8 days a large necrotic lesion was produced. At the lower level, using an impact velocity of 0.43m/s with an impact depth of 2mm, no contusion or lesion was produced. As a result of difference in debilitation of the two injuries, different behavioral paradigms were necessary to be able to discern between injured and sham. The injury and behavior schedule is presented in chapter 4, Table 4.1. For the more severely injured group, the neurological severity score (NSS) and the Morris water maze (MWM) was used. For the mild injured group, the rotarod was employed followed by the spatial object recognition (SOR), and contextual fear conditioning (CFC).

dnSNARE Breeding

dnSNARE animals were bred as described in Pascual et al (2005). Animals were bred under 12hr light/dark cycles. Pups were weaned at 3 weeks of age and genotyped. Details of producing GFAP.tTA and tetO.dnSNARE lines are as described elsewhere (Halassa, 2009; Halassa et al., 2007; Pascual et al., 2005). These lines were maintained in a heterozygous state and backcrossed onto a C57B16/J genetic background (Jackson Laboratories, Bar Harbor, ME). Bigenic offspring of these two lines (dnSNARE), and their wildtype littermates, were maintained on 40 mg/kg doxycycline (dox) containing food (Bioserv, Frenchtown, NJ). They were switched to a regular diet to allow transgene expression in the dnSNARE animals for a minimum of 2 weeks prior to use. A portion of the bigenic animals were kept on dox for the duration of the experiments. These animals were the control for the transgenic mice and should have similar results as that of wildtype littermates. Due to the potential effect progesterone has one the recovery of brain injury (Feeser and Loria, 2011; Shakeri et al., 2013), only male mice were used.

Table 5.1. Experimental groups

	Injury			Sham		
	CCI	mCCI		CCI	mCCI	
	8 day	24hr	8 day		24hr	8 day
dnSNARE	12	4	15	11	4	13
on Dox	13	4	16	13	NA	12
WT littermates	26	6	14	27	5	13
on Dox	26	NA	16	25	NA	13

Cortical Injury

All animal procedures were approved by University of Pennsylvania's Institutional Animal Care and Use Committee (IACUC). dnSNARE and wildtype (WT) littermate mice were divided into the groups listed in Table 5.1.

The cortical injury protocol was the same as described in chapter 4.

Histology

Please refer to the previous chapter for the histology protocols.

Behavior Tests

The following behavioral tests were conducted in this study: rotarod, SOR, MWM, and NSS. The protocol is the same as the previous chapter.

Statistical Analysis

All statistical tests were carried out using JMP10. Two-way ANOVA was used to determine the effect of the transgene with injury. For behavior, on dox groups were compared independently of off dox groups where possible. For histology, the on dox transgenic injured group was compared to the WT injured group with a Student's t-test. For GFAP staining, a three-way ANOVA was

used to compare the interaction between genotype, hemisphere of brain, and injury. A two-way repeated measures ANOVA was used in the rotarod, MWM, and NSS behavioral tests.

RESULTS

Morris water maze deficits after moderate cortical impact injury are significantly improved in dnSNARE animals

Cortical impact injury created immediate impairments in both MWM and NSS by increasing time to platform in the former and by decreasing the number of tasks accomplished in the later. The NSS outcome immediately after injury or in the days following did not differ between littermate wildtype and dnSNARE animals (Figure 5.1, repeated measures ANOVA). Over time, there was a significant interaction between time and injury for both dnSNARE and WT injured groups, indicating both groups were significantly improving in their NSS outcome over the first week postinjury. However a lack of significance with geno×injury or geno×injury×time suggests that the transgene did not cause immediate behavioral changes or change rate of recovery.

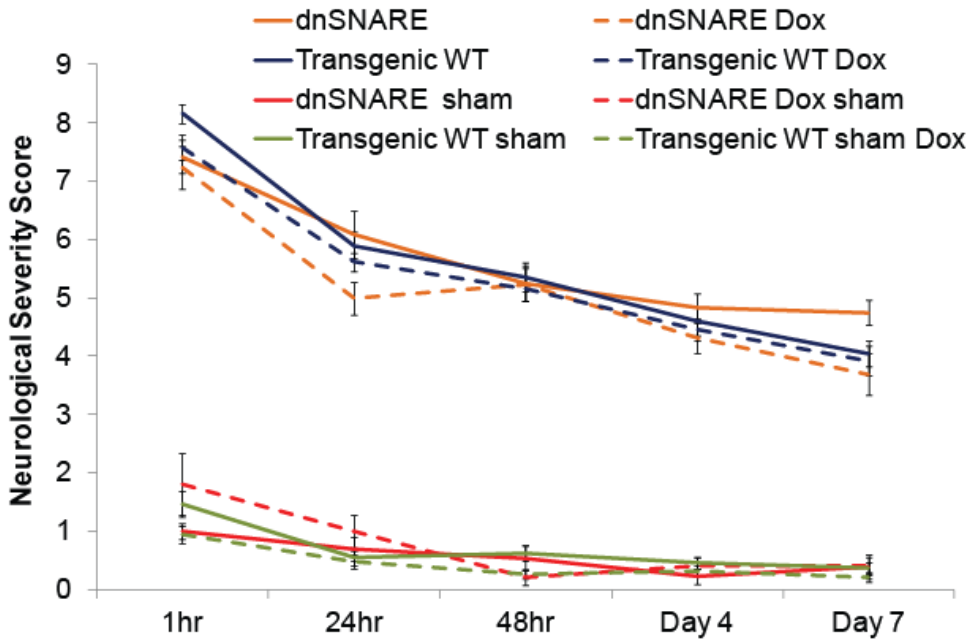

Figure 5.1. dnSNARE injured and sham mice had similar NSS performace as WT injured and sham mice.
NSS behavior did not vary across genotype for either sham or injured groups. All injured groups were significantly different from sham groups ($p<0.0001$, repeated measures ANOVA). There was no effect from genotype or genotype×injury. Data are expressed as Media ± Standard Error of the Mean (S.E.M.).

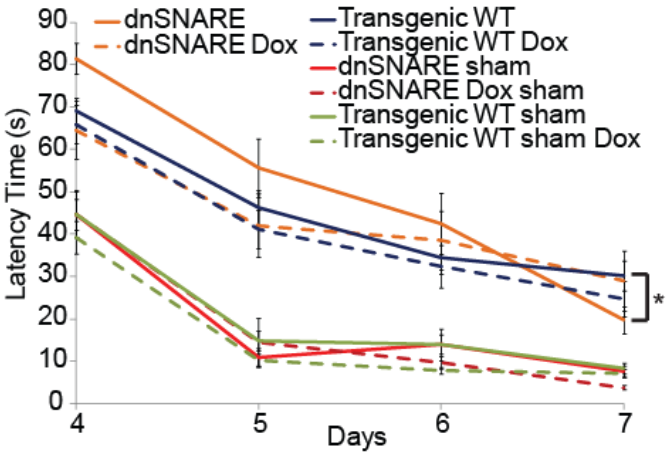

		Off Dox	On Dox
Between Subjects	Injury	p<0.0001*	p<0.0001*
	Genotype	p<0.0001*	p=0.1510
	Inj*Geno	p=0.5930	p=0.6008
Within Subjects	Time	p<0.0001*	p<0.0001*
	Time*Injury	p=0.0001*	p=0.2281
	Time*Geno	p=0.0270*	p=0.5508
	Time*Inj*Geno	p=0.0181*	p=0.1480
Day4 vs Day 5	Injury	p=0.1184	p=0.1292
	Genotype	p=0.3429	p=0.7309
	Inj*Geno	p=0.7199	p=0.5895
Day4 vs Day6	Injury	p=0.4397	p=0.2752
	Genotype	p=0.4537	p=0.8560
	Inj*Geno	p=0.3578	p=0.2220
Day4 vs Day7	Injury	p=0.0110*	p=0.7672
	Genotype	p=0.0074*	p=0.4069
	Inj*Geno	p=0.0070*	p=0.0512

Figure 5.2. Morris watermaze behavior across day 4 through day 7 post injury.
Injury and not genotype cause a significant difference in watermaze performance ($p<0.0001$). A repeated measures ANOVA showed a significant interaction between time and injury ($p<0.0001$) and time, genotype and injury ($p=0.0181$). On day 7, there was a significant interaction between genotype and injury ($p=0.0070$). Data are expressed as Media ± S.E.M.

Over the four day Morris water maze evaluation period, all injured groups showed significantly higher latency times relative to sham surgery groups ($p<0.0001$). Injured mice had a different recovery rate from sham (time×injury, $p=0.0001$); sham mice reached a learning plateau by the second day of MWM testing whereas the injured mice did not show reaching a similar learning plateau within the four days tested. A repeated measures ANOVA also showed significant interaction for time×injury×genotype ($p=0.0181$). When comparing the performance on Day 4 with Day 7, there was a significant interaction between genotype and injury ($p=0.0070$) suggesting that dnSNARE showed significant improvement in their latency times compared to WT injured animals over the course of the four days. There was no difference between the on dox groups. The statistics suggest that while dnSNARE injured animals had higher latency times over the course of the first three days, they had significantly better recovery rate than the other injured groups (on dox groups and WT injured) and significantly improved their performace by the end of the test. While dnSNARE on dox injured animals showed leaky transgene expression (Figure 5.3), this did not seem to translate to altered behavioral performance compared to WT on dox injured.

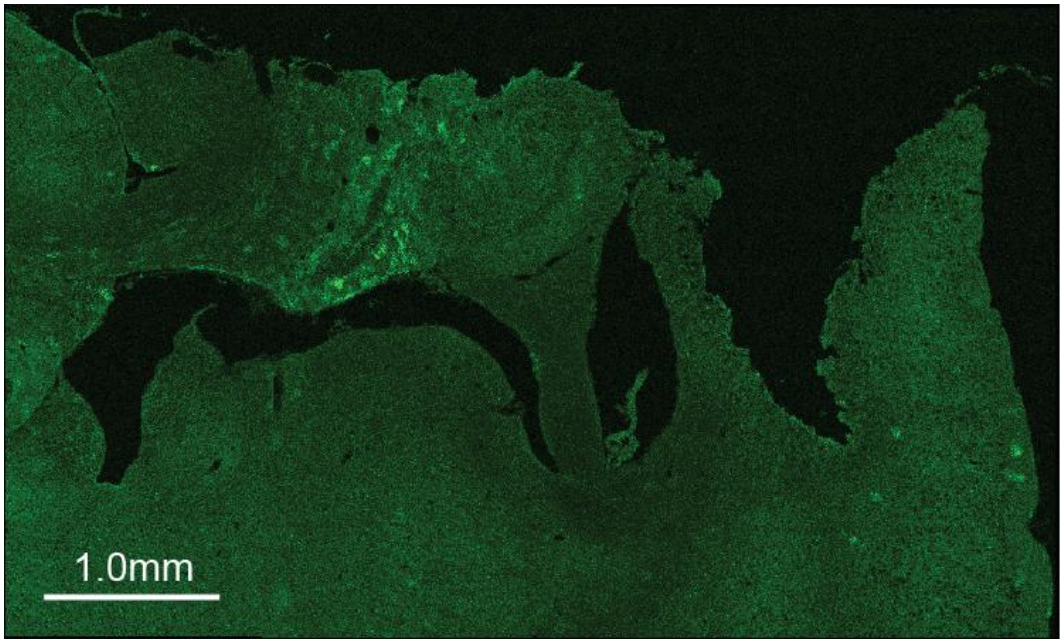

Figure 5.3. dnSNARE on dox with CCI
The transgene expression was not completely blocked in dnSNARE animals after CCI. GFP expression was detected in the hippocampus as well as the cortex.

A probe trial conducted one day after the completion of the water maze testing showed that injured animals performed significantly worse than sham across all groups, but there was no significant difference between dnSNARE and wildtype animals for this outcome measure after injury (Figure 5.4). We considered if these changes were influenced by a difference in swim speed among the groups, but we found that no differences existed among injured dnSNARE animals on dox, injured WT animals, or injured dnSNARE animals. Together, these data show that while dnSNARE mice might have faster recovery of spatial learning, this did not translate to improved spatial memory 24hrs later.

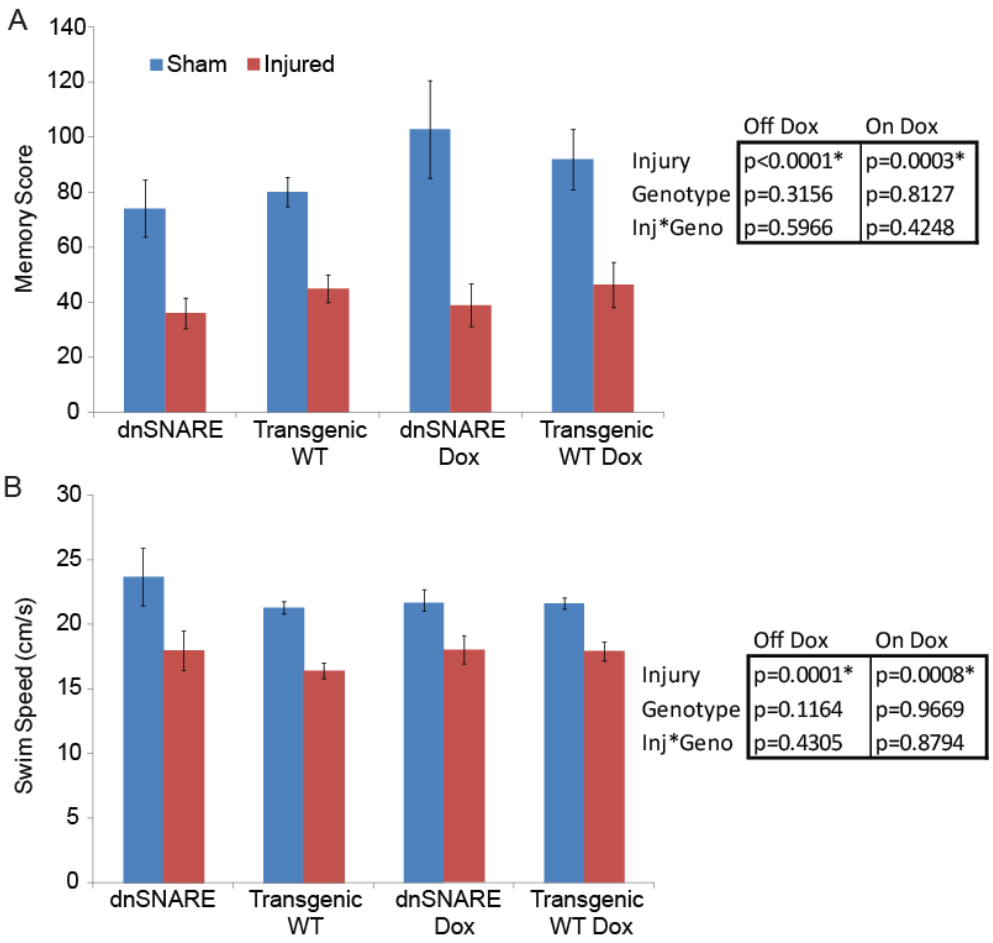

Figure 5.4. dnSNARE did not perform any differently on the probe trial.
There was significant difference between injured and sham memory score for all groups ($p<0.0001$, two-way ANOVA) (A) and for probe trial swim speed (B). Baseline performance between dnSNARE and WT transgenic animals were not different. There was no effect from genotype. Data are expressed as Media ± S.E.M.

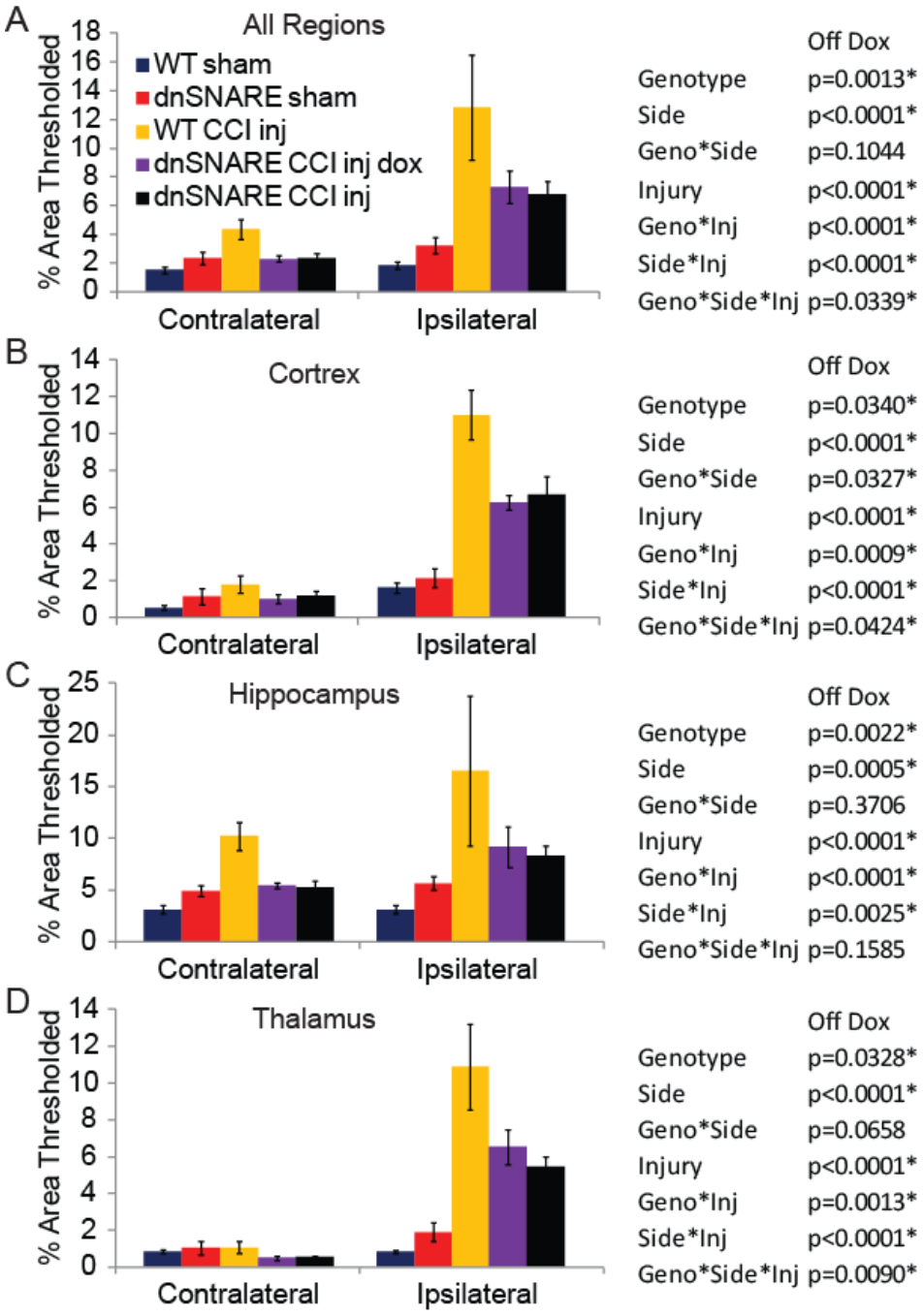

Figure 5.5. GFAP expression with CCI
dnSNARE injured animals showed significantly less GFAP expression than the WT CCI injured animals. The GFAP expression averaged across all regions (A), the cortex (B), the hippocampus (C), and the thalamus (D) all show that injury significantly increased GFAP expression in the ipsilateral compared to contralateral in a three-way ANOVA. CCI injured dnSNARE mice had reduced GFAP expression compared to WT and this reduction was mostly located on the ipsilateral side in the cortex and thalamus and on both contralateral and ipsilateral in the hippocampus. Data are expressed as Media ± S.E.M.

dnSNARE animals a significant reduction in GFAP reactivity, but no alteration in lesion volume eight days following moderate cortical impact injury

Examining the extent of GFAP reactivity across the ipsilateral and contralateral hemispheres revealed a significant difference between the injured and sham groups, and between injured WT and injured dnSNARE animals (Figure 5.5). Three-way ANOVA showed a significant difference in the volume of GFAP reactivity measured across 3 regions (cortex, hippocampus, thalamus) in both hemispheres across sham and injured groups (geno×side×inj, $p=0.0339$). Moreover, dnSNARE animals showed a significant reduction in GFAP expression for CCI injured mice in the ipsilateral cortex ($p=0.0424$), ipsilateral thalamus ($p=0.0090$), and both hippocampi ($p<0.0001$) when compared to injured, littermate wildtype animals. Individually comparing dnSNARE on dox injured to WT injured with t-tests showed that dnSNARE on dox had significantly reduced GFAP expression in the ipsilateral cortex ($p=0.0027$), the contralateral hippocampus ($p=0.0024$), and in the ipsilateral thalamus ($p=0.0452$). This reduction in dnSNARE dox injured animals could be due to the leaky transgene expression (Figure 5.3). There was also a larger error in the ipsilateral hippocampus of WT CCI injured mice due to the loss of the hippocampus in many of the mice reducing the number images taken from each sample from three down to two or one. These results suggeste that dnSNARE was able to reduce the level and spread of astrogliosis in CCI injured tissue. The reduction in GFAP expression was not matched by a change in lesion volume. Eight days after moderate cortical impact injury, the lesion volumes between all three CCI injured groups were not significantly different (Figure 5.6, Students's t-tests). dnSNARE injured mice had slight but not significantly increased tissue sparing compared to WT or dnSNARE on dox injured mice.

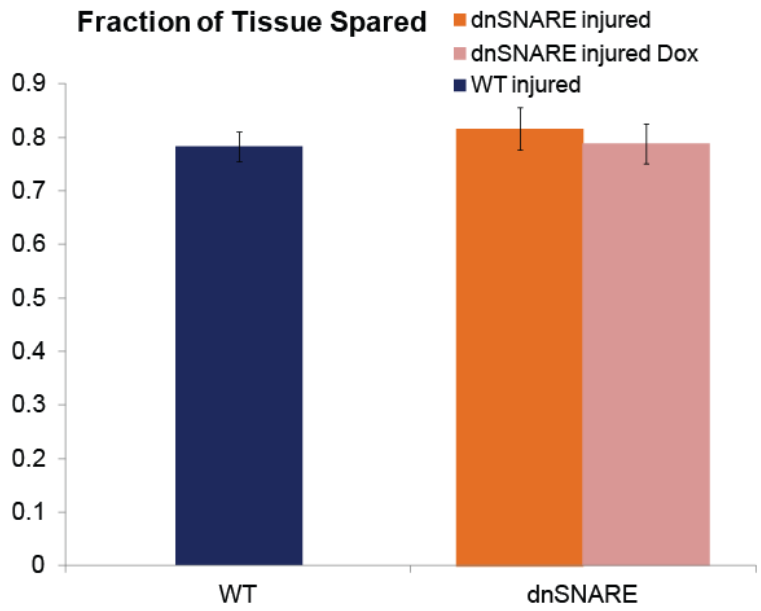

Figure 5.6. Lesion Volume.
The fraction of spared tissue on the ipsilateral side compared to the contralateral side was not different between the injured groups. Data are expressed as Media ± S.E.M.

Early behavioral impairments are eliminated in dnSNARE mice after mild cortical impact injury

Mice injured with the mild CCI (mCCI) exhibited early neuronal degeneration but no hemorrhagic contusion. There was a significant reduction in rotarod latency as measured with the fault parameter. In the mCCI test schedule (refer to chapter 3 and 4), mice were first tested on the rotarod. In this motor behavior test, dnSNARE injured mice on average performed better than dnSNARE sham mice, although not significantly (Figure 5.7, one-way repeated measures ANOVA). WT groups in contrast showed the opposite trends. In a two way repeated measures ANOVA, there was a significant interaction between genotype and injury for the fault parameter ($p=0.0201$) and trended toward significance for the fall parameter ($p=0.0675$). This suggests that dnSNARE was able to prevent early cortical injury deficits in mCCI. Comparison of the on dox groups revealed no statistical differences between dnSNARE and WT for both fault and fall latencies (in a two-way ANOVA). dnSNARE on dox injured animals also performed similarly to

WT injured (off dox) using a one-way ANOVA. dnSNARE on dox injured also significantly differed from dnSNARE injured (p=0.0077, one-way repeated measures ANOVA) but dox×time was not significant suggesting that both groups learned at a similar rate. These results suggest that

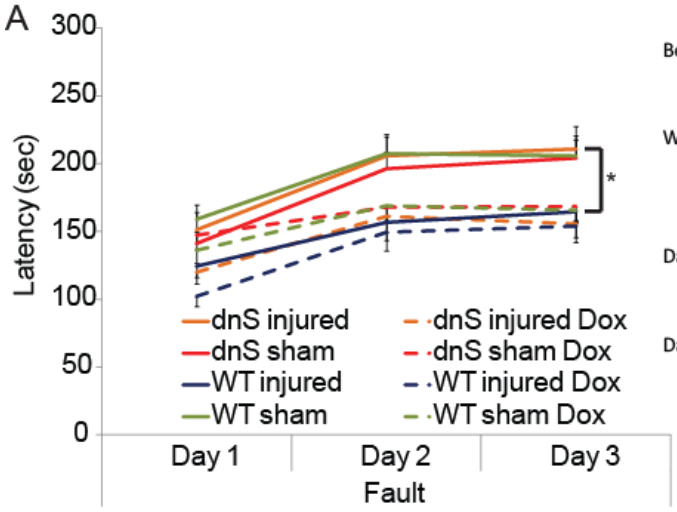

		Off Dox	On Dox
Between Subjects	Injury	p=0.1247	p=0.0396*
	Genotype	p=0.1592	p=0.4180
	Inj*Geno	p=0.0201*	p=0.7282
Within Subjects	Time	p<0.0001*	p<0.0001*
	Time*Injury	p=0.7622	p=0.1316
	Time*Geno	p=0.2910	p=0.4842
	Time*Inj*Geno	p=0.7221	p=0.7721
Day1 vs Day 2	Injury	p=0.4649	p=0.0674
	Genotype	p=0.1840	p=0.3380
	Inj*Geno	p=0.4993	p=0.7644
Day1 vs Day3	Injury	p=0.6719	p=0.0816
	Genotype	p=0.1245	p=0.2520
	Inj*Geno	p=0.8845	p=0.7008

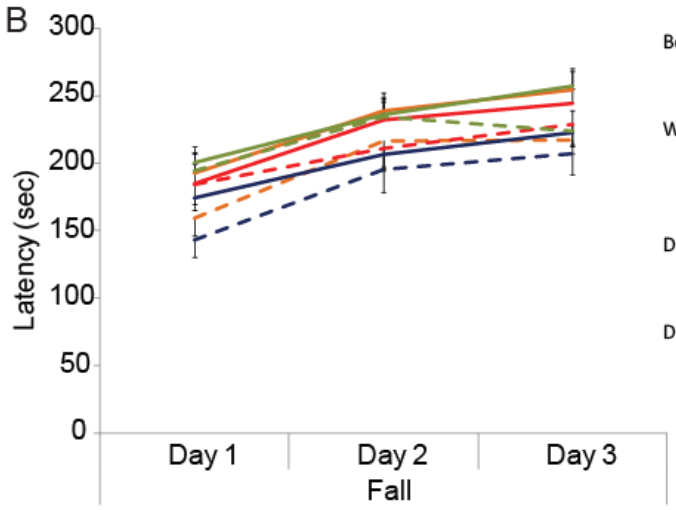

		Off Dox	On Dox
Between Subjects	Injury	p=0.2848	p=0.0512
	Genotype	p=0.4268	p=0.7889
	Inj*Geno	p=0.0675	p=0.2842
Within Subjects	Time	p<0.0001*	p<0.0001*
	Time*Injury	p=0.9729	p=0.1429
	Time*Geno	p=0.5710	p=0.8594
	Time*Inj*Geno	p=0.8671	p=0.4323
Day1 vs Day 2	Injury	p=0.8476	p=0.1521
	Genotype	p=0.3098	p=0.7853
	Inj*Geno	p=0.9287	p=0.5410
Day1 vs Day3	Injury	p=0.8148	p=0.0671
	Genotype	p=0.5706	p=0.7367
	Inj*Geno	p=0.6802	p=0.4107

Figure 5.7. dnSNARE mice did not have motor deficits in either the fault or fall parameter. (A) or in the fall (B) parameters. In both fault and fall parameters, dnSNARE injured mice on average had slightly greater latency times than dnSNARE sham, although not significant. There was a significant interaction between genotype and injury in a repeated measures ANOVA. Data are expressed as Media ± S.E.M.

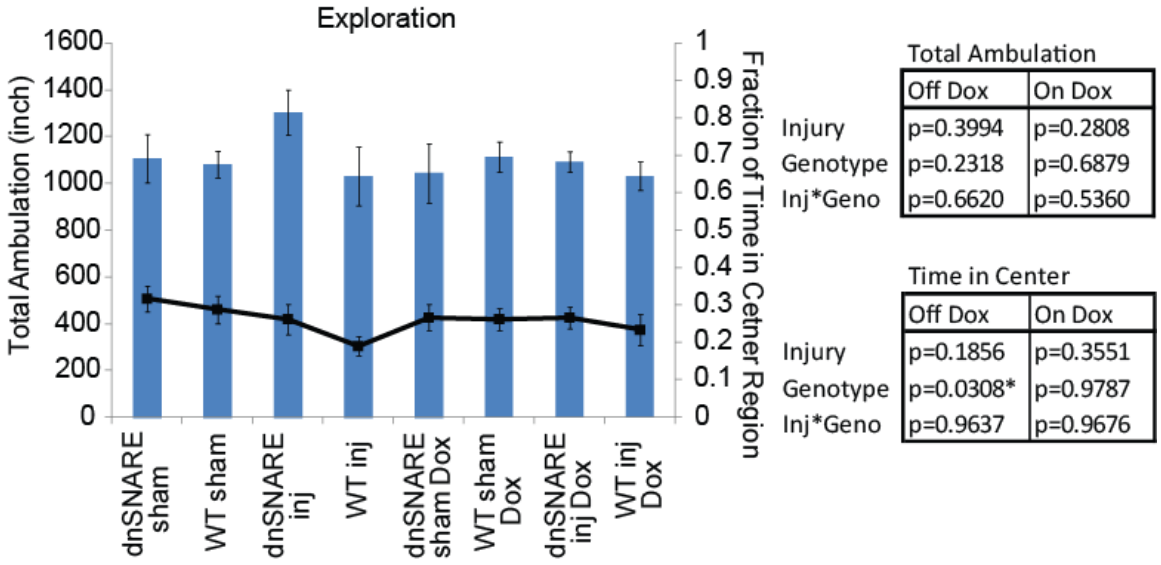

Figure 5.8. Analysis of exploratory behavior in session one of the SOR.
A two way ANOVA showed a significant interaction with injury (p=0.0295) but not with injury and genotype. Total ambulation data are depicted in blue bars; fraction of center region time data are depicted in contected data points. Data are expressed as Media ± S.E.M.

dnSNARE provides a significantly protective but acute effect after injury. The similarity in rotarod performance between the on dox injured and WT injured groups suggests that the transgene was being regulated properly. The dnSNARE expression also did not seem to affect baseline behavior.

Analyzing the exploratory behavior in session 1 of the SOR can determine the level of anxiety of the animal (Bailey and Crawley, 2009). There was no difference amongst the groups when comparing the total distance traveled in the SOR (Figure 5.8). This suggested that all the groups showed a similar level of exploratory activity. Although dnSNARE injured mice spent a greater fraction of time in the center region compared to WT injured (p=0.0308), a two way ANOVA failed to show a significant interaction for injury×genotype. The only significant interaction was due to the injury (p=0.0295).

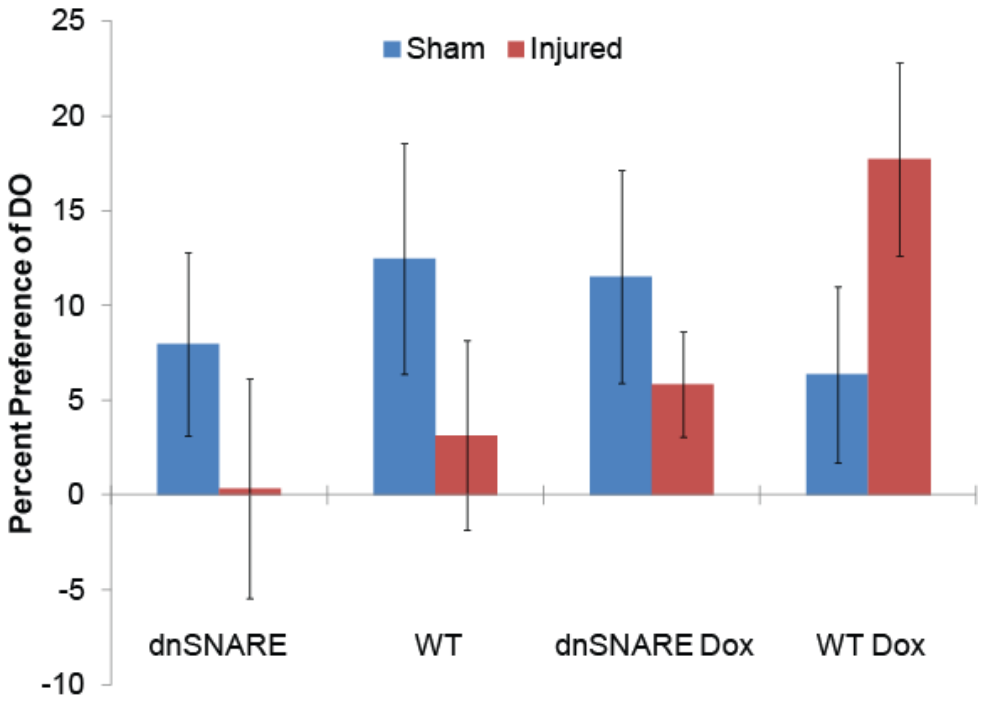

Figure 5.9. dnSNARE did not affect preference for the displace object in SOR.
The transgenic WT nor the dnSNARE sham animals did not have significant preference for the displace object more than injure animals. The dnSNARE on dox injured animals had similar percent preference as the injured transgenic WT. Data are expressed as Media ± S.E.M.

The SOR also looks at hippocampal dependent memory. A comparison between preference for the displaced objection in session 4 (object in original position) versus test day (object moved to new location), mice with better memory of the object in the original location will show renewed interest in the displaced object (Oliveira et al., 2010). Comparing the preference for the displace object between dnSNARE and WT mice showed no significant difference between the groups (Figure 5.9). As previously mentioned in chapter 2, the mCCI did not produce a significant behavioral difference in displaced object preference. dnSNARE animals show similar behavioral trends to WT mice as well as VIPP mice (Chapter 4). Comparing the time the mice spent exploring the two objects we can see if the groups had any differences in exploratory behavior which may affect overall performance in the SOR. All groups, injured and sham, showed similar amounts of time exploring the objects in both session 4 and in the test

session (Figure 5.10). Altogether, these data suggest that neither injury nor genotype had any effect on general exploratory behavior.

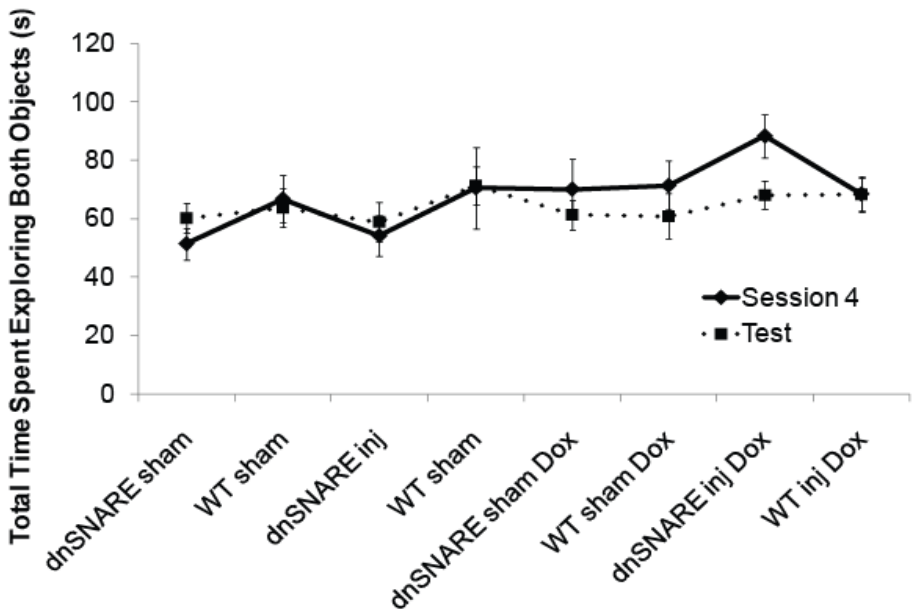

Figure 5.10. All groups spent similar amounts of times exploring the objects in session 4 and on test day.
There was no significance from genotype, injury, or in their interaction in a two-way ANOVA. Data are expressed as Media ± S.E.M.

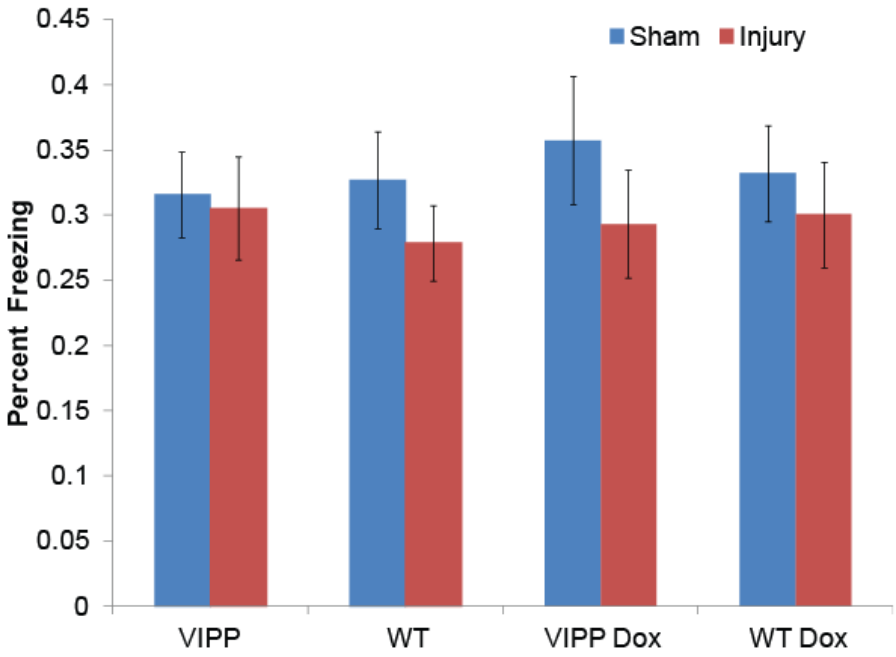

Figure 5.11. Overall freeze fraction in CFC.
There was no significant effect of injury or genotype on CFC. Data are expressed as Media ± S.E.M.

When looking at another hippocampal dependent task – the CFC – all groups displayed similar freezing fractions (Figure 5.11). As stated in chapter 4, dorsal hippocampus seems to be more involved in spatial behavior and ventral hippocampus seems to be involved in more fear conditioning behavior. The lack of damage to the ventral part of the hippocampus or the amygdale region might explain why mCCI did not have an effect on CFC. It could also mean that by day 8 that any behavioral dysfunction was recovered. Majority of mTBI symptoms recover within a week (McCrea M et al., 2003) and the lack of behavioral significance in the SOR and in the CFC may reflect this recovery.

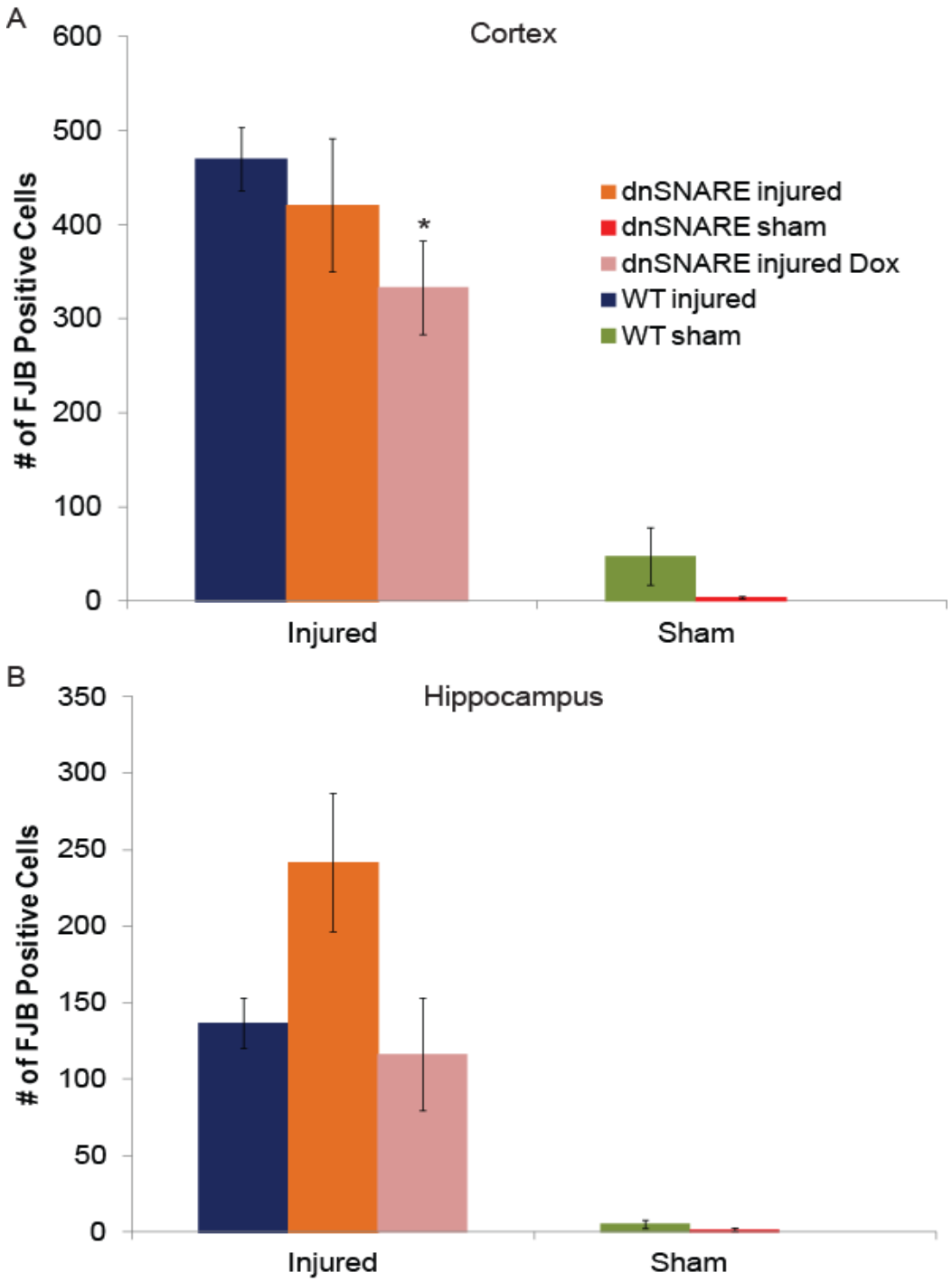

Figure 5.12. Cell death at 24hr from mCCI.
In the cortex, injured groups had significantly greater cell death in both the cortex (A) and the hippocampus (B). In neither regions was there a significant interaction between injury and genotype although for the hippocampus it was close to significance (p=0.0714, two way ANOVA). On dox injured mice had significantly reduced FJB cells in the cortex than WT injured mice (p=0.0292) but not in the hippocampus. Data are expressed as Media ± S.E.M.

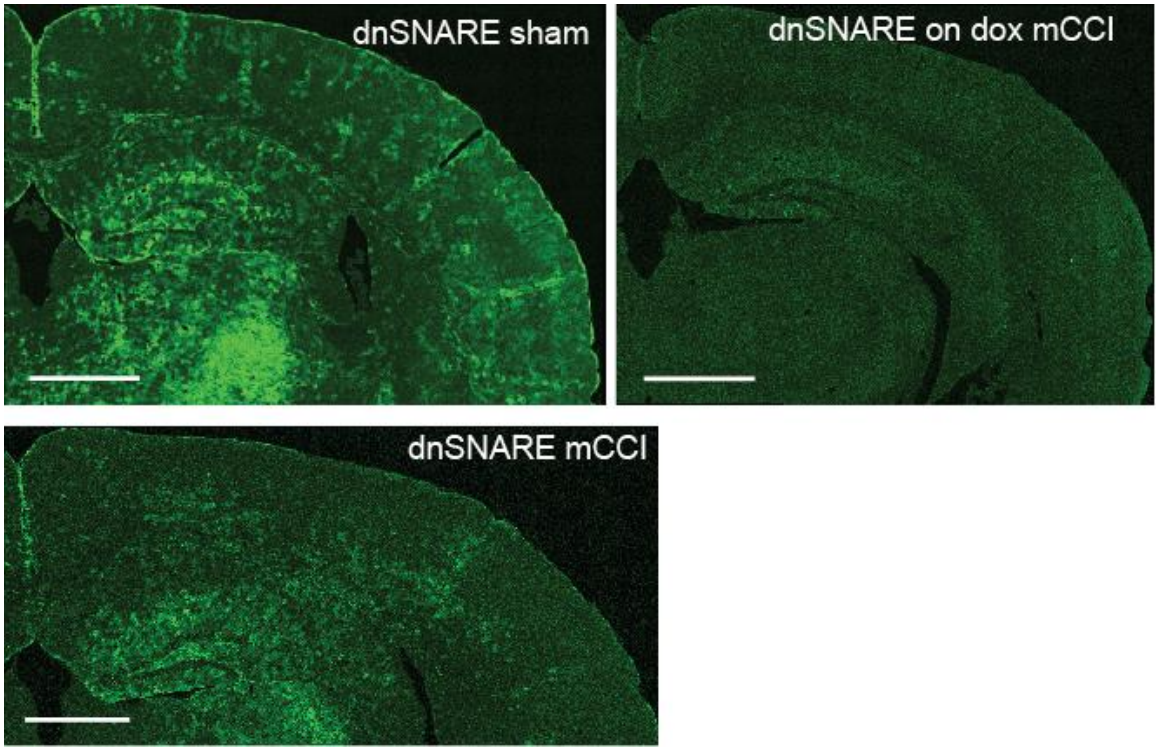

Figure 5.13. GFP expression in dnSNARE mTBI groups.
dnSNARE on dox injured animals have small amounts of leaky expression. Off dox animals show high levels of GFP expression. dnSNARE CCI show the highest level of GFP expression which corresponds to GFAP expression. Scale bars are 100µm. (GFP = green fluorescent protein)

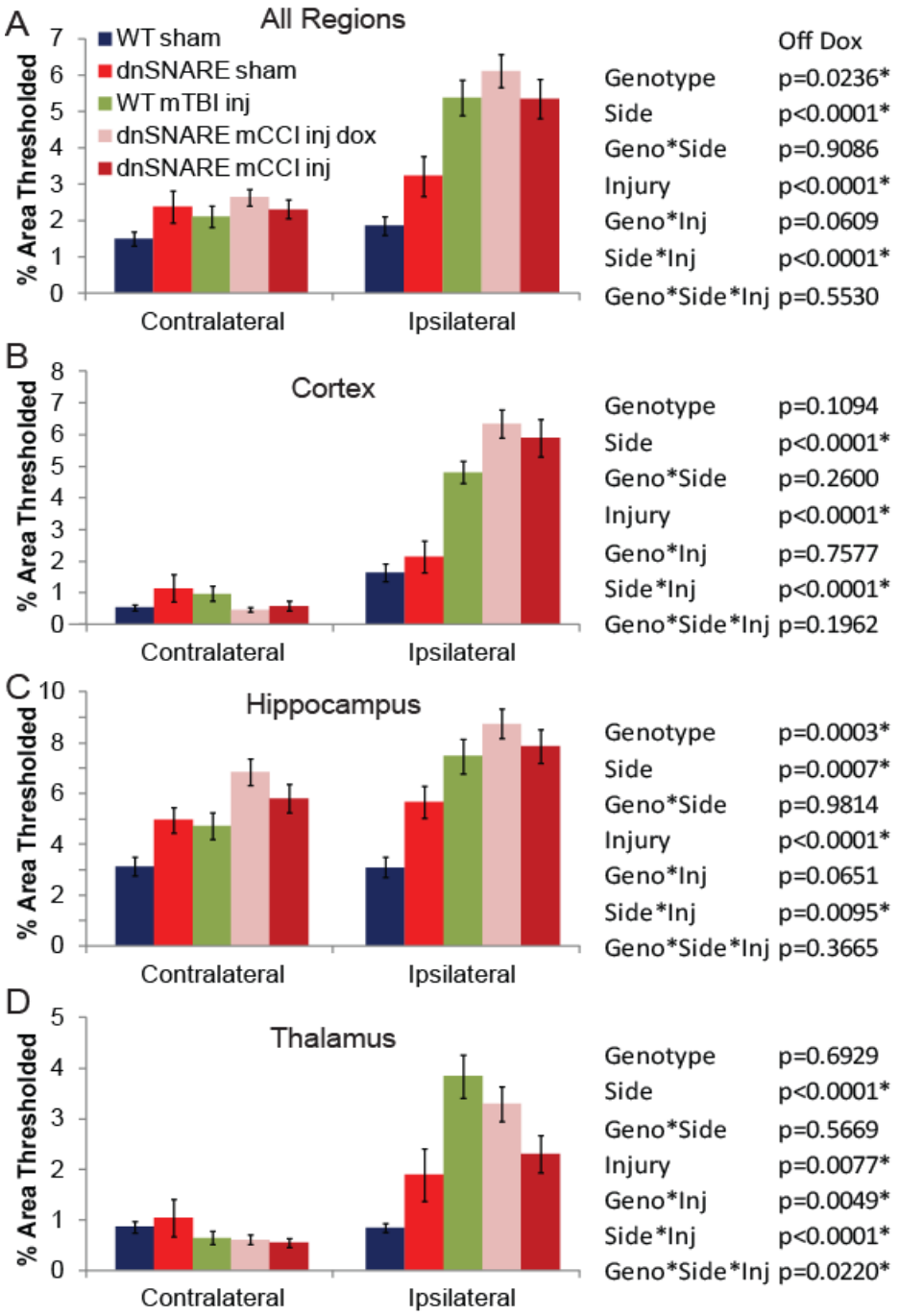

Figure 5.14. GFAP expression at day 8 after mTBI injury.
Baseline GFAP expression in dnSNARE mice was different from WT in the hippocampus ($p<0.0001$). dnSNARE on dox had elevated GFAP expression than WT injured in the contralateral hippocampus ($p=0.0063$) and ipsilateral cortex ($p=0.0103$). In mCCI dnSNARE on dox had reduced GFAP expression in the ipsilateral cortex ($p=0.0027$) and contralateral hippocampus ($p=0.0024$). There was an interaction between genotype and injury in the ipsilateral thalamus ($p=0.0220$) for mCCI injury. Data are expressed as Media ± S.E.M.

After mTBI, dnSNARE mice had increased cell death trends in the hippocampus and significantly reduced GFAP expression

Injury did cause significant neuronal degeneration in both the hippocampus and the cortex however dnSNARE did not provide any protection from neuronal degeneration. There was no significant interaction in a two way ANOVA between injury and genotype (Figure 5.12). In the hippocampus, genotype×injury was almost but not significant ($p=0.0714$) suggesting that dnSNARE potentially could increase cell death in the hippocampus. dnSNARE injured mice did perform slightly worse on average than WT animals in the SOR but this was not significant. dnSNARE on dox injured mice had significantly less cell death than WT injured in the cortex ($p=0.0292$), similar to VIPP on dox injured. The reduction in cell death in both dnSNARE and VIPP on dox mice suggests that the presence of dox and less likely the leaky transgene expression was responsible for the neuroprotection. Both CCI and mCCI injured on dox animals showed small levels of leaky dnSNARE expression as measured by the presence of green fluorescent protein (GFP) (Figure 5.13).

dnSNARE baseline GFAP expression was significantly elevated from when averaging across all three regions ($p=0.0236$) and more specifically in the hippocampus ($p=0.0003$); the other regions did not have significantly different baseline expression (Figure 5.14). dnSNARE also affected the GFAP expression levels after injury. After CCI, dnSNARE expression reduced GFAP expression and this was also the case after mCCI. For mCCI injured mice, GFAP expression was reduced in the ipsilateral thalamus ($p=0.0036$). The GFAP expression in the ipsilateral hippocampus of mCCI injured mice showed a potential significant interaction between genotype and injury ($p=0.0748$). Generally dnSNARE on dox injured GFAP expression followed those of WT injured with the following exceptions. In mCCI injured mice, dnSNARE on dox had significantly elevated expression in the contralateral hippocampus ($p=0.0063$) and in the ipsilateral cortex ($p=0.0103$). In contrast, CCI injured mice, dnSNARE on dox had significantly

reduced GFAP expression in the ipsilateral cortex (p=0.0027) and in the contralateral hippocampus (p=0.0024). These results suggested that dnSNARE in injury was able to reduce the level and spread of astrogliosis in both mCCI and CCI injured tissue. In mCCI, dnSNARE reduced glial reactivity in more distal areas to impact as seen by the reduction in the thalamus and slight reduction in the contralateral hippocampus. In CCI, dnSNARE significantly reduced astrogliosis in all regions where injury induced GFAP expression. Doxycycline also seemed to reduce the level of GFAP expression in CCI injured mice. This is likely in due to the noted anti-inflammatory effects of tetracyclines, minocycline (Jin et al., 2013; Siopi et al., 2012a, 2012b) and doxycycline (Bernardino et al., 2009; Jantzie et al., 2005; Lazzarini et al., 2013). However, in these studies, doxycycline did not seem to affect behavior as dnSNARE on dox animals largely performed on par with WT injured. It is also important to note that the relative expression of GFP correlated with the relative expression of GFAP (Figure 5.13 and 5.14).

The data suggests that while dnSNARE was able to preserve cortical motor function, the main mechanism was not due to a reduction of neuronal death. This is further supported by the fact that dnSNARE on dox mice had significantly less cell death than either WT injured and dnSNARE injured but most of the time had the worst latency times than either injured group.

DISCUSSION

In this study, we evaluated if controlling the release of gliotransmitters during the first week following TBI influenced either the histological or behavioral consequences of TBI. We evaluate the broad spectrum of injury severity using the controlled cortical impact model to either create a direct contusive injury with more widespread injury throughout the ipsilateral hemisphere, or a milder, non-hemorrhagic injury that created only a transient opening of the blood-brain barrier and transient behavioral deficit. In both injury models, dnSNARE showed aspects of improved behavior after injury. In the moderate CCI, dnSNARE animals had greater improvement of

Morris water maze latency over time. However, this improved learning did not transition to hippocampal memory in the probe trial. Moreover, we observed a significant reduction in the extent of GFAP reactivity eight days following injury in dnSNARE animals. In comparison, for mild cortical impact injury we observed that dnSNARE mice showed preservation of motor behavior in rotarod testing within the first three days of injury, a contrast to significant impairments observed in WT animals. We did not observe a significant effect of mild TBI on either SOR or CFC in WT mice, and therefore could not detect an improvement in either measure with dnSNARE mice. Overall, the improved behavior in both the CCI and mCCI injuries suggest that astrocyte gliotransmission through vesicles contribute significantly to outcome after TBI, although the histological mechanism(s) that mediate this improvement need further definition.

However dnSNARE have a hypofunction of NMDARs (Deng et al., 2011; Fellin et al., 2009). This is a major caveat in determining whether astrocytic release of gliotransmitters after mechanical injury is a major contributor to excitotoxicity because reducing NMDAR surface expression would also be neuroprotective after TBI. dnSNARE mice have already been shown to be neuroprotective in both stroke and NMDA excitotoxic injuries (Hines and Haydon, 2013).

In CCI injured rats, NMDAR antagonists reduced cell death, lowered brain edema, and improved BBB recovery (Dempsey et al., 2000; Raghavendra Rao et al., 2001). In FPI injury, NMDAR antagonists improved spatial memory and motor performance (Okiyama et al., 1997, 1998). CCI injured dnSNARE mice did not experience similar level of neuroprotection. There was no difference in NSS and there was only a small improvement in watermaze performance. This is likely due to the CCI being a hemorrhagic injury. Blood is toxic and is a source of excitotoxicity (Hawkins, 2009; Jaremko et al., 2010) and delayed BBB repair has been linked to worse behavioral outcome (Bush et al., 1999; Faulkner et al., 2004). Thrombin in blood activates protease activated recptor 1 (PAR1) (Coughlin, 1999) which phosphorylates and activates Src kinases. Phosphorylated Src kinates potentiates NMDAR activation and in turn α-amino-3-

hydroxy-5-methyl-4-isoxazolepropionic acid receptor (AMPAR) (Sharp et al., 2008). The neuroprotection from a hypofunction of NMDARs may have been negated by the presence of thrombin leading to a potentiation of NMDAR activity in the cells. In contrast, mCCI injured mice show preservation of motor function. mCCI injury also did not cause hemorrhaging and limited BBB extravastaion. The lack of blood and blood proteins in the brain parenchyma in the mCCI injury may have preserved the neuroprotective effects from dnSNARE induced NMDAR hypofunction.

Past research with NMDAR antagonists and TBI showed reduction of lesion volume and cell death. However, there was increased neurodegeneration in the hippocampus of dnSNARE injured mice in comparison to WT injured that was almost significant. This could potentially be due to a difference in cell death mechanism between dnSNARE and WT mice. Studies have shown that NMDAR dependent death leads to necrosis whereas NMDAR independent cell death pathways are apoptotic (Portera-Cailliau et al., 1997). Necrosis peaks at an earlier time point (Bien et al., 1999) and can be cleared away in a matter of hours (Rink et al., 1995) unlike apoptosis. With dnSNARE having reduced NMDAR surface expression in the cortex (Deng et al., 2011; Fellin et al., 2009), this could result in greater NMDAR independent cell death pathways in dnSNARE mice. FJB cannot differentiate between necrosis and apoptosis. It is possible that the increased cell death in dnSNARE hippocampus could be reflective of greater delayed cell death due to more apoptosis than necrosis. dnSNARE cortical degeneration was not greater than WT. This could be due to the difference in time course in degeneration between the brain regions. In vitro organotypic slice stretch models, cortical cells displayed faster degeneration (Elkin and Morrison III, 2007) than the hippocampus (Cater et al., 2006). The 24hr FBJ measure may not have accurately captured the peak cell death in the cortex for either dnSNARE or WT injured mice.

In addition to neurodegeneration as detected by FJB, we also looked at GFAP expression post injury for both CCI and mCCI. In both cases, we saw a significant reduction in GFAP expression of dnSNARE mice after injury compared to WT controls. These results suggest that the inhibition of vesicular release through dnSNARE expression resulted in a major effect in the pathophysiology after injury. NMDAR antagonism *in vivo* TBI studies have not shown a significant reduction in GFAP expression. In a focal ischemia model, rats treated with MK-801 did not have reduced GFAP in regions near the lesion (Schroeter et al., 1995). MK801 has also been shown to increase GFAP expression in a dose dependent manner in the cortex (O'Callaghan, 1994). If the sole effects from dnSNARE expression were from a hypofunction of NMDARs in the brain, then GFAP expression would not be so significantly reduced, especially in the CCI injured animals. Purinergic signaling in contrast has been shown to affect GFAP expression both *in vitro* and *in vivo* (Franke et al., 2012). Treatment with apyrase reduced the level of GFAP expression in injured cultures to that of naïve (Miller et al., 2009). Activation of P_2Y_1 and P_2Y_{12} receptors have a role in the activation of astrocytes (Franke et al., 2001). Blocking P2 receptor signaling with PPADS or suramin decreased GFAP expression in a spinal cord injury (Rodríguez-Zayas et al., 2012) and in a cortical stab wound (Franke et al., 1999; Di Prospero et al., 1998). Inhibition of purinergic signaling by antagonizing P_2Y_1 receptors with MRS2179 *in vitro* and *in vivo* reduced cell death after stretch and improved behavior after CCI injury (Choo et al., 2013).

Furthermore, the FJB cell death count in the mCCI also did not match behavior as there was not an increase in cortical FJB positive cells in WT compared to dnSNARE. This suggested that the level of cellular degeneration likely did not drive the behavioral dysfunction. It is possible that mCCI induced sublethal signaling dysfunction in neurons. Sublethal stretch injury has been shown to affect neuronal activity synchronicity which was blocked by treatment with apyrase or BAPTA-AM (Choo et al., 2013). This suggests that extracellular ATP can affect neuronal function that does not necessarily lead to cell death. Together this data suggests that the

behavioral preservation seen in dnSNARE animals was likely due to a reduction of astrocytic ATP.

If under mechanical input, astrocytes release of gliotransmitters was a major source of excitotoxic factors and drove neurodysfunction, then dnSNARE injured animals would reduce these effects. It would also suggest that if there was another greater source of excitoxic factors, then dnSNARE would not be able to block the subsequent dysfunction and degeneration. Our results show this. In a non-hemorrhagic injury, mCCI injured dnSNARE mice were essentially able to preserve behavior. However, in a hemorrhagic injury, CCI injured dnSNARE mice showed little neuroprotective effect. Blood is a major source of excitotoxic factors and complicates outcome. In clinical TBI, the increased presence of intracranial bleeding is associated with an increased risk of mortality (Perel et al., 2009) and worse prognosis (Godoy, 2013). Complicated mTBIs, as defined by having an intracranial abnormality on a MRI or CT scan, had significantly longer recovery times than those with uncomplicated mTBIs (Iverson et al., 2012).

It is important to note that dnSNARE expression can also block endogenous neuroprotective pathways. While dnSNARE inhibited release of extracellular ATPs could have the beneficial role of preventing neuronal signaling dysfunction, a reduction of extracellular ATP also leads to a reduction of extracellular adenosine. Reduced release of adenosine from astrocytes significantly reduced sleep pressure in sleep deprived mice (Halassa et al., 2009). Adenosine through activation of A_1 and A_{2A} receptors is also neuroprotective after injury (Cunha, 2005). CCI injured mice treated with 2-CA, a broad P1 receptors agonist had improved motor function and reduced cell death compared to untreated mice (Varma et al., 2002). Chronic treatment of caffeine, A_1 and A_{2A} receptor agonist, improved neurological deficits, histopathology, and reduced inflammation in CCI injured mice (Li et al., 2008). dnSNARE reduces a significant source of extracellular adenosine through inhibition of astrocytic ATP release (Florian et al., 2011; Halassa et al., 2009) and may reduce endogenous neuroprotective mechanisms after TBI.

We showed that targeting glial transmission prevented trauma induced behavioral deficits after mild CCI and improved the rate of spatial learning in more severe CCI injury. Regardless of the mechanism of neuroprotection (hypofunction of NMDAR, reduced excitotoxicity, or both) targeting astrocytes and gliotransmission is a potential theraputic strategy for TBI. The use of two injury models with different severities showed that the effectiveness of targeting astrocytes is greater in milder, non-hemorrhagic injuries.

Chapter 6 Summary and Conclusions

Past research on the astrocytic response to TBI was largely done *in vitro* cultures. This dissertation looks to expand this field into *in vivo* models. To do so, we first needed to create an injury model that had greater biomechanical fidelity to human mild TBI. Then by modifying the mild injury model we were able to simultaneously image and injure under a 2-photon microscope to determine if impact injury caused astrocytic calcium waves. Once we had established *in vivo* that stretch does induce intercellular calcium waves (ICW) similar to those *in vitro*, we wanted to determine if the ICWs release of extracellular adenosine triphosphate (ATP) contributed to degeneration and dysfunction after TBI. *In vitro* and *in vivo* studies both showed blocking purinergic signaling to be a potential therapeutic target. However, the use of drugs cannot differentiate the effect of astrocytes from other cell types. Using two transgenic animals with inhibited gliotransmission we were able to test the effect of astrocytic signaling on the recovery of TBI.

SUMMARY AND KEY CONCLUSIONS

New animal models of TBI need to incorporate aspects of human TBI biomechanics

Past animal TBI models studied the effect of brain injury types on dysfunction and degeneration. The exact mechanism used to create the injury was considered less important (Gennarelli, 1994). For this dissertation work, we needed an injury model that would allow us to study mild human TBI in the mouse and could also be adapted for *in vivo* imaging. Instead of using past strategies that relied on mimicking behavioral deficits or injury types to create the mild TBI in the mouse, we incorporated mild human TBI biomechanics. The resulting injury shares many of the same behavioral and histopathological symptoms as human mild TBI.

In vitro injury threshold studies showed that strain rate is a factor that affects cell death (Elkin and Morrison III, 2007) and that injury severity can affect which biochemical pathways dominate (Choo et al., 2013). These data make a case for needing to incorporate human TBI biomechanics to properly model human injury in animals. Comparing our mild controlled cortical impact (mCCI) to current CCI injury models we show the impact of varying strain rate on injury. The impact depth of mCCI was double the CCI impact depth used in these studies (2mm versus 1mm respectively). However comparing actual behavior and histopathology post injury, the strain rate difference between the two models largely dictated injury severity. A large contusion and lesion was created with CCI. But with impact speeds that create strain rates found in human mild TBI, greater injury depths can be achieved with less neurological damage. The similar staining patterns with the different histological stains in mCCI injured animals potentially show a link between injury mechanics and subsequent biochemical pathways.

Impact injury causes intercellular calcium waves in astrocytes *in vivo*

Astrocytes have been noted to have altered calcium signaling dynamics in different neuropathological states like ischemia (Ding et al., 2009) and status epilepticus (Ding et al., 2007). *In vitro* TBI research also showed astrocytes responding to stretch injury with a large ICW (Choo et al., 2013). With astrocyte cultures being a poor model for studying astrocytic functions (Agulhon et al., 2008; Lange et al., 2012), we needed to first validate that this stretch injury response occurred *in vivo*. We modified the mCCI device to conduct simultaneous *in vivo* imaging during the injury. With impact, the cortical astrocytes immediately responded with an ICW that originated from the site of impact. Without impact, the cortical astrocytes remained quiescent. We next tested to see what mechanism caused the ICW *in vivo*. The *in vitro* studies showed that percent stretch affected the signaling pathway responsible for ICW generation. At all levels of sublethal stretch tested, purinergic signaling was a dominant mechanism of ICWs.

Pretreating the cortex with apyrase reduced the injury response to near baseline levels. This suggests that the dominate mechanism of *in vivo* ICW was from extracellular ATP. Due to the limitations of 2-photon imaging, we were not able to test multiple levels of injury. However, based on the sublethal injury tested, we were able to partially validate *in vitro* results *in vivo*.

Reducing IP_3 signaling in vivo worsen behavioral outcome in a moderate severity injury

With venus tagged inosital triphosphatase (VIPP) mice, in the moderate CCI, there was a worse behavioral deficit in the watermaze compared to wildtype (WT). This was an unexpected finding. Past research with phospholipase C (PLC) inhibitors showed that blocking the inosital-1,4,5-triphosphate (IP_3) pathway provided both behavioral and histopathological protection. VIPP mice failed not only to improve behavioral outcome but worsened it. In the mCCI injury, VIPP fared slightly better. While the behavior did not show a significant interaction between genotype and injury, VIPP mice did not experience the same level of mild TBI induced deficit. This suggests that injury severity will dictate whether targeting IP3 is an effective approach.

Reducing astrocytic vesicular release preserves motor behavior after TBI.

With dnSNARE mice, in both mCCI and CCI injuries, we showed improved behavior but not improved histopathology. Preventing vesicular release specifically in astrocytes was able to reduce behavioral deficits. In CCI injury, acute time points showed no improvement. It was not until the last day of the watermaze (day7 post-injury) was there any difference in the dnSNARE injured group. With mCCI, the first few days post injury showed the greatest retention in behavior. These results suggest that preventing gliotransmitter release is neuroprotective. While it is possible the protection was from the inherent hypofunction of N-methyl-D-aspartate receptors (NMDAR) in dnSNARE mice, the reduction of gliosis is symptomatic of inhibited purinergic signaling and less of inhibited ionotropic glutamatergic signaling.

Severity of brain injury is an important factor to consider in the effectiveness of therapies.

The data in this dissertation together show that the biomechanics of the injury affects which downstream biochemical pathways dominate, affecting the efficacy of potential therapies. The difference between mCCI and CCI results with VIPP mice suggest that the level of injury can affect downstream signaling pathways and highlights the need to create models that reproduce the human TBI biomechanics to more accurately study subsequent biochemical changes. With dnSNARE, the difference in the time course of protection between the two injury levels again suggests that biomechanics will alter the effectiveness of the pathway in question. The data in this dissertation together with past *in vitro* work together suggest that the level of injury is an important consideration when looking at the treatment. Treatment methods that may work for milder injuries may not work for more severe injuries and vice versa. This is likely due to the differences in pathways that are activated in response to the difference in mechanism used to create the injury.

LIMITATIONS AND FUTURE WORK

The work in this thesis showed that astrocytic calcium signaling can potentially be a theraputic target for TBI. However, there are limitations to this work and much more research is needed before this strategy can become a therapy. The first is to have better understanding of the connection between mechanical input and the subsequent biochemical processes. In chapter three, we were able to validate some of the *in vitro* stretch results *in vivo*. Much of our understanding of the pathobiological pathways post TBI are derived from *in vitro* research ranging from tissue tolerances to changes in signaling. Future work needs to expand on the research into tissue tolerances and finding the link between the biomechanics and the biochemistry. What are the

results of blood brain barrier (BBB) breakdown? Will the injury response be different with and without BBB extravasation? With and without hemorrhage? With and without neuronal death?

Altered calcium signaling has been found to occur *in vitro*. We validate that this event also occurs *in vivo*. However, we were only able to test a limited injury spectrum. There needs to be more work in understanding the acute response under different injury conditions and how this acute response evolves long term.

The use of transgenic animals is also a major limitation. While transgenic mice in this study allowed us to specifically test the contribution of astrocyte signaling in contrast to using drugs which would affect multiple cell types, the presence of transgenes might also have other unanticipated effects. For instance with dnSNARE mice, an unintended effect was a hypofunction of N-methyl-D-aspartate receptor (NMDAR) in neurons. To study TBI, this unintended effect makes it difficult to determine which pathway or both provided the neuroprotective results. The VIPP transgene might also have other affects that have yet to be discovered that may affect the interpretation of our results.

While we found that the astrocytic signaling can be a therapeutic target in TBI, it is difficult to translate into a clinical treatment. Furthermore, the effects of the transgene are constitutive and present prior to injury. For a treatment to be effective, it must work post-injury. Future work needs to determine if targeting these pathways are effective in the hours to days post injury.

CONCLUSIONS

TBI is a potentially debilitating disorder with lifelong effects for many patients. Our work provided a method to better understand biochemical differences between mild TBI and moderate/severe TBI. The mCCI model will help to create greater understanding of tissue tolerances and the link between biomechanics and subsequent evoked biochemical pathways.

Having injury models that are modeled after human TBI biomechanics may allow us to study the right biochemical pathways post-injury and in this manner create better treatment strategies.

We also show that astrocyte signaling can be a potential theraputic target. While transgenic mice research is not directly translatable into clinical therapies, these studies do show that targeting astrocytes can preserve or reduce injury induced behavioral deficits. The transgenes also did not affect baseline behaviors which may imply that targeting astrocytes may cause minimal side effects, unlike the therapies that target neurons. We also show that injury severity does change the effectiveness of astrocytes as a theraputic target. At more severe injuries, the effectiveness was reduced and in some cases worsened outcome. Much more work needs to be done and hopefully the insights here contributed to the body of TBI research and guides future work.

Bibliography

Abbott, N.J., Rönnbäck, L., and Hansson, E. (2006). Astrocyte–endothelial interactions at the blood–brain barrier. Nat. Rev. Neurosci. *7*, 41–53.

Agulhon, C., Petravicz, J., McMullen, A.B., Sweger, E.J., Minton, S.K., Taves, S.R., Casper, K.B., Fiacco, T.A., and McCarthy, K.D. (2008). What Is the Role of Astrocyte Calcium in Neurophysiology? Neuron *59*, 932–946.

Agulhon, C., Sun, M.-Y., Murphy, T., Myers, T., Lauderdale, K., and Fiacco, T.A. (2012). Calcium Signaling and Gliotransmission in Normal vs. Reactive Astrocytes. Front. Pharmacol. *3*.

Albert-Weissenberger, C., and Sirén, A.-L. (2010). Experimental traumatic brain injury. Exp. Transl. Stroke Med. *2*, 16.

Albert-Weissenberger, C., Várrallyay, C., Raslan, F., Kleinschnitz, C., and Sirén, A.-L. (2012). An experimental protocol for mimicking pathomechanisms of traumatic brain injury in mice. Exp. Transl. Stroke Med. *4*, 1.

Alexander, M.P. (1995). Mild traumatic brain injury: pathophysiology, natural history, and clinical management. Neurology *45*, 1253–1260.

Alonso, A., Reinz, E., Fatar, M., Hennerici, M.G., and Meairs, S. (2011). Clearance of albumin following ultrasound-induced blood–brain barrier opening is mediated by glial but not neuronal cells. Brain Res.

Anderson, K.J., Fugaccia, I., and Scheff, S.W. (2003). Fluoro-Jade B Stains Quiescent and Reactive Astrocytes in the Rodent Spinal Cord. J. Neurotrauma *20*, 1223–1231.

Andriessen, T.M.J.C., Jacobs, B., and Vos, P.E. (2010). Clinical characteristics and pathophysiological mechanisms of focal and diffuse traumatic brain injury. J. Cell. Mol. Med. *14*, 2381–2392.

Bailey, K.R., and Crawley, J.N. (2009). Anxiety-Related Behaviors in Mice. In Methods of Behavior Analysis in Neuroscience, J.J. Buccafusco, ed. (Boca Raton (FL): CRC Press),.

Bain, A.C., and Meaney, D.F. (1999). Thresholds for Mechanical Injury to the in Vivo White Matter (Warrendale, PA: SAE International).

Bain, A.C., and Meaney, D.F. (2000). Tissue-Level Thresholds for Axonal Damage in an Experimental Model of Central Nervous System White Matter Injury. J. Biomech. Eng. *122*, 615–622.

Baldwin, S.A., and Scheff, S.W. (1996). Intermediate filament change in astrocytes following mild cortical contusion. Glia *16*, 266–275.

Bannerman, D.., Grubb, M., Deacon, R.M.., Yee, B.., Feldon, J., and Rawlins, J.N.. (2003). Ventral hippocampal lesions affect anxiety but not spatial learning. Behav. Brain Res. *139*, 197–213.

Bayly, P.V., Black, E.E., Pedersen, R.C., Leister, E.P., and Genin, G.M. (2006). In vivo imaging of rapid deformation and strain in an animal model of traumatic brain injury. J. Biomech. *39*, 1086–1095.

Beauchamp, K., Mutlak, H., Smith, W.R., Shohami, E., and Stahel, P.F. (2008). Pharmacology of traumatic brain injury: where is the "golden bullet"? Mol. Med. *14*, 731.

Bennett, R.E., Mac Donald, C.L., and Brody, D.L. (2012). Diffusion tensor imaging detects axonal injury in a mouse model of repetitive closed-skull traumatic brain injury. Neurosci. Lett. *513*, 160–165.

Bernardino, A.L.F., Kaushal, D., and Philipp, M.T. (2009). The Antibiotics Doxycycline and Minocycline Inhibit the Inflammatory Responses to the Lyme Disease Spirochete Borrelia burgdorferi. J. Infect. Dis. *199*, 1379–1388.

Biedenkapp, J.C., and Rudy, J.W. (2009). Hippocampal and extrahippocampal systems compete for control of contextual fear: Role of ventral subiculum and amygdala. Learn. Mem. *16*, 38–45.

Bien, A., Seidenbecher, C.I., Böckers, T.M., Sabel, B.A., and Kreutz, M.R. (1999). Apoptotic versus necrotic characteristics of retinal ganglion cell death after partial optic nerve injury. J. Neurotrauma *16*, 153–163.

Bigler, E.D., and Maxwell, W.L. (2012). Neuropathology of mild traumatic brain injury: relationship to neuroimaging findings. Brain Imaging Behav. *6*, 108–136.

Blumbergs, P.C., Scott, G., Manavis, J., Wainwright, H., Simpson, D.A., and McLean, A.J. (1994). Stalning af amyloid percursor protein to study axonal damage in mild head Injury. The Lancet *344*, 1055–1056.

Blumbergs, P.C., Scott, G., Manavis, J., Wainwright, H., Simpson, D.A., and McLean, A.J. (1995). Topography of axonal injury as defined by amyloid precursor protein and the sector scoring method in mild and severe closed head injury. J. Neurotrauma *12*, 565–572.

Bowser, D.N., and Khakh, B.S. (2007). Vesicular ATP Is the Predominant Cause of Intercellular Calcium Waves in Astrocytes. J. Gen. Physiol. *129*, 485–491.

Brody, D.L., Mac Donald, C., Kessens, C.C., Yuede, C., Parsadanian, M., Spinner, M., Kim, E., Schwetye, K.E., Holtzman, D.M., and Bayly, P.V. (2007). Electromagnetic Controlled Cortical Impact Device for Precise, Graded Experimental Traumatic Brain Injury. J. Neurotrauma *24*, 657–673.

Bush, T.G., Puvanachandra, N., Horner, C.H., Polito, A., Ostenfeld, T., Svendsen, C.N., Mucke, L., Johnson, M.H., and Sofroniew, M.V. (1999). Leukocyte Infiltration, Neuronal Degeneration, and Neurite Outgrowth after Ablation of Scar-Forming, Reactive Astrocytes in Adult Transgenic Mice. Neuron *23*, 297–308.

C. Edward Dixon, Bruce G. Lyeth, John T. Povlishock, Robert L. Findling, Robert J. Hamm, Anthony Marmarou, Harold F. Young, and Ronald L. Hayes (1987). A fluid percussion model of experimental brain injury in the rat. J. Neurosurg. *67*, 110–119.

Carbonell, W.S., Maris, D.O., McCall, T., and Grady, M.S. (1998). Adaptation of the fluid percussion injury model to the mouse. J. Neurotrauma *15*, 217–229.

Cater, H.L., Sundstrom, L.E., and Morrison III, B. (2006). Temporal development of hippocampal cell death is dependent on tissue strain but not strain rate. J. Biomech. *39*, 2810–2818.

Cernak, I. (2005). Animal Models of Head Trauma. NeuroRx *2*, 410–422.

Charles, A.C., Merrill, J.E., Dirksen, E.R., and Sandersont, M.J. (1991). Intercellular signaling in glial cells: Calcium waves and oscillations in response to mechanical stimulation and glutamate. Neuron *6*, 983–992.

Chen, S., Pickard, J.., and Harris, N.. (2003). Time course of cellular pathology after controlled cortical impact injury. Exp. Neurol. *182*, 87–102.

Chen, T., Willoughby, K.A., and Ellis, E.F. (2004). Group I metabotropic receptor antagonism blocks depletion of calcium stores and reduces potentiated capacitative calcium entry in strain-injured neurons and astrocytes. J. Neurotrauma *21*, 271–281.

Chen, Y., Constantini, S., Trembovler, V., Weinstock, M., and Shohami, E. (1996). An experimental model of closed head injury in mice: pathophysiology, histopathology, and cognitive deficits. J. Neurotrauma *13*, 557–568.

Choo, A.M., Miller, W.J., Chen, Y.-C., Nibley, P., Patel, T.P., Goletiani, C., Morrison, B., 3rd, Kutzing, M.K., Firestein, B.L., Sul, J.-Y., et al. (2013). Antagonism of purinergic signalling improves recovery from traumatic brain injury. Brain J. Neurol. *136*, 65–80.

Ciallella, J.R., Ikonomovic, M.D., Paljug, W.R., Wilbur, Y.I., Dixon, C.E., Kochanek, P.M., Marion, D.W., and DeKosky, S.T. (2002). Changes in expression of amyloid precursor protein and interleukin-1β after experimental traumatic brain injury in rats. J. Neurotrauma *19*, 1555–1567.

Clasadonte, J., Dong, J., Hines, D.J., and Haydon, P.G. (2013). Astrocyte control of synaptic NMDA receptors contributes to the progressive development of temporal lobe epilepsy. Proc. Natl. Acad. Sci. *110*, 17540–17545.

Cloots, R.J., van Dommelen, J.A., Kleiven, S., and Geers, M.G. (2012). Multi-scale mechanics of traumatic brain injury: predicting axonal strains from head loads. Biomech. Model. Mechanobiol. 1–14.

Coughlin, S.R. (1999). How the protease thrombin talks to cells. Proc. Natl. Acad. Sci. *96*, 11023–11027.

Crawley, J.N. (2007). What's Wrong With My Mouse?: Behavioral Phenotyping of Transgenic and Knockout Mice, Second Edition (John Wiley & Sons, Inc.).

Creed, J.A., DiLeonardi, A.M., Fox, D.P., Tessler, A.R., and Raghupathi, R. (2011). Concussive Brain Trauma in the Mouse Results in Acute Cognitive Deficits and Sustained Impairment of Axonal Function. J. Neurotrauma *28*, 547–563.

Cullen, D.K., Simon, C.M., and LaPlaca, M.C. (2007). Strain rate-dependent induction of reactive astrogliosis and cell death in three-dimensional neuronal-astrocytic co-cultures. Brain Res. *1158*, 103–115.

Cullen, D.K., Vernekar, V.N., and LaPlaca, M.C. (2011). Trauma-Induced Plasmalemma Disruptions in Three-Dimensional Neural Cultures Are Dependent on Strain Modality and Rate. J. Neurotrauma *28*, 2219–2233.

Cunha, R.A. (2005). Neuroprotection by adenosine in the brain: From A1 receptor activation to A2A receptor blockade. Purinergic Signal. *1*, 111–134.

D'Hooge, R., and De Deyn, P.P. (2001). Applications of the Morris water maze in the study of learning and memory. Brain Res. Rev. *36*, 60–90.

Dempsey, R.J., Başkaya, M.K., and Doğan, A. (2000). Attenuation of brain edema, blood-brain barrier breakdown, and injury volume by ifenprodil, a polyamine-site N-methyl-D-aspartate receptor antagonist, after experimental traumatic brain injury in rats. Neurosurgery *47*, 399–404; discussion 404–406.

Deng, Q., Terunuma, M., Fellin, T., Moss, S.J., and Haydon, P.G. (2011). Astrocytic activation of A1 receptors regulates the surface expression of NMDA receptors through a Src kinase dependent pathway. Glia *59*, 1084–1093.

Dikmen, S., Machamer, J., and Temkin, N. (2001). Mild Head Injury: Facts and Artifacts. J. Clin. Exp. Neuropsychol. *23*, 729–738.

Ding, S., Fellin, T., Zhu, Y., Lee, S.-Y., Auberson, Y.P., Meaney, D.F., Coulter, D.A., Carmignoto, G., and Haydon, P.G. (2007). Enhanced Astrocytic Ca2+ Signals Contribute to Neuronal Excitotoxicity after Status Epilepticus. J. Neurosci. *27*, 10674–10684.

Ding, S., Wang, T., Cui, W., and Haydon, P.G. (2009). Photothrombosis ischemia stimulates a sustained astrocytic Ca2+signaling in vivo. Glia *57*, 767–776.

Dixon, C.E., Lighthall, J.W., and Anderson, T.E. (1988). Physiologic, Histopathologic, and Cineradiographic Characterization of a New Fluid–Percussion Model of Experimental Brain Injury in the Rat. J. Neurotrauma *5*, 91–104.

Dixon, C.E., Clifton, G.L., Lighthall, J.W., Yaghmai, A.A., and Hayes, R.L. (1991). A controlled cortical impact model of traumatic brain injury in the rat. J. Neurosci. Methods *39*, 253–262.

Dokko, Y., Anderson, R., Manavis, J., Blumburgs, P., McLean, J., Zhang, L., Yang, K.H., and King, A.I. (2003). Validation of the human head FE model against pedestrian accident and its tentative application to the examination of the existing tolerance curve. In The 18 Th International Technical Conference on the Enhanced Safety of Vehicles (ESV) Proceedings, Nagoya, Japan, May, pp. 19–22.

Duhaime, A.-C., Gennarelli, L.M., and Yachnis, A. (1994). Acute subdural hematoma: is the blood itself toxic? J. Neurotrauma *11*, 669–678.

Ekmark-Lewén, S., Lewén, A., Israelsson, C., Li, G.L., Farooque, M., Olsson, Y., Ebendal, T., and Hillered, L. (2010). Vimentin and GFAP responses in astrocytes after contusion trauma to the murine brain. Restor. Neurol. Neurosci. *28*, 311–321.

Elewa, H.F., Hilali, H., Hess, D.C., Machado, L.S., and Fagan, S.C. (2006). Minocycline for Acute Neuroprotection. Pharmacotherapy *26*, 515–521.

Elkin, B.S., and Morrison III, B. (2007). Region-specific tolerance criteria for the living brain. Stapp Car Crash J *51*, 127–138.

Ellingson, B.M., Fijalkowski, R.J., Pintar, F.A., Yoganandan, N., and Gennarelli, T.A. (2005). New mechanism for inducing closed head injury in the rat. Biomed. Sci. Instrum. *41*, 86–91.

Fanselow, M.S., and Dong, H.-W. (2010). Are The Dorsal and Ventral Hippocampus functionally distinct structures? Neuron *65*, 7.

Farkas, O., Lifshitz, J., and Povlishock, J.T. (2006). Mechanoporation Induced by Diffuse Traumatic Brain Injury: An Irreversible or Reversible Response to Injury? J. Neurosci. *26*, 3130–3140.

Faul, M., Wald, M., and Coronado, V. (2010). Traumatic brain injury in the United States: emergency department visits, hospitalizations, and deaths.

Faulkner, J.R., Herrmann, J.E., Woo, M.J., Tansey, K.E., Doan, N.B., and Sofroniew, M.V. (2004). Reactive astrocytes protect tissue and preserve function after spinal cord injury. J. Neurosci. *24*, 2143–2155.

Feeney, D.M., Boyeson, M.G., Linn, R.T., Murray, H.M., and Dail, W.G. (1981). Responses to cortical injury: I. Methodology and local effects of contusions in the rat. Brain Res. *211*, 67–77.

Feeser, V.R., and Loria, R.M. (2011). Modulation of traumatic brain injury using progesterone and the role of glial cells on its neuroprotective actions. J. Neuroimmunol. *237*, 4–12.

Fellin, T., Pascual, O., Gobbo, S., Pozzan, T., Haydon, P.G., and Carmignoto, G. (2004). Neuronal Synchrony Mediated by Astrocytic Glutamate through Activation of Extrasynaptic NMDA Receptors. Neuron *43*, 729–743.

Fellin, T., Halassa, M.M., Terunuma, M., Succol, F., Takano, H., Frank, M., Moss, S.J., and Haydon, P.G. (2009). Endogenous nonneuronal modulators of synaptic transmission control cortical slow oscillations in vivo. Proc. Natl. Acad. Sci. *106*, 15037–15042.

Fiacco, T.A., and McCarthy, K.D. (2006). Astrocyte calcium elevations: Properties, propagation, and effects on brain signaling. Glia *54*, 676–690.

Fijalkowski, R.J., Stemper, B.D., Pintar, F.A., Yoganandan, N., Crowe, M.J., and Gennarelli, T.A. (2007). New Rat Model for Diffuse Brain Injury Using Coronal Plane Angular Acceleration. J. Neurotrauma *24*, 1387–1398.

Fijalkowski, R.J., Yoganandan, N., Zhang, J., and Pintar, F.A. (2009). A finite element model of region-specific response for mild diffuse brain injury. Stapp Car Crash J. *53*, 193–213.

Flierl, M.A., Stahel, P.F., Beauchamp, K.M., Morgan, S.J., Smith, W.R., and Shohami, E. (2009). Mouse closed head injury model induced by a weight-drop device. Nat. Protoc. *4*, 1328–1337.

Florian, C., Vecsey, C.G., Halassa, M.M., Haydon, P.G., and Abel, T. (2011). Astrocyte-derived Adenosine and A1 Receptor Activity Contribute to Sleep Loss-Induced Deficits in Hippocampal Synaptic Plasticity and Memory in Mice. J. Neurosci. Off. J. Soc. Neurosci. *31*, 6956–6962.

Floyd, C.L., Rzigalinski, B.A., Weber, J.T., Sitterding, H.A., Willoughby, K.A., and Ellis, E.F. (2001). Traumatic injury of cultured astrocytes alters inositol (1, 4, 5)–trisphosphate-mediated signaling. Glia *33*, 12–23.

Floyd, C.L., Rzigalinski, B.A., Sitterding, H.A., Willoughby, K.A., and Ellis, E.F. (2004). Antagonism of group I metabotropic glutamate receptors and PLC attenuates increases in inositol trisphosphate and reduces reactive gliosis in strain-injured astrocytes. J. Neurotrauma *21*, 205–216.

Franke, H., Krügel, U., and Illes, P. (1999). P2 receptor-mediated proliferative effects on astrocytes in vivo. Glia *28*, 190–200.

Franke, H., Krügel, U., Schmidt, R., Grosche, J., Reichenbach, A., and Illes, P. (2001). P2 receptor-types involved in astrogliosis in vivo. Br. J. Pharmacol. *134*, 1180–1189.

Franke, H., Verkhratsky, A., Burnstock, G., and Illes, P. (2012). Pathophysiology of astroglial purinergic signalling. Purinergic Signal. *8*, 629–657.

Geddes, D.M., Cargill, R.S., and LaPlaca, M.C. (2003). Mechanical stretch to neurons results in a strain rate and magnitude-dependent increase in plasma membrane permeability. J. Neurotrauma *20*, 1039–1049.

Gennarelli, T.A. (1994). Animate models of human head injury. J. Neurotrauma *11*, 357–368.

Gennarelli, T.A., Thibault, L.E., Adams, J.H., Graham, D.I., Thompson, C.J., and Marcincin, R.P. (1982). Diffuse axonal injury and traumatic coma in the primate. Ann. Neurol. *12*, 564–574.

Godoy, D.A. (2013). Intensive Care in Neurology and Neurosurgery. Pathophysiological Basis for the Management of Acute Cerebral Injury (SEEd).

Golding, E.M., and Vink, R. (1994). Inhibition of phospholipase C with neomycin improves metabolic and neurologic outcome following traumatic brain injury. Brain Res. *668*, 46–53.

Goldmsith, W. (1972). Biomechanics of Head Injury. In Biomechanics, Its Foundations and Objectives, Y. Fung, N. Perrone, and M. Anliker, eds. (Prentice-Hall), pp. 585–634.

Goodman, J.C., Cherian, L., Bryan Jr, R.M., and Robertson, C.S. (1994). Lateral cortical impact injury in rats: pathologic effects of varying cortical compression and impact velocity. J. Neurotrauma *11*, 587–597.

Halassa, M.M. (2009). Neuromodulatory roles for astrocytes: Synapses, circuits & behavior. Ph.D. University of Pennsylvania.

Halassa, M.M., Fellin, T., Takano, H., Dong, J.-H., and Haydon, P.G. (2007). Synaptic Islands Defined by the Territory of a Single Astrocyte. J. Neurosci. *27*, 6473–6477.

Halassa, M.M., Florian, C., Fellin, T., Munoz, J.R., Lee, S.-Y., Abel, T., Haydon, P.G., and Frank, M.G. (2009). Astrocytic Modulation of Sleep Homeostasis and Cognitive Consequences of Sleep Loss. Neuron *61*, 213–219.

Hall, E.D., Bryant, Y.D., Cho, W., and Sullivan, P.G. (2008). Evolution of post-traumatic neurodegeneration after controlled cortical impact traumatic brain injury in mice and rats as assessed by the de Olmos silver and fluorojade staining methods. J. Neurotrauma *25*, 235–247.

Hamilton, N.A., and Keller, M.S. (2010). Mild traumatic brain injury in children. Semin. Pediatr. Surg. *19*, 271–278.
Hashmi, A.M., Butt, Z., and Umair, M. (2013). Is depression an inflammatory condition? A review of available evidence. JPMA J. Pak. Med. Assoc. *63*, 899–906.
Hawkins, R.A. (2009). The blood-brain barrier and glutamate. Am. J. Clin. Nutr. *90*, 867S–874S.
Hines, D.J., and Haydon, P.G. (2013). Inhibition of a SNARE-Sensitive Pathway in Astrocytes Attenuates Damage following Stroke. J. Neurosci. *33*, 4234–4240.
Hinkle, D.A., Baldwin, S.A., Scheff, S.W., and Wise, P.M. (1997). GFAP and S100beta expression in the cortex and hippocampus in response to mild cortical contusion. J. Neurotrauma *14*, 729–738.
Ho, J., and Kleiven, S. (2007). Dynamic response of the brain with vasculature: A three-dimensional computational study. J. Biomech. *40*, 3006–3012.
Huh, J.W., Widing, A.G., and Raghupathi, R. (2007). Repetitive Mild Non-Contusive Brain Trauma in Immature Rats Exacerbates Traumatic Axonal Injury and Axonal Calpain Activation: A Preliminary Report. J. Neurotrauma *24*, 15–27.
Hylin, M.J., Orsi, S.A., Zhao, J., Bockhorst, K., Perez, A., Moore, A.N., and Dash, P.K. (2013). Behavioral and Histopathological Alterations Resulting from Mild Fluid Percussion Injury. J. Neurotrauma *30*, 702–715.
Iverson, G.L., Lange, R.T., Wäljas, M., Liimatainen, S., Dastidar, P., Hartikainen, K.M., Soimakallio, S., and Öhman, J. (2012). Outcome from Complicated versus Uncomplicated Mild Traumatic Brain Injury. Rehabil. Res. Pract. *2012*, 1–7.
James, G., and Butt, A.M. (2002). P2Y and P2X purinoceptor mediated Ca2+ signalling in glial cell pathology in the central nervous system. Eur. J. Pharmacol. *447*, 247–260.
Jantzie, L.L., Cheung, P.-Y., and Todd, K.G. (2005). Doxycycline reduces cleaved caspase-3 and microglial activation in an animal model of neonatal hypoxia-ischemia. J. Cereb. Blood Flow Metab. *25*, 314–324.
Jaremko, K.M., Chen-Roetling, J., Chen, L., and Regan, R.F. (2010). Accelerated hemolysis and neurotoxicity in neuron-glia-blood clot co-cultures. J. Neurochem. no–no.
Jin, W.-J., Feng, S.-W., Feng, Z., Lu, S.-M., Qi, T., and Qian, Y.-N. (2013). Minocycline improves postoperative cognitive impairment in aged mice by inhibiting astrocytic activation: NeuroReport 1.
Kilbourne, M., Kuehn, R., Tosun, C., Caridi, J., Keledjian, K., Bochicchio, G., Scalea, T., Gerzanich, V., and Simard, J.M. (2009). Novel model of frontal impact closed head injury in the rat. J. Neurotrauma *26*, 2233–2243.
Kimpara, H., and Iwamoto, M. (2012). Mild Traumatic Brain Injury Predictors Based on Angular Accelerations During Impacts. Ann. Biomed. Eng. *40*, 114–126.
Kleiven, S. (2007). Predictors for traumatic brain injuries evaluated through accident reconstructions. Stapp Car Crash J. *51*, 81–114.
Kleiven, S., and Hardy, W.N. (2002). Correlation of an FE Model of the Human Head with Local Brain Motion--Consequences for Injury Prediction. Stapp Car Crash J. *46*, 123–144.
Kochanek, P.M., Marion, D.W., Zhang, W., Schiding, J.K., White, M., Palmer, A.M., Clark, R.S.B., O'Malley, M.E., Styren, S.D., and Ho, C. (1995). Severe controlled cortical impact in rats: assessment of cerebral edema, blood flow, and contusion volume. J. Neurotrauma *12*, 1015–1025.
Kuchibhotla, K.V., Lattarulo, C.R., Hyman, B.T., and Bacskai, B.J. (2009). Synchronous Hyperactivity and Intercellular Calcium Waves in Astrocytes in Alzheimer Mice. Science *323*, 1211–1215.
Kushner, D. (1998). Mild traumatic brain injury: Toward understanding manifestations and treatment. Arch. Intern. Med. *158*, 1617–1624.

Laird, M.D., Vender, J.R., and Dhandapani, K.M. (2008). Opposing Roles for Reactive Astrocytes following Traumatic Brain Injury. Neurosignals *16*, 154–164.

Lamy, M., Baumgartner, D., Yoganandan, N., Stemper, B.D., and Willinger, R. (2013). Experimentally validated three-dimensional finite element model of the rat for mild traumatic brain injury. Med. Biol. Eng. Comput. *51*, 353–365.

Lange, S.C., Bak, L.K., Waagepetersen, H.S., Schousboe, A., and Norenberg, M.D. (2012). Primary Cultures of Astrocytes: Their Value in Understanding Astrocytes in Health and Disease. Neurochem. Res. *37*, 2569–2588.

Laurer, H.L., Bareyre, F.M., Lee, V.M., Trojanowski, J.Q., Longhi, L., Hoover, R., Saatman, K.E., Raghupathi, R., Hoshino, S., and Grady, M.S. (2001). Mild head injury increasing the brain's vulnerability to a second concussive impact. J. Neurosurg. *95*, 859–870.

Lazzarini, M., Martin, S., Mitkovski, M., Vozari, R.R., Stühmer, W., and Bel, E.D. (2013). Doxycycline restrains glia and confers neuroprotection in a 6-OHDA Parkinson model. Glia *61*, 1084–1100.

Le, T.H., and Gean, A.D. (2009). Neuroimaging of traumatic brain injury. Mt. Sinai J. Med. J. Transl. Pers. Med. *76*, 145–162.

Lee, B., and Newberg, A. (2005). Neuroimaging in Traumatic Brain Imaging. NeuroRx *2*, 372–383.

Levchakov, A., Linder-Ganz, E., Raghupathi, R., Margulies, S.S., and Gefen, A. (2006). Computational studies of strain exposures in neonate and mature rat brains during closed head impact. J. Neurotrauma *23*, 1570–1580.

Li, W., Dai, S., An, J., Li, P., Chen, X., Xiong, R., Liu, P., Wang, H., Zhao, Y., Zhu, M., et al. (2008). Chronic but not acute treatment with caffeine attenuates traumatic brain injury in the mouse cortical impact model. Neuroscience *151*, 1198–1207.

Lighthall, J.W. (1988). Controlled cortical impact: a new experimental brain injury model. J. Neurotrauma *5*, 1–15.

Lindgren, S., and Rinder, L. (1966). Experimental studies in head injury. II. Pressure propagation in "percussion concussion."Biophysik *3*, 174–180.

Longhi, L., Saatman, K.E., Fujimoto, S., Raghupathi, R., Meaney, D.F., Davis, J., McMillan, A., Conte, V., Laurer, H.L., Stein, S., et al. (2005). Temporal Window of Vulnerability to Repetitive Experimental Concussive Brain Injury. Neurosurgery *56*, 364–374.

Lusardi, T.A., Smith, D.H., Wolf, J.A., and Meaney, D.F. (2003). The separate roles of calcium and mechanical forces in mediating cell death in mechanically injured neurons. Biorheology *40*, 401–409.

Lyeth, B.G., Gong, Q.-Z., Shields, S., Muizelaar, J.P., and Berman, R.F. (2001). Group I Metabotropic Glutamate Antagonist Reduces Acute Neuronal Degeneration and Behavioral Deficits after Traumatic Brain Injury in Rats. Exp. Neurol. *169*, 191–199.

Macdonald, C., Dikranian, K., Song, S., Bayly, P., Holtzman, D., and Brody, D. (2007). Detection of traumatic axonal injury with diffusion tensor imaging in a mouse model of traumatic brain injury. Exp. Neurol. *205*, 116–131.

Malec, J.F., Brown, A.W., Leibson, C.L., Flaada, J.T., Mandrekar, J.N., Diehl, N.N., and Perkins, P.K. (2007). The Mayo Classification System for Traumatic Brain Injury Severity. J. Neurotrauma *24*, 1417–1424.

Manley, G.T., Rosenthal, G., Lam, M., Morabito, D., Yan, D., Derugin, N., Bollen, A., Knudson, M.M., and Panter, S.S. (2006). Controlled Cortical Impact in Swine: Pathophysiology and Biomechanics. J. Neurotrauma *23*, 128–139.

Mao, H., and Yang, K.H. (2011). Investigation of brain contusion mechanism and threshold by combining finite element analysis with in vivo histology data. Int. J. Numer. Methods Biomed. Eng. *27*, 357–366.

Mao, H., Zhang, L., Yang, K.H., and King, A.I. (2006). Application of a finite element model of the brain to study traumatic brain injury mechanisms in the rat. Stapp Car Crash J. *50*, 583–600.

Mao, H., Jin, X., Zhang, L., Yang, K.H., Igarashi, T., Noble-Haeusslein, L.J., and King, A.I. (2010a). Finite Element Analysis of Controlled Cortical Impact-Induced Cell Loss. J. Neurotrauma *27*, 877–888.

Mao, H., Yang, K.H., King, A.I., and Yang, K. (2010b). Computational neurotrauma--design, simulation, and analysis of controlled cortical impact model. Biomech. Model. Mechanobiol. *9*, 763–772.

Margulies, S.S., and Thibault, L.E. (1992). A proposed tolerance criterion for diffuse axonal injury in man. J. Biomech. *25*, 917–923.

Margulies, S.S., Thibault, L.E., and Gennarelli, T.A. (1990). Physical model simulations of brain injury in the primate. J. Biomech. *23*, 823–836.

Marmarou, A., Foda, M.A.A.-E., Brink, W. van den, Campbell, J., Kita, H., and Demetriadou, K. (1994). A new model of diffuse brain injury in rats: Part I: Pathophysiology and biomechanics. J. Neurosurg. *80*, 291–300.

Matz, P.G., Lewén, A., and Chan, P.H. (2001). Neuronal, but not microglial, accumulation of extravasated serum proteins after intracerebral hemolysate exposure is accompanied by cytochrome c release and DNA fragmentation. J. Cereb. Blood Flow Metab. *21*, 921–928.

McAllister, T.W., Ford, J.C., Ji, S., Beckwith, J.G., Flashman, L.A., Paulsen, K., and Greenwald, R.M. (2012). Maximum Principal Strain and Strain Rate Associated with Concussion Diagnosis Correlates with Changes in Corpus Callosum White Matter Indices. Ann. Biomed. Eng. *40*, 127–140.

McCrea M, Guskiewicz KM, Marshall SW, and et al (2003). Acute effects and recovery time following concussion in collegiate football players: The ncaa concussion study. JAMA *290*, 2556–2563.

McIntosh, T.K., Noble, L., Andrews, B., and Faden, A.I. (1987). Traumatic brain injury in the rat: characterization of a midline fluid-percussion model. Cent. Nerv. Syst. Trauma *4*, 119–134.

McIntosh, T.K., Vink, R., Noble, L., Yamakami, I., Fernyak, S., Soares, H., and Faden, A.L. (1989). Traumatic brain injury in the rat: Characterization of a lateral fluid-percussion model. Neuroscience *28*, 233–244.

McKinlay, A. (2010). Controversies and outcomes associated with mild traumatic brain injury in childhood and adolescences. Child Care Health Dev. *36*, 3–21.

Meaney, D., and Thibault, L.E. (1990). Physical model studies of cortical brain deformation in response to high strain rate inertial loading. (Lyon, France: International Conference on the Biomechanics of Impacts).

Meaney, D.F., Ross, D.T., Winkelstein, B.A., Brasko, J., Goldstein, D., Bilston, L.B., Thibault, L.E., and Gennarelli, T.A. (1994). Modification of the cortical impact model to produce axonal injury in the rat cerebral cortex. J. Neurotrauma *11*, 599–612.

Meaney, D.F., Smith, D.H., Shreiber, D.I., Bain, A.C., Miller, R.T., Ross, D.T., and Gennarelli, T.A. (1995). Biomechanical analysis of experimental diffuse axonal injury. J. Neurotrauma *12*, 689–694.

Miller, W.J. (2009). Mechanism of Astrocytic Calcium Wave Propagation and In Vitro Hippocampal Cell Death are Determined by the Magnitude of Mechanical Injury. University of Pennsylvania.

Miller, R.T., Margulies, S.S., Leoni, M., Nonaka, M., Chen, X., Smith, D.H., and Meaney, D.F. (1998). Finite Element Modeling Approaches for Predicting Injury in an Experimental Model of Severe Diffuse Axonal Injury (Warrendale, PA: SAE International).

Miller, W.J., Leventhal, I., Scarsella, D., Haydon, P.G., Janmey, P., and Meaney, D.F. (2009). Mechanically Induced Reactive Gliosis Causes ATP-Mediated Alterations in Astrocyte Stiffness. J. Neurotrauma *26*, 789–797.

Morrison, B., Elkin, B.S., Dollé, J.-P., and Yarmush, M.L. (2011). In Vitro Models of Traumatic Brain Injury. Annu. Rev. Biomed. Eng. *13*, 91–126.

Morrison III, B., MEANEY, D.F., Margulies, S.S., and McINTOSH, T.K. (2000). Dynamic Mechanical Stretch of Organotypic Brain Slice Cultures Induces Differential Genomic Expression: Relationship to Mechanical Parameters. Tech. BRIEFS.

Morrison III, B., Cater, H.L., Wang, C.C.-B., Thomas, F.C., Hung, C.T., Ateshian, G.A., and Sundstrom, L.E. (2003). A tissue level tolerance criterion for living brain developed with an in vitro model of traumatic mechanical loading. Stapp Car Crash J. *47*, 93–105.

Morrison III, B., Cater, H.L., Benham, C.D., and Sundstrom, L.E. (2006). An in vitro model of traumatic brain injury utilising two-dimensional stretch of organotypic hippocampal slice cultures. J. Neurosci. Methods *150*, 192–201.

Mulligan, S.J., and MacVicar, B.A. (2004). Calcium transients in astrocyte endfeet cause cerebrovascular constrictions. Nature *431*, 195–199.

Mungenast, A.E. (2011). Diacylglycerol Signaling Underlies Astrocytic ATP Release. Neural Plast. *2011*.

Myer, D.J., Gurkoff, G.G., Lee, S.M., Hovda, D.A., and Sofroniew, M.V. (2006). Essential protective roles of reactive astrocytes in traumatic brain injury. Brain *129*, 2761–2772.

Nadal, A., Fuentes, E., Pastor, J., and McNaughton, P.A. (1995). Plasma albumin is a potent trigger of calcium signals and DNA synthesis in astrocytes. Proc. Natl. Acad. Sci. *92*, 1426–1430.

National Center for Injury Prevention and Control (2003). Report to Congress on Mild Traumatic Brain Injury in the United States: Steps to Prevent a Serious Public Health Problem.

Neary, J.T., Kang, Y., Willoughby, K.A., and Ellis, E.F. (2003). Activation of Extracellular Signal-Regulated Kinase by Stretch-Induced Injury in Astrocytes Involves Extracellular ATP and P2 Purinergic Receptors. J. Neurosci. *23*, 2348–2356.

Newman, E.A. (2003). New roles for astrocytes: Regulation of synaptic transmission. Trends Neurosci. *26*, 536–542.

Nimmerjahn, A., Kirchhoff, F., Kerr, J.N.D., and Helmchen, F. (2004). Sulforhodamine 101 as a specific marker of astroglia in the neocortex in vivo. Nat. Methods *1*, 31–37.

O'Callaghan, J.P. (1994). Biochemical analysis of glial fibrillary acidic protein as a quantitative approach to neurotoxicity assessment: advantages, disadvantages and application to the assessment of NMDA receptor antagonist-induced neurotoxicity. Psychopharmacol. Bull. *30*, 549–554.

Oberheim, N.A., Wang, X., Goldman, S., and Nedergaard, M. (2006). Astrocytic complexity distinguishes the human brain. Trends Neurosci. *29*, 547–553.

Okiyama, K., Smith, D.H., White, W.F., Richter, K., and McIntosh, T.K. (1997). Effects of the novel NMDA antagonists CP-98,113, CP-101,581 and CP-101,606 on cognitive function and regional cerebral edema following experimental brain injury in the rat. J. Neurotrauma *14*, 211–222.

Okiyama, K., Smith, D.H., White, W.F., and McIntosh, T.K. (1998). Effects of the NMDA antagonist CP-98,113 on regional cerebral edema and cardiovascular, cognitive, and neurobehavioral function following experimental brain injury in the rat. Brain Res. *792*, 291–298.

Oliveira, A.M.M., Hawk, J.D., Abel, T., and Havekes, R. (2010). Post-training reversible inactivation of the hippocampus enhances novel object recognition memory. Learn. Mem. *17*, 155–160.

Oliveira, A.M.M., Estévez, M.A., Hawk, J.D., Grimes, S., Brindle, P.K., and Abel, T. (2011). Subregion-specific p300 conditional knock-out mice exhibit long-term memory impairments. Learn. Mem. *18*, 161–169.

Ommaya, A.K., and Gennarelli, T.A. (1974). Cerebral concussion and traumatic unconsciousness. Correlation of experimental and clinical observations of blunt head injuries. Brain J. Neurol. *97*, 633–654.

Ommaya, A.K., Hirsch, A.E., Flamm, E.S., and Mahone, R.H. (1966). Cerebral concussion in the monkey: an experimental model. Science *153*, 211–212.

Ommaya, A.K., Yarnell, P., Hirsch, A.E., and Harris, E.H. (1967). Scaling of Experimental Data on Cerebral Concussion in Sub-Human Primates to Concussion Threshold for Man (Warrendale, PA: SAE International).

Paradise, M.B., Naismith, S.L., Norrie, L.M., Graeber, M.B., and Hickie, I.B. (2012). The role of glia in late-life depression. Int. Psychogeriatr. *24*, 1878–1890.

Parpura, V., Basarsky, T.A., Liu, F., Jeftinija, K., Jeftinija, S., and Haydon, P.G. (1994). Glutamate-mediated astrocyte–neuron signalling. Nature *369*, 744–747.

Pascual, O., Casper, K.B., Kubera, C., Zhang, J., Revilla-Sanchez, R., Sul, J.-Y., Takano, H., Moss, S.J., McCarthy, K.D., and Haydon, P.G. (2005). Astrocytic Purinergic Signaling Coordinates Synaptic Networks. Science *310*, 113–116.

Patki, G., Solanki, N., Atrooz, F., Allam, F., and Salim, S. (2013). Depression, anxiety-like behavior and memory impairment are associated with increased oxidative stress and inflammation in a rat model of social stress. Brain Res. *1539*, 73–86.

Peña, A., Pickard, J.D., Stiller, D., Harris, N.G., and Schuhmann, M.U. (2005). Brain tissue biomechanics in cortical contusion injury: a finite element analysis. Acta Neurochir. Suppl. *95*, 333–336.

Perea, G., Navarrete, M., and Araque, A. (2009). Tripartite synapses: astrocytes process and control synaptic information. Trends Neurosci. *32*, 421–431.

Perel, P., Roberts, I., Bouamra, O., Woodford, M., Mooney, J., and Lecky, F. (2009). Intracranial bleeding in patients with traumatic brain injury: A prognostic study. BMC Emerg. Med. *9*, 15.

Peters, O., Schipke, C.G., Hashimoto, Y., and Kettenmann, H. (2003). Different Mechanisms Promote Astrocyte Ca2+ Waves and Spreading Depression in the Mouse Neocortex. J. Neurosci. *23*, 9888–9896.

Pfister, B.J., Weihs, T.P., Betenbaugh, M., and Bao, G. (2003). An In Vitro Uniaxial Stretch Model for Axonal Injury. Ann. Biomed. Eng. *31*, 589–598.

Pifarré, P., Prado, J., Giralt, M., Molinero, A., Hidalgo, J., and Garcia, A. (2010). Cyclic GMP phosphodiesterase inhibition alters the glial inflammatory response, reduces oxidative stress and cell death and increases angiogenesis following focal brain injury. J. Neurochem. *112*, 807–817.

Pleasant, J.M., Carlson, S.W., Mao, H., Scheff, S.W., Yang, K.H., and Saatman, K.E. (2011). Rate of Neurodegeneration in the Mouse Controlled Cortical Impact Model Is Influenced by Impactor Tip Shape: Implications for Mechanistic and Therapeutic Studies. J. Neurotrauma *28*, 2245–2262.

Portera-Cailliau, C., Price, D.L., and Martin, L.J. (1997). Non-NMDA and NMDA receptor-mediated excitotoxic neuronal deaths in adult brain are morphologically distinct: Further evidence for an apoptosis-necrosis continuum. J. Comp. Neurol. *378*, 88–104.

Powell, J.M., Ferraro, J.V., Dikmen, S.S., Temkin, N.R., and Bell, K.R. (2008). Accuracy of Mild Traumatic Brain Injury Diagnosis. Arch. Phys. Med. Rehabil. *89*, 1550–1555.

Di Prospero, N.A., Zhou, X.R., Meiners, S., McAuliffe, W.G., Ho, S.Y., and Geller, H.M. (1998). Suramin disrupts the gliotic response following a stab wound injury to the adult rat brain. J. Neurocytol. *27*, 491–506.

Raghavendra Rao, V.L., Dogan, A., Todd, K.G., Bowen, K.K., and Dempsey, R.J. (2001). Neuroprotection by memantine, a non-competitive NMDA receptor antagonist after traumatic brain injury in rats. Brain Res. *911*, 96–100.

Rákos, G., Kis, Z., Nagy, D., Lür, G., Farkas, T., Hortobágyi, T., Vécsei, L., and Toldi, J. (2007). Evans Blue fluorescence permits the rapid visualization of non-intact cells in the perilesional rim of cold-injured rat brain. Acta Neurobiol. Exp. (Warsz.) *67*, 149–154.

Rashid, B., Destrade, M., and Gilchrist, M.D. (2012). Mechanical characterization of brain tissue in tension at dynamic strain rates. J. Mech. Behav. Biomed. Mater.

Raslan, F., Schwarz, T., Meuth, S.G., Austinat, M., Bader, M., Renné, T., Roosen, K., Stoll, G., Sirén, A.-L., and Kleinschnitz, C. (2010). Inhibition of bradykinin receptor B1 protects mice from focal brain injury by reducing blood–brain barrier leakage and inflammation. J. Cereb. Blood Flow Metab. *30*, 1477–1486.

Raslan, F., Albert-Weißenberger, C., Ernestus, R.-I., Kleinschnitz, C., and Sirén, A.-L. (2012). Focal brain trauma in the cryogenic lesion model in mice. Exp. Transl. Stroke Med. *4*, 6.

Richmond, M.A., Yee, B.K., Pouzet, B., Veenman, L., Rawlins, J.N., Feldon, J., and Bannerman, D.M. (1999). Dissociating context and space within the hippocampus: effects of complete, dorsal, and ventral excitotoxic hippocampal lesions on conditioned freezing and spatial learning. Behav. Neurosci. *113*, 1189–1203.

Rinder, L. (1969). "Concussive Response" and Intracranial Pressure Changes at Sudden Extradural Fluid Volume Input in Rabbits. Acta Physiol. Scand. *76*, 352–360.

Rink, A., Fung, K.-M., Trojanowski, J.Q., Lee, V.M., Neugebauer, E., and McIntosh, T.K. (1995). Evidence of apoptotic cell death after experimental traumatic brain injury in the rat. Am. J. Pathol. *147*, 1575.

Rodríguez-Zayas, A.E., Torrado, A.I., Rosas, O.R., Santiago, J.M., Figueroa, J.D., and Miranda, J.D. (2012). Blockade of P2 Nucleotide Receptors After Spinal Cord Injury Reduced the Gliotic Response and Spared Tissue. J. Mol. Neurosci. *46*, 167–176.

Ross, D.T., Meaney, D.F., Sabol, M.K., Smith, D.H., and Gennarelli, T.A. (1994). Distribution of Forebrain Diffuse Axonal Injury Following Inertial Closed Head Injury in Miniature Swine. Exp. Neurol. *126*, 291–299.

Ruan, J.S., Khalil, T.B., and King, A.I. (1993). Finite Element Modeling of Direct Head Impact (Warrendale, PA: SAE International).

Ruan, J.S., Khalil, T., and King, A.I. (1994). Dynamic response of the human head to impact by three-dimensional finite element analysis. J. Biomech. Eng. *116*, 44–50.

Rudy, J.W., and Matus-Amat, P. (2005). The ventral hippocampus supports a memory representation of context and contextual fear conditioning: implications for a unitary function of the hippocampus. Behav. Neurosci. *119*, 154–163.

Ruff, R.M., Iverson, G.L., Barth, J.T., Bush, S.S., Broshek, D.K., and the NAN Policy and Planning Committee (2009). Recommendations for Diagnosing a Mild Traumatic Brain Injury: A National Academy of Neuropsychology Education Paper. Arch. Clin. Neuropsychol. *24*, 3–10.

Rzigalinski, B.A., Weber, J.T., Willoughby, K.A., and Ellis, E.F. (1998). Intracellular free calcium dynamics in stretch-injured astrocytes. J. Neurochem. *70*, 2377–2385.

Saatman, K.E., Duhaime, A.-C., Bullock, R., Maas, A.I.R., Valadka, A., and Manley, G.T. (2008). Classification of Traumatic Brain Injury for Targeted Therapies. J. Neurotrauma *25*, 719–738.

Sasaki, M., and Dunn, L. (2001). A model of acute subdural hematoma in the mouse. J. Neurotrauma *18*, 1241–1246.
Scemes, E. (2000). Components of astrocytic intercellular calcium signaling. Mol. Neurobiol. *22*, 167–179.
Scemes, E., and Giaume, C. (2006). Astrocyte calcium waves: What they are and what they do. Glia *54*, 716–725.
Schroeter, M., Schiene, K., Kraemer, M., Hagemann, G., Weigel, H., Eysel, U.T., Witte, O.W., and Stoll, G. (1995). Astroglial responses in photochemically induced focal ischemia of the rat cortex. Exp. Brain Res. Exp. Hirnforsch. Expérimentation Cérébrale *106*, 1–6.
Shakeri, M., Boustani, M.R., Pak, N., Panahi, F., Salehpour, F., Lotfinia, I., Meshkini, A., Daghighi, S., vahedi, P., Khani, M., et al. (2013). Effect of progesterone administration on prognosis of patients with diffuse axonal injury due to severe head trauma. Clin. Neurol. Neurosurg. *115*, 2019–2022.
Shapira, Y., Shohami, E., Sidi, A., Soffer, D., Freeman, S., and Cotev, S. (1988). Experimental closed head injury in rats: mechanical, pathophysiologic, and neurologic properties. Crit. Care Med. *16*, 258–265.
Sharp, F., Liu, D.Z., Zhan, X., and Ander, B.P. (2008). Intracerebral hemorrhage injury mechanisms: glutamate neurotoxicity, thrombin, and Src. Acta Neurochir. Suppl. *105*, 43–46.
Shitaka, Y., Tran, H.T., Bennett, R.E., Sanchez, L., Levy, M.A., Dikranian, K., and Brody, D.L. (2011). Repetitive Closed-Skull Traumatic Brain Injury in Mice Causes Persistent Multifocal Axonal Injury and Microglial Reactivity. J. Neuropathol. Exp. Neurol. *70*, 551–567.
Shohami, E., Shapira, Y., and Cotev, S. (1988). Experimental closed head injury in rats: prostaglandin production in a noninjured zone. Neurosurgery *22*, 859–863.
Shreiber, D.I. (1998). Experimental and computational modeling of traumatic brain injury: In vivo thresholds for mechanical disruption of the blood-brain barrier. Ph.D. University of Pennsylvania.
Shreiber, D.I., Bain, A.C., and Meaney, D.F. (1997). In Vivo Thresholds for Mechanical Injury to the Blood-Brain Barrier (Warrendale, PA: SAE International).
Shreiber, D.I., Bain, A.C., Ross, D.T., Smith, D.H., Gennarelli, T.A., McIntosh, T.K., and Meaney, D.F. (1999). Experimental investigation of cerebral contusion: histopathological and immunohistochemical evaluation of dynamic cortical deformation. J. Neuropathol. Exp. Neurol. *58*, 153–164.
Shultz, S.R., MacFabe, D.F., Foley, K.A., Taylor, R., and Cain, D.P. (2011). A single mild fluid percussion injury induces short-term behavioral and neuropathological changes in the Long–Evans rat: Support for an animal model of concussion. Behav. Brain Res. *224*, 326–335.
Signoretti, S., Vagnozzi, R., Tavazzi, B., and Lazzarino, G. (2010). Biochemical and neurochemical sequelae following mild traumatic brain injury: summary of experimental data and clinical implications. Neurosurg. Focus *29*, E1.
Singh, A., Lu, Y., Chen, C., Kallakuri, S., and Cavanaugh, J.M. (2006). A new model of traumatic axonal injury to determine the effects of strain and displacement rates. Stapp Car Crash J. *50*, 601–623.
Siopi, E., Llufriu-Dabén, G., Fanucchi, F., Plotkine, M., Marchand-Leroux, C., and Jafarian-Tehrani, M. (2012a). Evaluation of late cognitive impairment and anxiety states following traumatic brain injury in mice: The effect of minocycline. Neurosci. Lett. *511*, 110–115.

Siopi, E., Calabria, S., Plotkine, M., Marchand-Leroux, C., and Jafarian-Tehrani, M. (2012b). Minocycline Restores Olfactory Bulb Volume and Olfactory Behavior after Traumatic Brain Injury in Mice. J. Neurotrauma *29*, 354–361.

Smith, D.H., Okiyama, K., Thomas, M.J., Claussen, B., and McINTOSH, T.K. (1991). Evaluation of Memory Dysfunction Following Experimental Brain Injury Using the Morris Water Maze. J. Neurotrauma *8*, 259–269.

Smith, D.H., Soares, H.D., Pierce, J.S., Perlman, K.G., Saatman, K.E., Meaney, D.F., Dixon, C.E., and McINTOSH, T.K. (1995). A Model of Parasagittal Controlled Cortical Impact in the Mouse: Cognitive and Histopathologic Effects. J. Neurotrauma *12*, 169–178.

Sofroniew, M.V., and Vinters, H.V. (2010). Astrocytes: biology and pathology. Acta Neuropathol. (Berl.) *119*, 7–35.

Spaethling, J.M., Geddes-Klein, D.M., Miller, W.J., von Reyn, C.R., Singh, P., Mesfin, M., Bernstein, S.J., and Meaney, D.F. (2007). Linking impact to cellular and molecular sequelae of CNS injury: Modeling in vivo complexity with in vitro simplicity. In Progress in Brain Research, John T. Weber and Andrew I.R. Maas, ed. (Elsevier), pp. 27–39.

Spain, A., Daumas, S., Lifshitz, J., Rhodes, J., Andrews, P.J., Horsburgh, K., and Fowler, J.H. (2010). Mild fluid percussion injury in mice produces evolving selective axonal pathology and cognitive deficits relevant to human brain injury. J. Neurotrauma *27*, 1429–1438.

Sullivan, H.G., Martinez, J., Becker, D.P., Miller, J.D., Griffith, R., and Wist, A.O. (1976). Fluid-percussion model of mechanical brain injury in the cat. J. Neurosurg. *45*, 520–534.

Teasdale, G., and Jennett, B. (1974). Assessment of coma and impaired consciousness: a practical scale. The Lancet *304*, 81–84.

Thibault, L.E., Meaney, D.F., Anderson, B.J., and Marmarou, A. (1992). Biomechanical aspects of a fluid percussion model of brain injury. J. Neurotrauma *9*, 311–322.

Thompson, H.J., Lifshitz, J., Marklund, N., Grady, M.S., Graham, D.I., Hovda, D.A., and McIntosh, T.K. (2005). Lateral fluid percussion brain injury: a 15-year review and evaluation. J. Neurotrauma *22*, 42–75.

Ucar, T., Tanriover, G., Gurer, I., Onal, M.Z., and Kazan, S. (2006). Modified Experimental Mild Traumatic Brain Injury Model: J. Trauma Inj. Infect. Crit. Care *60*, 558–565.

Varma, M.R., Dixon, C.E., Jackson, E.K., Peters, G.W., Melick, J.A., Griffith, R.P., Vagni, V.A., Clark, R.S.., Jenkins, L.W., and Kochanek, P.M. (2002). Administration of adenosine receptor agonists or antagonists after controlled cortical impact in mice: effects on function and histopathology. Brain Res. *951*, 191–201.

Vaslin, A., Puyal, J., Borsello, T., and Clarke, P.G.H. (2007). Excitotoxicity-related endocytosis in cortical neurons. J. Neurochem. *102*, 789–800.

Vaslin, A., Naegele-Tollardo, S., Puyal, J., and Clarke, P.G.H. (2011). Excitotoxicity-induced endocytosis mediates neuroprotection by TAT-peptide-linked JNK inhibitor. J. Neurochem. *119*, 1243–1252.

Verkhratsky, A., Rodríguez, J.J., and Parpura, V. (2012). Calcium signalling in astroglia. Mol. Cell. Endocrinol. *353*, 45–56.

Viano, D.C., and Pellman, E.J. (2005). Concussion in professional football: biomechanics of the striking player--part 8. Neurosurgery *56*, 266–280; discussion 266–280.

Viano, D.C., Casson, I.R., Pellman, E.J., Zhang, L., King, A.I., and Yang, K.H. (2005). Concussion in professional football: brain responses by finite element analysis: part 9. Neurosurgery *57*, 891–916; discussion 891–916.

Viano, D.C., Casson, I.R., and Pellman, E.J. (2007). CONCUSSION IN PROFESSIONAL FOOTBALL. Neurosurgery *61*, 313–328.

Vorhees, C.V., and Williams, M.T. (2006). Morris water maze: procedures for assessing spatial and related forms of learning and memory. Nat. Protoc. *1*, 848–858.
Ward, C.C., and Thompson, R.B. (1975). The Development of a Detailed Finite Element Brain Model (Warrendale, PA: SAE International).
Weber, J.T. (2012). Altered Calcium Signaling Following Traumatic Brain Injury. Front. Pharmacol. *3*.
Weber, J.T., Rzigalinski, B.A., and Ellis, E.F. (2001). Traumatic Injury of Cortical Neurons Causes Changes in Intracellular Calcium Stores and Capacitative Calcium Influx. J. Biol. Chem. *276*, 1800–1807.
Werner, C., and Engelhard, K. (2007). Pathophysiology of traumatic brain injury. Br. J. Anaesth. *99*, 4–9.
Wilhelm, A., Volknandt, W., Langer, D., Nolte, C., Kettenmann, H., and Zimmermann, H. (2004). Localization of SNARE proteins and secretory organelle proteins in astrocytes in vitro and in situ. Neurosci. Res. *48*, 249–257.
Williams, A.J., Hartings, J.A., Lu, X.-C.M., Rolli, M.L., Dave, J.R., and Tortella, F.C. (2005). Characterization of a New Rat Model of Penetrating Ballistic Brain Injury. J. Neurotrauma *22*, 313–331.
Williams, A.J., Hartings, J.A., Lu, X.-C.M., Rolli, M.L., and Tortella, F.C. (2006). Penetrating ballistic-like brain injury in the rat: differential time courses of hemorrhage, cell death, inflammation, and remote degeneration. J. Neurotrauma *23*, 1828–1846.
Williams, A.J., Wei, H.H., Dave, J.R., and Tortella, F.C. (2007). Acute and delayed neuroinflammatory response following experimental penetrating ballistic brain injury in the rat. J. Neuroinflammation *4*, 17.
Willinger, R., Kang, H.S., and Diaw, B. (1999). Three-dimensional human head finite-element model validation against two experimental impacts. Ann. Biomed. Eng. *27*, 403–410.
Xiong, Y., Mahmood, A., and Chopp, M. (2013). Animal models of traumatic brain injury. Nat. Rev. Neurosci. *14*, 128–142.
Yeates, K.O. (2010). Mild Traumatic Brain Injury and Postconcussive Symptoms in Children and Adolescents. J. Int. Neuropsychol. Soc. JINS *16*, 953–960.
Yoganandan, N., Li, J., Zhang, J., Pintar, F.A., and Gennarelli, T.A. (2008). Influence of angular acceleration–deceleration pulse shapes on regional brain strains. J. Biomech. *41*, 2253–2262.
Zhang, L., Yang, K.H., and King, A.I. (2001). Comparison of Brain Responses Between Frontal and Lateral Impacts by Finite Element Modeling. J. Neurotrauma *18*, 21–30.
Zhang, L., Bae, J., Hardy, W.N., Monson, K.L., Manley, G.T., Goldsmith, W., Yang, K.H., and King, A.I. (2002). Computational study of the contribution of the vasculature on the dynamic response of the brain. Stapp Car Crash J. *46*, 145–164.
Zhang, L., Yang, K.H., King, A.I., and Viano, D.V. (2003). A new biomechanical predictor for mild traumatic brain injury–A preliminary finding. In Proc. 2003 Summer Bioengineering Conference, pp. 137–138.
Zhang, L., Yang, K.H., and King, A.I. (2004). A proposed injury threshold for mild traumatic brain injury. J. Biomech. Eng. *126*, 226–236.
Zhang, L., Gurao, M., Yang, K.H., and King, A.I. (2011). Material Characterization and Computer Model Simulation of Low Density Polyurethane Foam Used in a Rodent Traumatic Brain Injury Model. J. Neurosci. Methods *198*, 93–98.
Zorec, R., Araque, A., Carmignoto, G., Haydon, P.G., Verkhratsky, A., and Parpura, V. (2012). Astroglial excitability and gliotransmission: an appraisal of Ca2+ as a signalling route. ASN NEURO *4*, 103–119.